THE HYDROCHEMICAL AND ISOTOPIC CHARACTERIZATION OF GROUNDWATER IN SOUTHERN MOZAMBIQUE

Sabine Henry | HNRSAB003
University of Cape Town
February 2020

Declaration

I am presenting this dissertation in FULL fulfilment of the requirements for my degree.

I know the meaning of plagiarism and declare that all of the work in the dissertation, save for that which is properly acknowledged, is my own.

I hereby grant the University of Cape Town free license to reproduce for the purpose of research either the whole or any portion of the contents in any manner whatsoever of the above dissertation.

Abstract

A groundwater chemistry sampling campaign was run over two sampling seasons in 2018. Groundwater samples were taken across the region of southern Mozambique, between the towns of Namaacha, Catuane, Ponta do Ouro and Marracuene. Major anions and cations were analyzed by two labs at Stellenbosch University, and stable isotopes of oxygen and hydrogen, and radiogenic isotopes of strontium were analyzed at the Department of Geological Sciences at the University of Cape Town. The aim of this study was to characterize the isotopic and hydrochemical composition of groundwater in the southern Mozambique study area, using major ions and stable isotopes. Samples were categorized into different zones based on the underlying geology in which the borehole was sited. Overall, the dominant anions and cations are: $Cl>HCO_3>SO_4$ and Na> Ca=Mg>K. 68% of samples plotted in the Na-Cl water type, whilst 30% plotted in the Na-HCO_3 water type of the Piper and Chadha diagrams. Salinization is the mechanism controlling the Na-Cl water types, whilst recharge is mechanism controlling the Na-HCO_3 water types. Saturation indices of calcite, dolomite, halite, and gypsum. Saturation indices were calculated using the thermodynamic software PHREEQC. All samples were undersaturated with respect to gypsum and halite, suggesting that the conditions were thermodynamically favored for their dissolution. Samples that were from boreholes that plotted in the limestone layers and >40m depth in basalts, and quaternary sediments were oversaturated with respect to calcite and dolomite, indicating that the conditions were thermodynamically favored for their precipitation out of solution. Samples that plotted in the rhyolite, shallow basalts and quaternary sediments were undersaturated with respect to calcite and dolomite, suggesting dissolution into solution. Sixty-two percent of sample had an NA/Cl ration greater than one, indicating silicate weathering as a major process affecting the chemical character of the water. Samples in the basalts however had Na/Cl ratios less than one, and δ^2H and $\delta^{18}O$ values out of the range of seawater, suggesting ion exchange as a process affecting the chemistry of groundwater in these areas. Since there is no established Local Meteoric Water Line (LMWL) in the area, LMWL from Pretoria and Durban were used as proxies, and the Global Meteoric Water Line (GMWL) was also plotted. Samples in the rhyolites, basalts and quaternary sediments has high d-excess values, and showed a strong evaporation trend. The mechanisms for groundwater salinization in these areas is strongly influenced by evapoconcentaion effects. Geographical features such as seasonal variation, latitude, elevation and distance from coast do not appear to be a major factor affecting the isotopic composition of the groundwaters. The strontium isotopes and elemental strontium concentrations indicate that groundwater mixing likely occurred in each zone, however no end-members were established.

Acknowledgments

- Prof. Chris Harris, for all the guidance, supervision and advice;
- Prof. Jodie Miller, for co-supervision and providing the opportunity and funding to do this Masters;
- Conseng Engineering (Mozambique), Oscar and Claudio for taking us around to collect samples;
- Jared van Rooyen, for being an excellent field assistant and providing lots of wisdom;
- To Sherissa Roopnarain and Warrick Joe for isotope analysis at UCT stable isotope laboratory at UCT;
- The Central Analytical Facility at Stellenbosch University;
- My family for all their support and guidance;
- Félicie, Katie and Claire for their friendship and support;.
- WE-consult Uganda and Umvoto Africa for the opportunity to broaden my understanding of hydrogeology.

Table of Contents

List of Tables

List of Figures

1. Introduction

Water is essential to life and is effectively the most valuable resource available to mankind. In Mozambique, only 49% of the urban population has access to clean water, decreasing to 35% in rural areas. Of this, 60% is supplemented by groundwater (World Bank, 2007). Southern Mozambique's growing population is becoming more dependent on groundwater resources as the demand for freshwater for agricultural and domestic use increases. Many of the government-issued boreholes, such as the community hand pumps at the center of most villages are sunk into shallow sedimentary aquifers, without knowing the quality of the water (Chairuca et al., 2018).

The chemistry of water is an important factor in determining its use for domestic, agricultural and industrial purposes. Natural groundwater contains a wide variety of inorganic and organic constituents, primarily a result of the interaction with geological material and to a lesser extent atmospheric contribution and anthropogenic sources. Hydrochemistry governs water quality and therefore it is imperative to understand the hydrochemical processes responsible for temporal and spatial changes in the chemistry of groundwater.

As groundwater moves through rocks, the soluble products of rock weathering minerals dissolve and dilute through various rock-water interactions, releasing ions of various types and concentrations and resulting in a unique chemical signature. In addition to this, the chemistry of water may be altered as a result of various contamination from agricultural and industrial activities. Chemical ion ratios and correlations can be used to predict the origin of mineralization, thus serving as an important technique for several geochemical problems, such as predicting groundwater quality and deducing the source of salinity.

The stable isotopes of oxygen and hydrogen occur in a fixed relative abundance and are an important tool in many hydrogeological studies (Craig, 1961; Dansgaard, 194; IAEA,2007). Because these elements make up the water molecule and are conservative, they are the ideal environmental tracer - waters of different origins will present different isotope ratios. This thesis will investigate the hydrochemical and isotopic characteristics of 72 boreholes in Southern Mozambique using major anions and cations and stable isotopes, oxygen, and hydrogen.

1.1. Aims and Objectives

Aim: The overall aim of this study is to characterize the isotopic and hydrochemical composition of groundwater in southern Mozambique, in order to understand the mechanisms controlling the groundwater chemistry.

Objective 1: Delineate different zones based on the geological formation where the boreholes is located.

Objective 2: Using major ion ratios, and calculated saturation indices, determine the major controls of the groundwater chemistry.

Objective 3: Using stable isotopes of oxygen and hydrogen, and radiogenic isotope strontium, to infer the source of groundwater and delineate external processes (i.e. evaporation).

1.2. Stable Isotopes in the Hydrological Cycle

Stable isotope geochemistry is a highly developed branch of Earth Sciences, based upon natural variations of relative abundances of stable isotopes of different elements. Isotopes are atoms of the same element, but with different atomic masses due to a different number of neutrons in their nuclei. Stable isotopes are non-radioactive forms of atoms that can be used to trace the origin, sources, sinks, and interactions of water bodies (IAEA, 2007).

1.2.1. The Hydrological Cycle

The hydrosphere is a complex and dynamic system in which water (of different states, whether it be liquid, solid or gas) is in a perpetual flux between different reservoirs of the hydrological cycle. The different reservoirs in the hydrological cycle can be seen as different storage units for water, each having a different mass of water substance and different movement.

On a global scale, the hydrological cycle represents a system that is close to equilibrium (Clarke and Fritz, 1997). As water evaporates from the oceans, 90% of the return flux is back into the oceans via atmospheric precipitation. The remaining 10% of the moisture precipitates over continents, where it is stored in several reservoirs for variable amounts of time. Only about 1/3 of water vapor on land comes from oceanic water, the remaining comes from continent based reservoirs (Sharp,2005). As these reservoirs feed into one another, the water is recycled several times before, at some stage in the process, it eventually returns returning to the ocean through a river or groundwater runoff (Gat, 1996).

1.2.2. Reference Standards and Measurement of delta ^{18}O and ^{2}H

The oceans represent the largest reservoir of surface water and are relatively homogenous in isotopic composition. Therefore, it was chosen by Craig (1961) as the reference standard - the Standard Mean Ocean Water (SMOW) in which all $\delta^{18}O$- and $\delta^{2}H$ - concentrations are measured against. The Vienna Standard Mean Ocean Water (VSMOW) replaced SMOW over a decade after it was introduced after the original SMOW standard ran out.

Stable isotope data for O and H are expressed as the difference between measured ratios of the heavy and light isotopes of the same element and the reference, VSMOW (Coplen, 1993). This is known as the delta notation, δ.

$$\delta = \frac{R_{sample} - R_{standard}}{R_{standard}} \times 1000$$

An increasing δ value corresponds to an increased proportion of the heavy isotope to the lighter isotope, whereas a decreasing δ value corresponds to an increased proportion of the light isotope to the heavy isotope.

1.2.3. Fractionation Processes

Chemically speaking, isotopes of the same element behave in a very similar manner, physically however, they exhibit different properties due to mass differences. These differences manifest during physical processes, leading to isotope fractionation and thus changes in delta values. The most salient mechanisms responsible for the shift in the delta value are as follows:

1. Equilibrium fractionation is the exchange of isotopes of an element between different substances that contain that element in a closed system. When the flux of evaporation is equal to the flux of condensation and the two fluxes of isotopes are in balance, the system is said to be in isotopic equilibrium. For this to arise, the reactant and product reservoirs must be well mixed, otherwise, equilibrium will only be met at the interfaces of two reservoirs. Furthermore, chemical equilibrium must exist and for a significant amount of time, such that the forward and backward reaction rates are the same, this is to ensure that the isotopes mix between the reactants and products. To attain an isotopic equilibrium, one reservoir, usually, the smaller one must react completely with the other one. The whole reaction is assisted by mixing within the reservoirs (Clarke and

Fritz, 1997).

2. Kinetic Fractionation (non-equilibrium fractionation), is the differential distribution of isotopes during unidirectional non-equilibrium chemical reactions. In kinetic processes, the products are in instantaneous equilibrium with the reactants. A non-equilibrium state can be reached in response to the removal or additions of bulk product, relative to the bulk reactant. This would result in the deceleration of the reverse reaction and can either enhance or diminish mass-discrimination during fractionation. Kinetic fractionation effects in standing bodies of water are strongly affected by wind-speed, salinity, surface temperature, and humidity. At lower humidity, evaporation progressively becomes a non-equilibrium process as the water-vapor exchange is reduced.

3. Physical fractionation is the separation of isotopes during physical processes such as diffusion, evaporation, sublimation, melting, freezing, condensation and evaporation. In any thermodynamic reaction, an isotopic fraction will occur due to differences in reaction rates and vapor pressures of different molecular species. Reaction rates are governed by bond strength, with heavier isotopes having stronger bonds as they have more mass and therefore have more energy between the bonds. During evaporation, hydrogen bonds between polar water molecules must break. With the heavier isotopes, more energy is required to break this bond. Vapor pressure is the pressure of a vapor in contact with its liquid or solid forms. The vapor pressure of an element is inversely proportional to its atomic mass. Therefore, lighter isotopes are more volatile and preferentially evaporate and diffuse, whereas heavier isotopes will preferentially condense. This results in a disproportionate concentration of the lighter isotopes in the vapor phases. It should be noted that during precipitation, the condensation flux is a function of concentration of isotopes and not hydrogen bond strength (Craig, 1961).

The degree of isotopic fractionation between two phases is known as the fractionation factor, α:

$$\alpha_{A-B} = \frac{R_A}{R_B}$$

Where R_A and R_B are the isotopic ratios of an element in two phases, A and B. Give the equation that relates alpha, R and delta:

$$\alpha_{A-B} = (1000 + dA)/(1000 + dB)$$

1.2.4. Meteoric Water Lines

The isotopic compositions of meteoric (meteorological) waters behave in a surprisingly predictable fashion (Craig, 1961;). In physical processes involving evaporation and condensation, hydrogen isotopes fractionate in proportion to oxygen isotopes due to differences in corresponding vapor pressures between H_2O and HDO, and $H_2{}^{16}O$ and $H_2{}^{18}O$. Every step in the hydrological cycle amongst fresh-water reservoirs partitions $\delta^{18}O$ and $\delta^{2}H$, resulting in unique isotopic compositions for each reservoir. This has been found useful for determining the provenance of groundwaters. Craig (1961) defined the relationship between $\delta^{18}O$ and $\delta^{2}H$ in worldwide freshwater samples, resulting in the Global Meteoric Water Line (GMWL). The GMWL is effectively the line of best fit through the weighted mean of all Local Meteoric Water Lines (LMWL). The relationship was defined as:

$$\delta D = 8\delta^{18}O + 10‰ \ SMOW.$$

A LMWL differs from the GMWL depending on different climatic regimes and most LMWLs are less steep than the GMWL. This has been found to be extremely useful in characterizing groundwater recharge environments. Some notable observations are that colder climatic regimes are isotopically depleted and have steeper gradients in comparison to warmer climatic regimes, which are isotopically enriched and have shallower gradients (Craig, 1961; Dansgaard, 1964).

1.2.5. Evaporation, Deuterium Excess ‘d’ and its effects on the GMWL

The interface between a water body and the atmosphere can be broken down into three layers. The first layer, known as the boundary layer, is situated directly above the water surface. This layer is only a few microns thick and is 100% saturated with vapor, consequently, it is under isotopic equilibrium with the water surface below. The preceding layer is a transition zone, where water vapor is moved between the boundary layer (below) and the atmosphere above in both directions. The water vapor in this zone moves via molecular diffusion, where lighter isotopes have a greater diffusivity than heavier isotopes, this is de facto a physical fractionation process. What this means, is that when humidity is low, the transition becomes enriched in the less diffusive, heavier isotopes, a result of evaporation, where transport of vapor away from the liquid-vapor interface is fast. At higher humidity, however, no net diffusive fractionation occurs as diffusion ensues in both directions. It should be noted that this diffusive fractionation is greater in ^{18}O- than in ^{2}H- (**Figure 1-1**).

Global atmospheric water vapor has an average humidity of 85% (Dansgaard, 1964). This is reflected in the GMWL, which is displaced from the reference standard, seawater. If evaporation only occurred as an effect of physiochemical equilibrium, then the GMWL would pass through the reference standard, as it would be in isotopic equilibrium with seawater. However, evaporation results in non-equilibrium fractionation, whereas precipitation is a largely equilibrium process is a strong factor and displaces the GMWL from seawater by 10‰ for delta ^{2}H.

$$\delta^2 H = 8\delta^{18} O + 10‰ SMOW$$

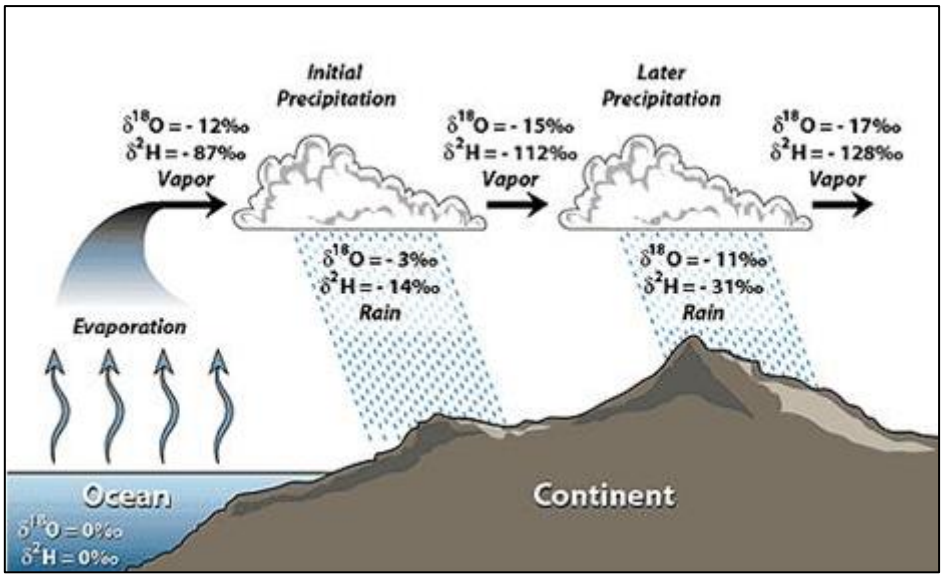

Figure 1-1 **Conceptual model of stable isotopes oxygen and hydrogen in precipitation. Waters of different sources are distinguished by their differing ratios. (based on Hoefs, 1997 and Coplen et al., 2000)**

1.3. Hydrochemical Processes

Hydrochemical processes determine the chemistry of the groundwater and they can be divided into two domains: external and internal. External controls on groundwater chemistry include processes or factors that occur outside of groundwater reservoirs. Such controls include, the composition of rainfall, evaporation processes prior to infiltration and uptake by vegetation. Internal controls include processes that occur within the groundwater reservoir. Internal controls are useful in the sense that they can give insight into the inherent nature of the aquifer. The major controls of water quality are listed below:

1. *Redox Processes*: refers to the loss (oxidation) or gain (reduction) of electrons. Redox processes are related to the decay of organic matter. The decay of organic matter is an oxidation reaction, whereby oxygen is used in the process and an acid is produced. This is of

importance in the CFA, whereby fossil organic matter (peat) is oxidized. Once oxygen is depleted, other electron acceptors such as NO_3^-, Fe-oxides and sulphate may facilitate the oxidation of organic matter.

Fe-oxides → Fe-concentrate

Sulphate → hydrogen sulphide

Organic matter → methane

2. *Weathering and dissolution of minerals*: the release of elements into the groundwater, resulting in different water types. The groundwater type is usually a function of the lithology of the aquifer matrix. Since different minerals have different rates of dissolution and solution kinetics, elemental concentrations also vary as a function of lithology. Mineral dissolution rates can be affected by changes in pH, brought about by redox reactions and changes in thermodynamic and acid-base equilibria, brought about by sudden shifts of water chemistry (point source pollution).
3. *Mineral precipitation*: the weathering of minerals, such as silicates, produces secondary minerals (clays), which tend to be more stable. The composition of the resulting clay minerals reflects the parent rock. As clay minerals dissolve, they are stripped of their cations first, then their silicon's and lastly their Al-hydroxides or Fe-oxides.
4. *Ion exchange reactions*: the chemistry of the water may profoundly change when infiltrating water differs from that of the already present water. This is particularity prominent in coastal aquifers, pollution plumes and acid rain.
5. *Mixing* of different waters occurs in coastal zones, near springs, seepage zones or waters that have different water qualities because of different lithologies/sources and anthropogenic sources. In 2018, it was reported that in Cape Town, 36% of water is lost due to leaking water pipes (Armitage, 2018). In addition to this, many of the WWTW sludge and maturation ponds are not lined.
6. *Anthropogenic sources*: include a wide variety of constituents that are leached into the groundwater system. Constituents vary from ordinary table salt (NaCl) used in everyday household products, to heavy metals and organic matter. Anthropogenic sources even include acid rain and air pollution from the burning of fossil fuels.
7. *Evaporation:* affects the concentration of ions in solution and the delta value of stable isotopes.
8. *Precipitation*: wet (e.g. rainfall) and dry (e.g. dust) deposition.

The geochemistry was assessed based on the measurements of major anions (chloride, bicarbonate alkalinity, sulphate) and cations (sodium, calcium, magnesium, potassium). Based on these results, hydrochemical zones were delineated using Chadha plots.

A Chadha plot expresses the difference in milliequivalent percentage between alkaline earth metals (calcium and magnesium) and alkalis (sodium and potassium), and weak acidic anions (bicarbonate) and strong acidic anions (chloride and sulphate) (Chadha, 1999). The different water types are a result of different controlling mechanisms. The following lists defines the water types and their respective controlling mechanism:

- Na-Cl: Salinization
- Na-HCO_3: Base Ion Exchange (BIE)
- Ca-Mg-HCO_3: Recharging water
- Ca-Cl_2: Reverse Ion Exchange (RIE)

1.3.1. Ion Exchange Processes

Ion exchange processes are useful when deciphering the geochemical patterns and conditions in an aquifer. In geochemistry, the word *exchange* refers to the replacement of one chemical for another one at a solid surface. In a steady state system, the cation exchanger (solid surface) will be in chemical equilibrium with the groundwater. However, when the water composition changes as a result of pollution or exploitation, the cation exchanger will re-adjust its composition to the new groundwater composition. In this sense, the cation ion exchanger acts as a temporary buffer, and the water composition may still reflect chemical characteristics of the former groundwater (Apello and Potsma, 2009).

Typically, coastal aquifers, with a shelly geology like that of the quaternary sediments of the study area are dominated by calcium and bicarbonate ions as a result of calcite dissolution. The cation exchanger will therefore be dominated by calcium ions. When Na-Cl intrudes into a freshwater body, of Ca-HCO_3 waters, *ion exchange* (reverse ion exchange) occurs, whereby sodium is taken up by the exchanger and calcium is released. Since chloride is chemically 'inert', it remains in solution and the water composition changes from Na-Cl to Ca-Cl_2 type:

$$Na^+ + 1/2Ca\text{-}X_2 \rightarrow Na\text{-}X + 1/2Ca^{2+}$$

Conversely, base ion exchange occurs when fresh water (dominated by calcium and bicarbonate) infiltrates Na-Cl of water, a process known as *freshening,* and calcium ions are absorbed onto the cation exchanger, whilst Na^+ ions are released, resulting in Na-HCO_3 water type:

$$1/2Ca^{2+} + Na\text{-}X \rightarrow 1/2Ca\text{-}X_2 + Na^+$$

1.3.2. Saturation Indices

The saturation index (SI) indicates the state of saturation of a groundwater sample with respect to a given mineral. In this case, the SI were calculated for anhydrite, aragonite, calcite, dolomite, fluorite, and halite. Based on the SI value, the trend of precipitation or dissolution can be determined. Minerals that are oversaturated (SI>0.1) will tend to precipitate, whereas minerals that are undersaturated (SI<0.1) will tend to dissolve. Equilibrium is taken to be between SI = -0.1 to 0.1. The SI values were calculated using the thermodynamic software PHREEQC using the formula below.

$$SI = log \frac{IAP}{KT}$$

***SI* - Saturation Index**

***IAP* - Ion Activity Product**

***KT* – Solubility Product**

The Ion Activity Product (IAP) is the effective concentration of any ion in solution, and it is usually less than the actual concentration of ions in solution. The IAP of the dissociated chemical species in solution and KT is the equilibrium solubility product for the chemical involved at the sample temperature. Such an index reflects groundwater discharging from an aquifer containing ample amount of the mineral with enough residence time to reach equilibrium (Appelo and Postma, 2009). Saturation indices can be used in conjunction with major ion ratios to infer mineral dissolution contribution to the overall geochemical character of the water.

1.3.3. Oxidation-Reduction Reactions

Reduction and oxidation processes exert an important control on the natural concentrations of oxygen, iron, sulphate, hydrogen sulphide, methane etc. in groundwater. In addition to this, they also determine the fate of some pollutants, such as nitrates leaching from agricultural practices,

contaminants leaching from landfills, industrial spills, or heavy metals in acid mine drainage. Redox reactions can be defined as a chemical reaction, in which electrons are transferred between two reactants participating in the reaction. The order in which they proceed can be predicted from standard equilibrium thermodynamics. Redox processes in groundwater typically occur through the addition of an oxidant, such as O_2 or NO_3^- to an aquifer containing a reductant. However, the addition of a reductant, such as Dissolved Organic Matter (*DOC*) that leaches from soils or landfills can also be important (Apello & Postma, 2009).

The oxidation state is an important factor in determining the behaviour of elements in the natural environment. For example, Fe^{2+} (ferrous iron), is more soluble in water than Fe^{3+} (ferric iron). If water containing high amounts of Fe^{2+} is exposed to oxygen (from a fluctuating water table, or injection water containing a high amount of dissolved oxygen), the ferrous iron will oxidize to ferric iron, losing an electron and gaining a positive charge. This is problematic because iron hydroxide would precipitate out of solution, clogging pore spaces and changing the physical nature of aquifer material. There are many redox reactions that occur in aquifers, **Figure 1-2** displays some of the more important processes that can occur in groundwater systems.

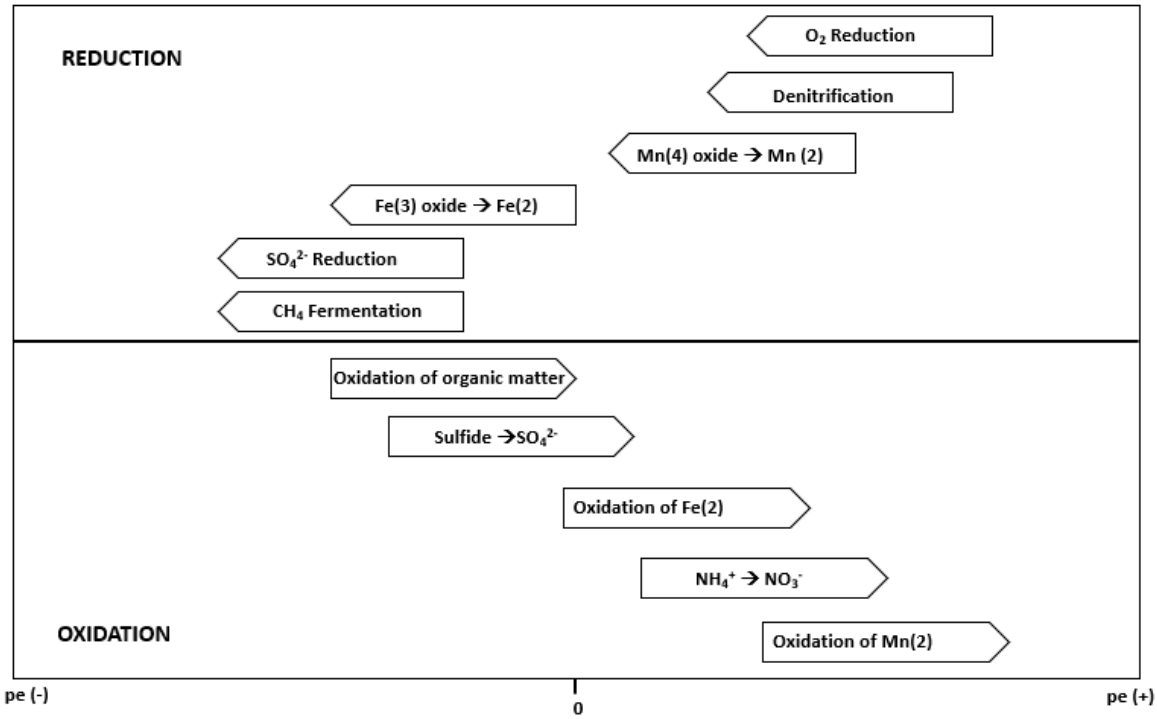

Figure 1-2 **Some major oxidation-reduction processes in groundwater systems (adapted from Appello and Potsma, 2009)**

1.3.4. Salinization Processes

Groundwater salinization is a worldwide phenomenon and is one of the most conspicuous causes of

water quality degradation. Salinization presents itself as a major environmental and economic adversity, affecting both soil and water resources, agricultural development, and disturbances in natural ecosystems. Essentially, salinity is the total concentration of dissolved constituents, namely, sodium, chloride, sulphate, boron, fluoride, and radioactivity. A multitude of issues arise from the salinization of groundwater, and include – degrading the quality of water supplied for domestic and agricultural purposes; changing the chemical composition of natural water resources; ecosystem transformation via loss of biodiversity and taxonomical replacement of halotolerant species; loss of fertile soil; enhanced mobilization of toxic trace elements; health issues and lastly, change in local climatic conditions due to vegetation loss soil deterioration.

In general, there are three sources of groundwater salinity. Primary salinity, also known as natural salinity, is a result of the dissolution of minerals from either the host lithology or the accumulation of rainfall over time. Such minerals are highly soluble and release ions into solution upon contact with water. Typical minerals include, halite, gypsum, carbonates, anhydrite, fluoride salts and sulphate salts. Secondary/dry land salinity is caused by fluctuating water levels, which bring salts to the ground surface. The accumulation of salts in the soil profile can be enhanced by the removal of vegetation. Seasonal affects can be observed in salt concentrations, with higher rainfall months resulting in salts percolating down to the water table and drier months leading to an increased concertation on the surface. Lastly, tertiary/irrigated salinity occurs as a result of over irrigation, ensuing in a build-up of salts in the groundwater.

1.4. Study Area

The study is in the Maputo Province of southern Mozambique, in the Boane, Namaacha, Matutuine, Maputo, Matola and Marracuene districts. The study area is bordered by Swaziland to the west, the Kwazulu-Natal Province of South Africa to the south, the Indian Ocean to the east and the Moamba district of the Maputo Province to the north. The study covers a total area of 11,562 $km^{2.}$, and a map of the study area can be found in **Figure 1-3**.

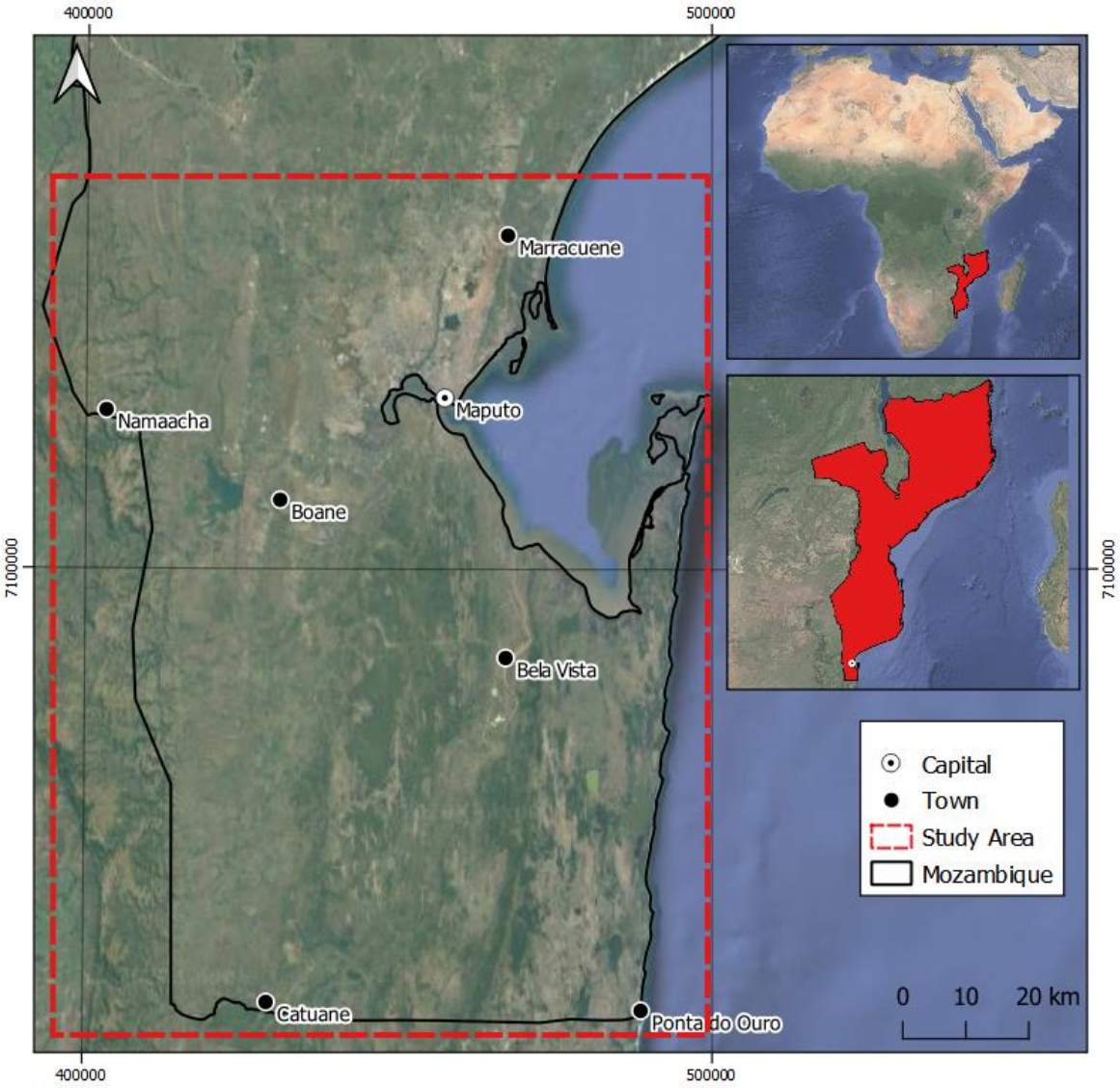

Figure 1-3 Map of the study area and some of the major towns.

1.4.1. Geology

The Lebombo monocline is a 700 km long, between 5-30 km wide, E-dipping linear flexure that formed along the border of Mozambique and South Africa/Swaziland. The location of the Lebombo monocline is thought to be controlled by either the rapid transition between stretched and normal continental crust or between the normal lithospheric upper mantle and thick Archean lithospheric mantle, all of which formed part of the Kalahari Craton (Manninen *et al.,* 2008). A geological map of the area can be found in **Figure 1-4**.

A W-E cross-section of the Lebombo monocline through Swaziland and Mozambique, reveals that Karoo sediments lie unconformably over crystalline basement rocks. The next major lithological units after Karoo sediments are the Karoo volcanics, and are as follows in chronological order from

oldest to youngest; Sabie River Basalt Formation, Mbuluzi Formation, Movene Basalt Formation (with Sica beds) and the Cretaceous sedimentary cover of the Maputo and Grudja Formations (Melluso *et al.*, 2008). The Karoo volcanics (Sabie River Basalt Formation – Movene Basalt Formation) dip to the east, with the dip angle becoming progressively steeper westward (45-65^{o}), which is indicative of active downward flexing during emplacement.

The Umbeluzi Formation is a collective term for two petrographically distinct formations, the Jozini and Mbuluzi Rhyolite Formations. The younger Mbuluzi Rhyolite Formation is pervasive within Mozambique and can be distinguished from the Jozini formation by the presence of quartz phenocrysts. The basal unit of the Mbuluzi Rhyolite Formation is known as the Oribi beds, which is characterized by a high concentration of quartz phenocrysts (Cleverly and Bistow, 1979, 1984).

The Grandes (Big) Lebombo mountain range that borders Mozambique and South Africa/Swaziland comprise of the Mbuluzi Formation; however further west in Mozambique (and within the study area) are the Pequenos (Little) Lebombo Mountains comprised of the Movene Basalt Formation rhyolites, known as the Sicia Beds. The Mbuluzi rhyolites can be differentiated from the Movene rhyolites on a petrographic basis. The rhyolite sequences of the Grandes and Pequenos Lebombos form positive topographic features, known as cuesta-type geomorphology (Manninen *et al.,* 2008). Between the Grandes and Pequenos Lebombos is a relatively, topographically flat area covered by a savannah-type landscape. This area encompasses the Movene basalts, which represent the capping unit of the Lebombo Group and thus, the Karoo Supergroup (Eales *et al.,* 1984). The Movene basalts are mainly tholeiitic in nature, with high-Ti content (Manninen *et al.,* 2008). The Movene basalts are interbedded with the Sicia beds, indicating bi-modal volcanism at the time (Manninen *et al.,* 2008). It is estimated that the Karoo lavas once covered an area of 2, 000, 000 km^{2} however today only erosional remnant remains, covering an approximate area of 140, 000 km^{2}(Cox, 1970, 1972).

The Mozambique Basin covers a total area of 380,000 km^{2}, with the present-day onshore area covering 275,000 km^{2} and offshore covering 105,000 km^{2} (Coster *et al.,*1989; Matthews *et al.,* 2001). The basin is bounded by the Lebombo monocline on the south-west, the Nuanetsi-Sabi monocline on the north-west and igneous outcrops of the Karoo Supergroup in the west (Gwavava *et al.,* 1992).

Due to the repetitive cycles of transgression and regression in the Mozambique Basin, a number of Cretaceous sedimentary deposits of both marine and continental origins can be distinguished. Laying unconformably over the Movene Formation is the Lupata Formation, which consists of continental red-beds of eroded Karoo volcanics (Afonso *et al*., 1969). The transition to

marine sediments is defined by the Maputo Formation and is made up of marly-glauconitic sandstones that grade upward into fine-grained sediments. This formation was deposited during the lower Cretaceous in the first transgression cycle and can be up to 200m thick (Soares and Silva, 1970; Salam and Abdula, 1995; Melluso *et al.*, 2008). The Lower Domo Shale Formation, Domo Sand Formation, and Upper Domo Shale Formation represent deep marine sediments. These formations are pervasive in the central parts of the basin but have not been identified within the study area. (Salman *et al.,* 1995).

Overlying the Maputo Formation (within the study area) is the Grudja Formation, which is comprised of clay layers intercalated by glauconite-quartz sandstones. These sandstones are an important reservoir of natural gas in Mozambique and in recent years have received a lot of attention (Mashaba and Altermann, 2015; Castelino *et al.,* 2015; Said *et al.,* 2015). In the more southern parts of the Mozambique Basin, and thus within the study area, this formation has been eroded and replaced by more shallow-water sandbanks (Salman and Abdula, 1995). Moving westward towards the Lebombo Mountains, the Grudja formation grades into the Singuedza/Elefantes Formation. The Singuedza/Elefantes formation is of continental-marine sediments of Cenomanian age and consists of conglomerates, marine-fauna bearing layers, red-sandstones, and silites (Lachelt, 2004; Flores, 1961).

During the Eocene, shallow-water facies in the form of limestone and calcareous sandstones are represented by the Cheringoma Formation. This formation is overlain by the Neogene marine Jofane/Morrumbene Formations which are collectively known as the Tembe Formation in southern Mozambique. They are comprised of shallow marine facies, comprising of sandstones and limestones. Lastly, the Mazamba Formation which is characterized by continental facies of arkosic and conglomeratic sands Afonso *et al*., 1998; Lachelt, 2004). It is important to note that there is evidence that the Karoo volcanics extend eastwards beneath the Cretaceous sedimentary cover, off the coast of Mozambique (Flores, 1970, 1973; Darracott and Kleywegt, 1974).

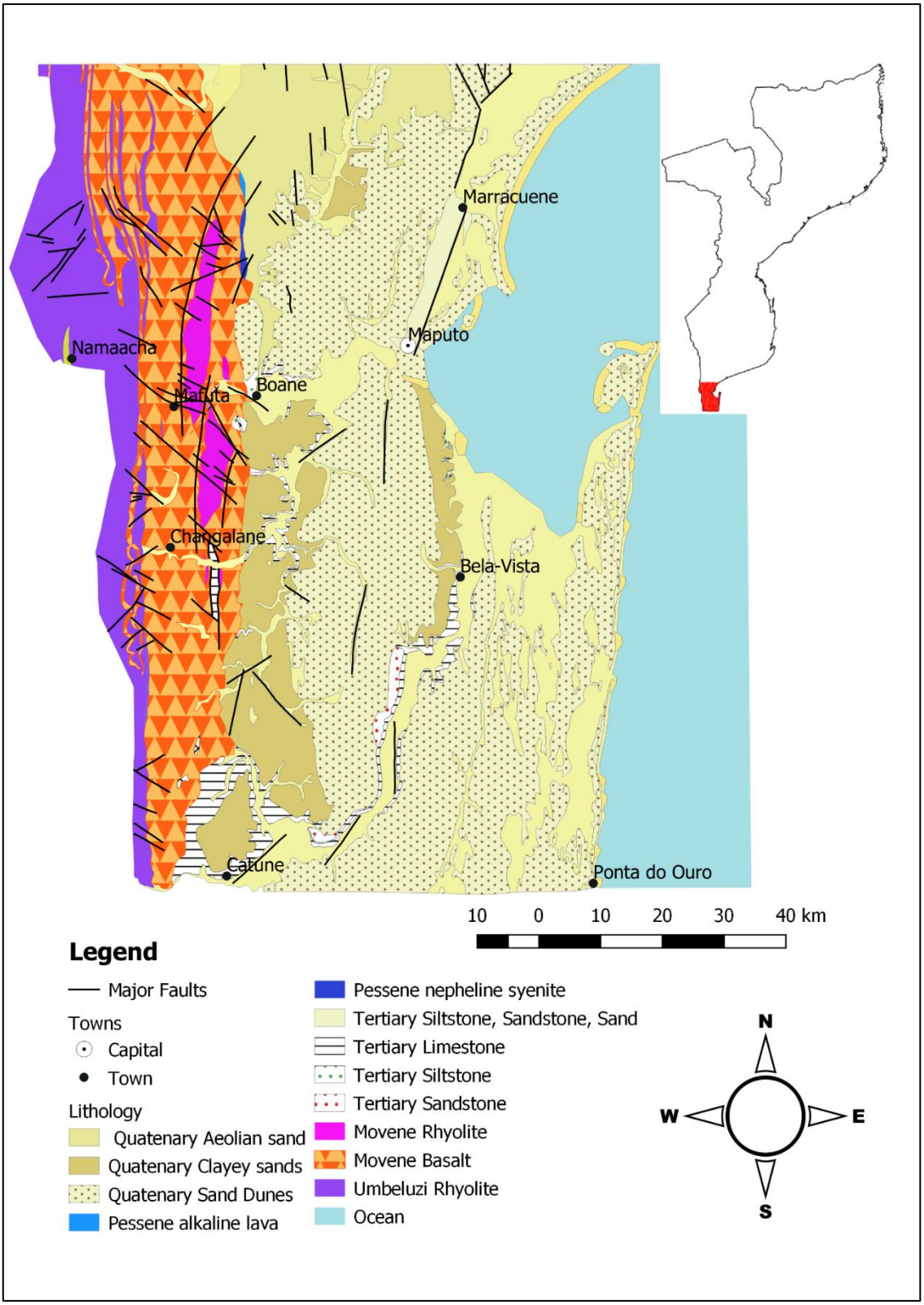

Figure 1-4 **Simplified geological map of the study area.(WE-consult, 2019)**

1.5. Hydrology

The study area can be divided into two physiographic regions. The Lebombo Range, comprised of gently tilting rhyolites and basalts, and the Coastal Plain, which is comprised of cretaceous mudrock and transported Quaternary and Tertiary soils.

1.5.1. Precipitation and Climate

The climate of the study area is classified as tropical to subtropical, with two distinct seasons that have an annual average temperature of over 20^{o}C. On a continental scale, seasonal changes are brought about by the movement of the Intertropical Convergence Zone (ITCZ). During the southern hemisphere winter months, the ITCZ shifts north of the equator, causing an area of high pressure. Thus, producing prevailing hot winds that inhibit rainfall events. The dry season in the study area extends from May to September and has an average temperature of 20^{o}C.

During the southern hemisphere summer months, the ITCZ shifts south of the equator, causing a zone of low pressure over the area. Warm, moisture-rich air of the subtropical maritime system rises above the landmass, causing it to cool, condense and rain. The rainy season extends from October to April and has an average temperature of 25^{o}C.

The town of Namaacha, which is situated in the western extremity of the study area and in the Lebombo Mountains (elevation of 600m) experiences a warm and temperate climate. The annual average temperature is 20.2^{o}C and annual precipitation is 958mm (Namaacha Monthly Climate Averages, 2018).

Maputo City on the other hand, which is situated in the eastern extremity of the study area and in the Coastal plains, experiences a tropical climate. The annual average temperature is 26^{o}C and annual precipitation is 710mm (Maputo City Month Climate Averages, 2018)).

1.5.2. Drainage Basins and River Systems

Within the study area, three main drainage basins can be identified: Maputo, Umbeluzi and Incomati basins (**Figure 1-5**).

The Maputo Basin covers an area of 30,000 km2 and is bordered by the Umbeluzi and Incomati drainage basins in the north and the Umhlatuze coastal catchment to the south. This basin

is shared between Mozambique, South Africa, and Swaziland, with the headwaters originating from South Africa. The Usuthu and Phongolo rivers are the two main tributaries to the Maputo River, which flows past Bela-Vista and out into Maputo Bay. The confluence of the Usuthu and Phongolo river is situated 15km east of Catuane.

The Umbeluzi basin, the smallest of the three basins in the study area, is sandwiched between the Maputo Basin to the south and the Incomati River Basin to the north. The basin covers a total area of 5400km2. The Umbeluzi river has two main tributaries, the White Umbeluzi and the Movene river. The river flows through the Espirito Santos estuary, south of Maputo City and into Maputo Bay.

The Incomati Basin covers an area of 75,156 km^2 and is bordered by the Umbeluzi and Maputo basins in the south. There are 6 main tributaries to t he Incomati River, they are as follows: Komati, Crocodile, Sabie, Massintonto, Unetze and Mazimechopes RIvers. All the tributaries originate from the highlands area of the Lebombo Range, except the Mazimechopes River. The Incomati River discharges into Maputo bay, north of Maputo City.

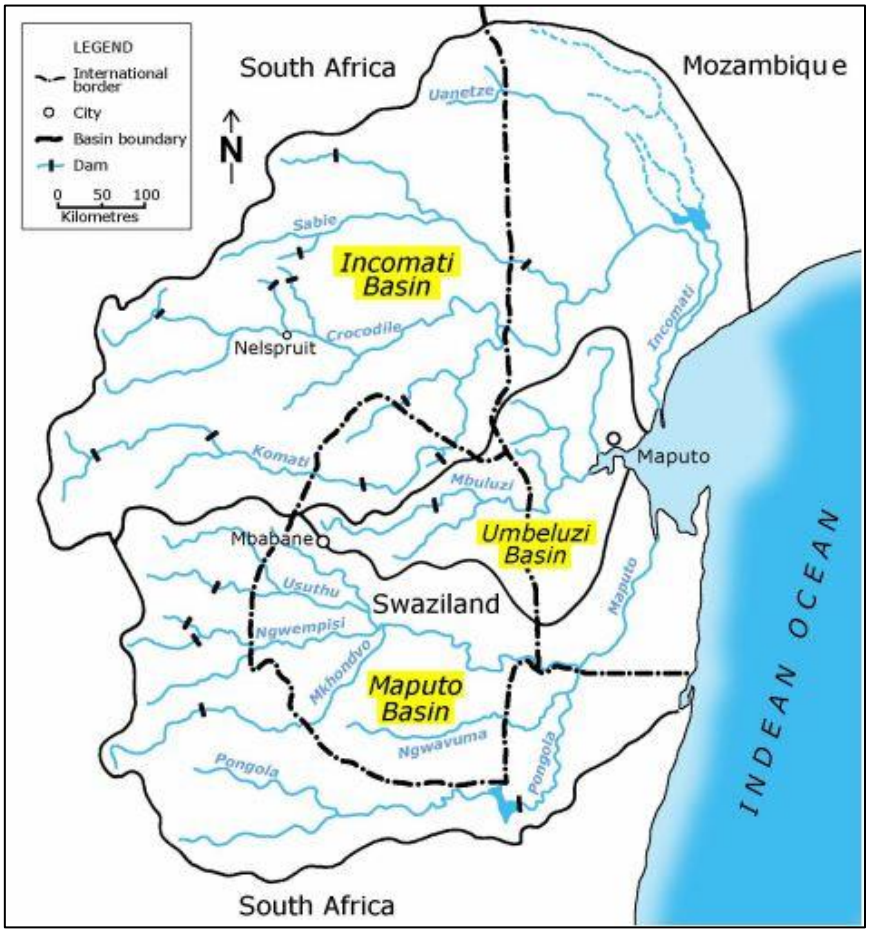

Figure 1-5 **Simplified map of major perennial rivers in the study area. Major drainage basins highlighted in yellow (Van and van der Zaag, 2001)**

1.5.3. Groundwater Occurrences and Estimated Yields

Within the study area two hydrogeological units can be identified based on geology and estimated yields; cretaceous and post-cretaceous sedimentary formations and karoo and post-karoo sedimentary formations (see **Table 1-1** and **Figure 1-6**).

The first unit comprised of cretaceous and post-cretaceous units forms part of the largest primary aquifer in southern Africa. These extensive unconfined aquifers represent some of the most productive in the country with variable quality (DNA, 1989). Within this unit, three sub-units can be identified. The first sub-unit is the intergranular and fractured argillaceous sandstones of the upper cretaceous Zululand group. Yields are estimated to be around 0.1 - 0.5 l/s. The second sub-unit consists of unconsolidated to semi-consolidated sediments of the Maputaland group that formed in the late Cenozoic. The estimated yields of this aquifer are between 0.5-2.0 l/s. The third sub-unit identified in this group is the tertiary and quaternary intergranular alluvium, with estimated yields between 0.1 - >5 l/s (Beuster and Clarke, 2008).

The second hydrogeological unit in the study area is composed of the karoo and post-karoo sedimentary rocks. This unit is of variable well discharge and generally poor quality (Smedley, 2002). Within this unit, two subunits can be identified. The first sub-unit is represented by the intergranular and fractured Lebombo rhyolites and basalts that form part of the Lebombo range. The estimated yields are between 0.1 - 0.5 l/s. However, localized fracturing in the Lebombo rhyolites (which generally tend to be non-water bearing) have recorded yields of up to 7 l/s (Piteau and Associates, 1992)The second sub-unit identified, is comprised of intergranular and fractured basalt alluvium, which has low quality but estimated yields of 0.5-2.0 l/s (Beuster and Clarke, 2008).

Table 1-1 **Major Hydro stratigraphic units in the study area (adapted from Piteau and Associates, 1992; Smedley 2002; Beuster and Clarke, 2008)**

	Type	Geohydrogeological Unit	Stratigraphy	Estimated Yield (l/s)
Cretaceous & post-cretaceous	Intergranular	Alluvium	Tertiary to quaternary deposits	0.1 - > 5

	Intergranular	Unconsolidated to semi-consolidated sediments (sands, calcrete, calcarnite, conglomerate and clay	Maputaland group – late Cenozoic	0.5 – 2.0
	Intergranular and fractured	Argillaceous sandstones	Zululand group – upper Cretaceous	0.1 – 0.5
Karoo & post-Karoo	Intergranular and fractured	Basalt Alluvium	Lower Jurassic	0.5 – 2.0
	Intergranular and fractured	Lebombo rhyolites and basalts	Upper Jurassic	0.1 – 0.5

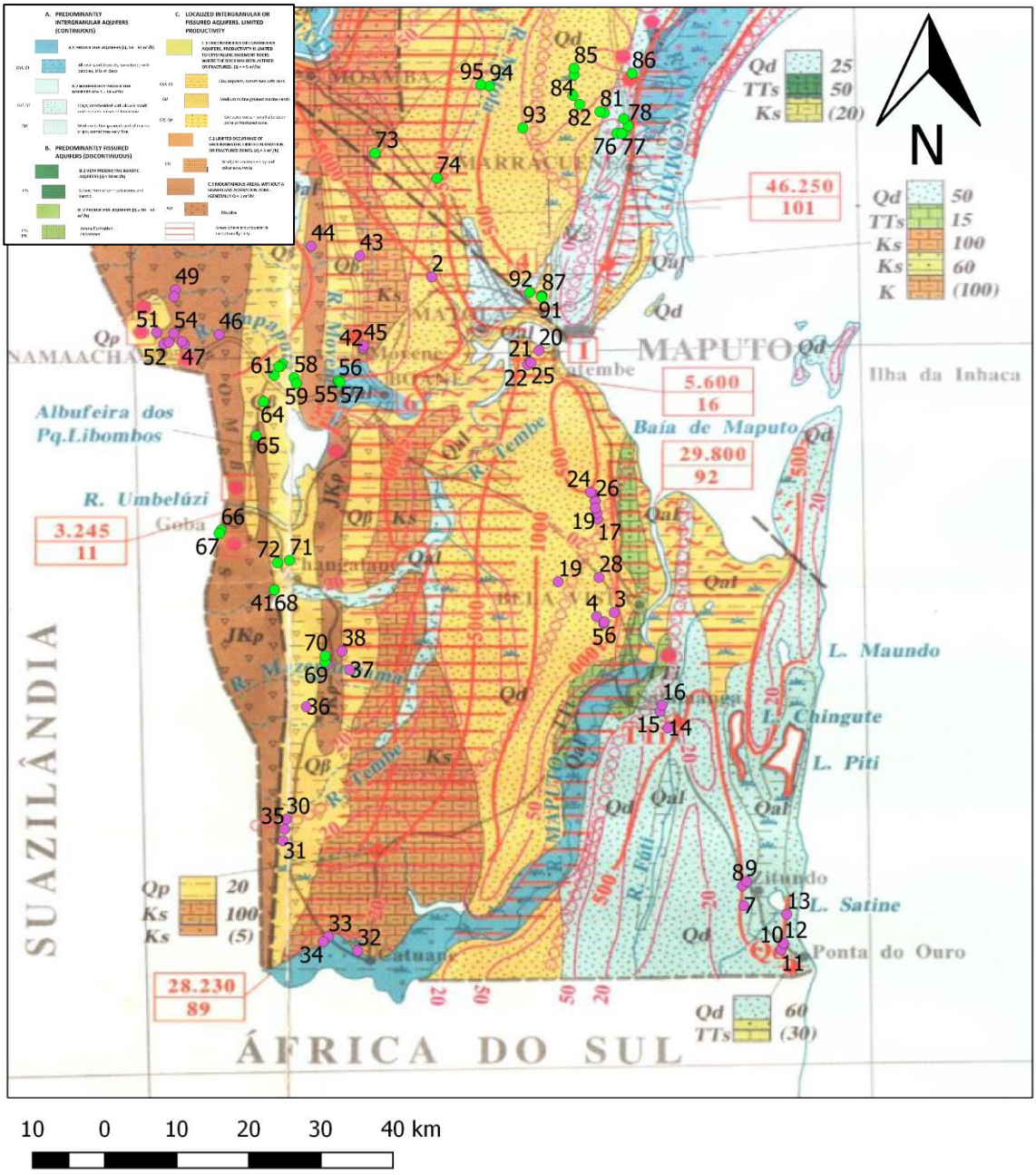

Figure 1-6 **Hydrogeological map of the study area, with sample locations. Pink dots represent samples taken in March 2019, whilst green dots represent samples taken in September 2019 (Carta Hidrogeológica do I.N.G, 19).**

2. Methodology

2.1. In-Field Sampling Procedure

The sampling of groundwater was undertaken in two sampling trips, the first between the 12-17th of March 2018 and the second, between the 3-6th of September 2018. During the March sampling trip, 54 samples were taken in and between the towns of Maputo, Matola, Bela Vista, Ponta do Ouro, Boane, Namaacha, Changalane, and Catuane. During the September sampling trip, 41 samples were taken in and between the towns of Changalane, Marracuene, Matola, and Mafuane (**Figure 1-6**). Samples were collected as a once off samples, as in there are no two boreholes that were sampled twice. Sampling was only possible for boreholes that were in close proximity to major roads connecting the respective towns. Only 24% of the boreholes sampled had electric pumps, the remaining 76% of the boreholes had community manual hand pumps (**Figure 2-1**).

Samples taken during this research are divided into zones based on what major lithology they plot in. Zone A represents samples that plot in Rhyolites, Zone B plots in basalts (Zone B1 <40m, Zone B2 >40m), Zone C plots in limestone, and Zone D2 plots in Quaternary sediments (Zone D1 <40m, Zone D2 >40m).

Infield, community boreholes were purged on average for 5 minutes before samples were collected at the surface. Only manual hand pumping options were available for the community boreholes. Electric boreholes were purged on average for 10 minutes. The depth to the water level could not be collected for any sample as the casing did not permit a dip-meter to be used. Therefore, there is a risk that boreholes were not purged for long enough, indicating that the samples may not be representative of the aquifer.

All sample bottles were pre-washed with the sample water. After this, samples were collected and immediately measured for temperature, EC, salinity, TDS, and resistivity using an Extech EC600. The pH was measured using a FieldScout SoilStik pH Meter. Both probes were calibrated every morning before sampling took place with the respective calibration solutions. The borehole locations and elevations were noted and recorded using a Garmin eTrex 10 handheld GPS. All samples were filtered on-site using 0.45µm, 25mm, sterile cellulose acetate filters. Each sample tube was labelled using a black permanent marker with a specific code. Anion and cation samples were collected separately in 50ml conical bottom centrifuge tubes, and O- and H- isotopes, Sr-isotopes, and blanks were collected in 15 ml conical bottom centrifuge tubes. The tops of the tubes were cello-taped and put in a sampling zip-lock bag designated for each borehole. Samples were put in a car-fridge at a temperature of 4°C.

Figure 2-1 Example of a community hand pump in Southern Mozambique.

2.2. Analytical Techniques

2.2.1. Major Cations

Major cation and trace element concentrations (mg/l) were analysed at the Central Analytical Facility (CAF) at Stellenbosch University. Samples were first prepared by being acidified to a pH less than 2 using an ultrapure concentrated nitric acid. Cations were analysed using an Agilent 7700 ICP-OES. The cations sampled included: calcium, magnesium, sodium and potassium.

2.2.2. Bicarbonate

HCO_3^- (mg/L) was analysed at the Department of Soil Science at Stellenbosch University using the Metrohm 905 Titrano Autotritator. Three samples, SH18015A, SH18017A, and SH18041A were titrated with 0.004N of HCL. The remaining samples were titrated with 0.1N of HCL. The alkalinity was calculated using the equation below:

$$\text{volume of titrant ml} \times \text{normality of acid (N)} \; \text{volume of sample (ml)} \times 50{,}000$$

2.2.3. Chloride and Sulphate

The major anions, Cl^- and SO_4^{2-} were analyzed at BemLabs in Somerset West, South Africa. Chloride concentration (mg/l) was measured using 0.02N Silver Nitrate ($AgNO_3$) titration using Methrom 904 Titrando. Sulfate was calculated from the sulfur content using the ICP-OES the Agilent 700 ICP series ICP.

2.2.4. Oxygen and Hydrogen isotopes

Oxygen and Hydrogen isotope ratios were prepared and analysed at the Department of Biological Sciences at the University of Cape Town. Two internal standards were analysed in duplicate (O) or triplicate (H) using isotope ratio mass spectrometry. For this study, the CTMP2010 (Cape Town Millipore Water 2010) and RMW (Rocky Mountain Water) were used and they have calibrated $\delta^{2}H$ and $\delta^{18}O$ values of -7.4‰ and -2.74‰ and -131.4‰ and -17.38‰, respectively. These were calibrated using international standards V-SMOW and standard light Arctic precipitation (SLAP). The raw data obtained from the internal standards were converted to the V-SMOW scale and corrected for scale compression. Groundwater samples were analysed by wavelength-scanned cavity ring-down spectroscopy (WS-CRDS) using an L2120-I (Picarro, Sunnyvale, CA, USA). Following the methodology of West et al. (2014), six injections were made for each sample, with the first three being discarded. All WS-CRDS samples were screened post-analysis Chemcorrect, version 1.0.0.

2.2.5. Strontium Isotopes

The $^{87}Sr/^{86}Sr$ isotope ratios were measured at the Department of Geological Sciences at the University of Cape Town using a NuPlasma HR MC-ICP-MS. The determination of $^{87}Sr/^{86}Sr$ ratios involves two steps. The first step was the preparation of samples (wet chemistry). Preparation involved decanting each filtered sample into 6 ml aliquots. Each sample was then dried down in a Teflon beaker. Following this, nitric acid was added to the remnant solution and the sample was dried down again. Proceeding this, 1.5ml of 2N of HNO_3^- was added. The second stage involves running the sample through the Spectrometer (Sr chemistry). Sr was extracted from each sample through the cation exchange column. The 200ppb 0.2% HNO_3 solution was analysed for $^{87}Sr/^{86}Sr$ ratios using a NuPlasma HR MC-ICP-MS. The standard reference is NIST987, which has a corresponding $^{87}Sr/^{86}Sr$ ratio of 0.710255. The Sr isotopic data was corrected for instrumental mass fractionation and Rubidium interference using the exponential law and a $^{87}Sr/^{86}Sr$ value of 0.1194.

2.2.6. Charge Balance

In a water sample, the number of positively charged ions in solution (cations) should balance the number of negatively charged ion (anions). It is possible to check whether this is true by performing a Charge Balance Error (CBE) calculation, with anion and cations expressed in meq/l:

$$CBE\ (\%\ difference) = \frac{\sum cations - \sum anions}{\sum cations + \sum anions} \times 100$$

This check should return a value of 0% if cations and anions are perfectly in balance, although it is accepted that values between ± 10% are satisfactory for this test. However, a value outside of the ±10% range does not necessarily mean an error since it is not practical to test for all cations and anions in a sample. As a result, the most encountered (major) cations and anions are generally analysed, which was done for CFA. These included:

- Anions: Nitrate (NO_3^-), sulphate (SO_4^{2-}), chloride (Cl^-) and bicarbonate alkalinity (HCO_3^-) and,
- Cations: Calcium (Ca^{2+}), magnesium (Mg^{2+}), potassium (K^+) and sodium (Na^+)

2.2.7. Saturation Indices

Saturation indices were calculated using the thermodynamic software, PHREEQC from the United States Geological Survey (USGS).

3. Results

Major cations, namely, calcium, magnesium, sodium and potassium; major anions, namely, chloride, sulphate and bicarbonate; physiochemical parameters, such as EC, pH and TDS; isotopes of oxygen, hydrogen and strontium are all presented in **Table 3-1**. A list of descriptive stattistcis are given for each chemical parameter in **Table 3-2**, showing minimum, maximum median, standard deviation and median values.

Table 3-1 Table of results showing major physiochemical parameters, elemental concentrations, and isotope composition.

Sample ID	Latitude, S	Longitude, E	Elevation	pH	EC	TDS	Ca	Mg	Na	K	Cl	SO4	HCO3	SiO2	Sr	87/86Sr	δ18O	δ2H	d-excess
	decimal degrees		meters		µS/cm	mg/L											‰		
ZONE A - RHYOLITE																			
SH18046	-25.97698	32.08995	228	7.2	189	80.2	1.4	2.6	20.1	2.7	28.8	2.0	22.5	19.2	0.02	0.716355	-3.70	-16.0	13.6
SH18047	-25.99015	32.04126	459	7.5	481	249.5	15.2	6.7	55.6	2.2	64.8	5.0	100.0	40.9	0.06	0.707370	-3.42	-16.2	11.2
SH18048	-25.98679	32.0378	464	7.5	539	295.7	16.1	7.3	62.8	1.9	93.6	4.0	110.0	42.1	0.07	0.708295	-3.70	-16.0	13.6
SH18052	-25.99008	32.01196	592	6.5	281	145.2	1.6	1.9	41.7	3.6	50.4	3.0	43.0	50.5	0.02	0.710866	-3.86	-17.7	13.2
SH18054	-25.97517	32.02642	541	6.7	334	189.9	8.7	4.4	42.2	2.3	48.9	3.0	80.5	53.5	0.05	0.708154	-3.56	-16.3	12.2
SH18065	-26.11902	32.14214	110	6.9	3200	1946.1	145.5	73.8	441.5	1.7	1017.1	12.0	254.5	75.1	0.60	0.708034	-3.10	-15.0	9.8
SH18066	-26.25186	32.09272	366	6.7	1045	648.8	48.6	27.8	121.4	4.9	205.5	5.0	235.5	62.5	0.25	0.707466	-3.53	-17.1	11.1
SH18067	-26.2565	32.09	389	6.9	1055	658.9	48.4	19.6	152.0	4.2	225.7	17.0	192.0	42.7	0.26	0.707259	-3.33	-15.9	10.8
ZONE B - BASALT																			
Zone B1 < 40m																			
SH18030	-26.65839	32.18454	122	7.1	2490	1461.0	102.5	67.3	224.8	3.9	408.1	6.0	648.5	75.7	0.11	0.708448	-2.68	-13.0	8.4
SH18031	-26.68875	32.18001	101	7.6	742	457.7	20.3	15.4	84.7	2.9	91.4	15.0	228.0	50.5	0.07	0.709536	-2.59	-10.9	9.9
SH18035	-26.67249	32.18206	109	7.3	1729	988.8	58.8	32.1	190.5	2.5	311.0	6.0	388.0	61.3	0.14	0.707439	-3.44	-15.7	11.8
SH18036	-26.5001	32.21267	77	7.2	1119	599.4	31.5	24.1	118.3	3.4	223.1	4.0	195.0	61.9	0.34	0.710222	-2.02	-9.7	6.5
SH18039	-26.44008	32.2425	62	7.6	1188	712.3	15.2	12.0	173.9	5.9	154.8	7.0	343.5	84.7	0.08	0.710898	-2.55	-12.8	7.6
SH18040	-26.33585	32.16769	102	7.4	1540	870.7	30.0	23.0	205.0	5.8	244.7	9.0	353.3	77.5	0.13	0.710589	-2.53	-12.5	7.8
SH18043	-25.86603	32.28794	143	8.0	1415	886.7	13.1	9.6	244.1	2.3	201.6	23.0	393.0	63.7	0.06	0.709973	-2.78	-15.2	7.0
SH18044	-25.85269	32.21954	83	7.5	2440	1567.6	39.5	31.7	379.7	2.8	354.9	12.0	747.0	72.7	0.18	0.709015	-2.75	-13.8	8.2
SH18045	-25.99243	32.29326	56	7.4	1633	1074.5	71.1	42.7	175.1	6.2	158.4	25.0	596.0	85.3	0.31	0.708561	-2.91	-14.5	8.8
SH18055	-26.04222	32.25683	150	7.1	2060	1397.3	50.4	35.2	405.9	4.1	431.2	61.0	409.5	66.7	0.26	0.710310	-0.60	0.0	4.9
SH18056	-26.04164	32.25764	150	7.1	3680	2302.1	80.6	69.6	666.2	17.4	966.7	70.0	431.5	62.5	0.68	0.709955	-3.17	-15.2	10.1
SH18057	-26.04333	32.26	40	6.9	2210	1333.7	95.0	69.7	299.2	4.0	444.9	62.0	359.0	76.3	0.64	0.709223	-1.03	-3.3	4.9
SH18059	-26.04544	32.19853	44	6.8	523	309.09	31.0	16.1	57.2	1.6	97.2	3.0	103.0	28.2	0.13	0.711020	-1.81	-6.5	8.0
SH18062	-26.02154	32.17659	67	6.6	465	322.1	26.8	12.3	46.1	1.4	81.0	2.0	152.5	36.1	0.08	0.710101	-1.88	-6.3	8.7
SH18070	-26.42883	32.23883	80	6.4	482	290.2	16.6	11.1	57.8	1.6	93.6	7.0	102.5	40.9	0.08	0.710668	-1.55	-6.4	6.0
SH18071	-26.29433	32.18894	93	7.1	1048	741.6	64.0	26.0	131.9	2.5	108.7	15.0	393.5	69.1	0.14	0.708711	-2.49	-13.6	6.3

Sample ID	Latitude, S	Longitude, E	Elevation	pH	EC	TDS	Ca	Mg	Na	K	Cl	SO4	HCO3	SiO2	Sr	87/86Sr	δ18O	δ2H	d-excess
Zone B2 >40m																			
SH18038	-26.42203	32.26295	54	7.2	1711	1018.9	85.6	54.2	134.4	6.0	280.7	8.0	450.0	79.9	0.34	0.709832	-2.83	-15.1	7.5
SH18042	-25.99578	32.29246	57	7.7	1834	1088.1	86.4	49.3	185.5	7.1	200.8	25.0	534.0	83.5	0.36	0.708532	-2.86	-15.6	7.3
SH18058	-26.0375	32.19519	59	6.8	1715	1014.8	90.0	15.5	255.9	1.1	469.7	25.0	157.5	49.9	0.16	0.706775	-3.47	-16.5	11.3
SH18064	-26.071033	32.152307	78	6.6	578	580.7	52.6	30.5	93.8	0.0	85.3	9.0	309.5	85.3	0.60	0.708179	-3.38	-17.1	10.0
SH18068	-26.33586	32.16772	325	6.8	360	201.8	14.0	8.9	39.9	1.6	75.9	7.0	54.5	39.1	0.06	0.710283	-1.63	-5.4	7.6
ZONE C - LIMESTONE																			
SH18032	-26.84328	32.28464	35	7.2	381	246.3	12.8	9.4	39.2	0.8	41.0	5.0	138.0	42.7	0.10	0.722076	-2.07	-6.0	10.6
SH18033	-26.82349	32.24373	39	9.9	11760	7655.4	174.1	224.7	1839.0	3.1	2829.0	1516.0	1069.5	69.1	1.90	0.714819	-2.57	-10.3	10.3
SH18034	-26.83054	32.23655	44	7.7	550	374.5	20.9	19.8	47.9	0.2	31.7	7.0	247.0	58.3	0.16	0.720483	-1.91	-5.2	10.1
SH18037	-26.44827	32.273863	49	7.4	2500	1390.5	69.9	53.0	309.0	6.7	372.9	13.0	566.0	95.5	0.34	0.709796	-2.65	-13.5	7.8
ZONE D - SAND																			
Zone D2 >40m																			
SH18002	-25.89578	32.38884	14	7.2	2030	14903.6	438.7	530.7	4306.0	50.6	8206.2	1174.0	197.5	16.2	13.23	0.706477	-3.40	-15.8	11.4
SH18008	-26.75196	32.8259	11	7.2	863	553.7	56.4	13.9	80.7	5.1	103.7	1.4	292.5	31.2	0.15	0.712852	-2.48	-7.9	11.9
SH18010	-26.83467	32.88349	16	6.1	737	345.8	5.7	12.0	92.0	5.9	149.7	67.0	13.5	15.6	0.09	0.711005	-3.39	-13.2	13.9
SH18011	-26.84204	32.88001	18	6.1	508	240.0	6.2	9.6	58.2	4.3	92.9	45.0	24.0	15.4	0.10	0.711372	-2.93	-11.3	12.1
SH18012	-26.83282	32.88396	17	6.3	437	187.3	9.8	7.4	48.5	3.8	79.2	16.0	22.5	13.6	0.09	0.710492	-3.11	-13.3	11.6
SH18013	-26.79199	32.8882	24	6.7	388	209.5	22.1	5.4	35.0	2.8	49.7	7.0	87.5	25.8	0.09	0.711493	-2.03	-7.1	9.2
SH18014	-26.52993	32.72123	18	6.9	4410	2144.8	246.4	169.8	279.4	19.5	1259.7	72.0	98.0	17.4	2.18	0.709095	-3.44	-14.2	13.3
SH18025	-26.01618	32.52846	29	7.5	1482	947.9	41.0	17.2	198.8	5.3	244.0	175.0	266.5	60.7	0.17	0.71253	-3.64	-18.6	10.5
SH18074	-25.75697	32.39642	57	6.8	3920	2208.0	177.8	125.6	474.4	13.0	1110.7	106.0	200.5	54.1	1.21	0.710950	-4.02	-20.3	11.8
SH18089	-25.92283	32.5435	4	6.7	12500	7095.1	77.1	194.2	2520.0	72.9	4059.9	1003.0	171.0	33.7	0.86	0.709398	-3.47	-16.5	11.3
SH18090	-25.92306	32.54353	6	6.5	1943	1139	1.7	4.3	420.6	12.0	426.5	79.0	195.0	34.9	0.02	0.709848	-3.68	-17.2	12.2
SH18091	-25.92408	32.5435	5	6.1	2220	1385.6	2.7	8.4	501.7	14.2	502.1	148.0	208.5	34.3	0.04	0.709478	-3.83	-18.7	11.9
SH18094	-25.62767	32.47028	63	6.0	732	388.3	9.6	8.5	120.9	5.7	116.6	86.0	41.0	71.5	0.08	0.713387	-4.28	-22.8	11.5
SH18095	-25.62564	32.45789	80	6.1	1756	1030.6	47.7	53.6	212.0	9.4	631.3	41.0	35.5	48.7	0.46	0.713387	-4.28	-22.8	11.5

Sample ID	Latitude, S	Longitude, E	Elevation	pH	EC	TDS	Ca	Mg	Na	K	Cl	SO4	HCO3	SiO2	Sr	87/86Sr	δ18O	δ2H	d-excess
ZONE D - SAND																			
Zone D2 > 40m																			
SH18002	-25.89578	32.38884	14	7.2	2030	14903.6	438.7	530.7	4306.0	50.6	8206.2	1174.0	197.5	16.2	13.23	0.706477	-3.40	-15.8	11.4
SH18008	-26.75196	32.8259	11	7.2	863	553.7	56.4	13.9	80.7	5.1	103.7	1.4	292.5	31.2	0.15	0.712852	-2.48	-7.9	11.9
SH18010	-26.83467	32.88349	16	6.1	737	345.8	5.7	12.0	92.0	5.9	149.7	67.0	13.5	15.6	0.09	0.711005	-3.39	-13.2	13.9
SH18011	-26.84204	32.88001	18	6.1	508	240.0	6.2	9.6	58.2	4.3	92.9	45.0	24.0	15.4	0.10	0.711372	-2.93	-11.3	12.1
SH18012	-26.83282	32.88396	17	6.3	437	187.3	9.8	7.4	48.5	3.8	79.2	16.0	22.5	13.6	0.09	0.710492	-3.11	-13.3	11.6
SH18013	-26.79199	32.8882	24	6.7	388	209.5	22.1	5.4	35.0	2.8	49.7	7.0	87.5	25.8	0.09	0.711493	-2.03	-7.1	9.2
SH18014	-26.52993	32.72123	18	6.9	4410	2144.8	246.4	169.8	279.4	19.5	1259.7	72.0	98.0	17.4	2.18	0.709095	-3.44	-14.2	13.3
SH18025	-26.01618	32.52846	29	7.5	1482	947.9	41.0	17.2	198.8	5.3	244.0	175.0	266.5	60.7	0.17	0.71253	-3.64	-18.6	10.5
SH18074	-25.75697	32.39642	57	6.8	3920	2208.0	177.8	125.6	474.4	13.0	1110.7	106.0	200.5	54.1	1.21	0.710950	-4.02	-20.3	11.8
SH18089	-25.92283	32.5435	4	6.7	12500	7095.1	77.1	194.2	2520.0	72.9	4059.9	1003.0	171.0	33.7	0.86	0.709398	-3.47	-16.5	11.3
SH18090	-25.92306	32.54353	6	6.5	1943	1139	1.7	4.3	420.6	12.0	426.5	79.0	195.0	34.9	0.02	0.709848	-3.68	-17.2	12.2
SH18091	-25.92408	32.5435	5	6.1	2220	1385.6	2.7	8.4	501.7	14.2	502.1	148.0	208.5	34.3	0.04	0.709478	-3.83	-18.7	11.9
SH18094	-25.62767	32.47028	63	6.0	732	388.3	9.6	8.5	120.9	5.7	116.6	86.0	41.0	71.5	0.08	0.713387	-4.28	-22.8	11.5
SH18095	-25.62564	32.45789	80	6.1	1756	1030.6	47.7	53.6	212.0	9.4	631.3	41.0	35.5	48.7	0.46	0.713387	-4.28	-22.8	11.5
ZoneD1 < 40m																			
SH18003	-26.36745	32.64569	23	7.0	4150	2532.7	109.6	80.9	604.2	9.8	750.1	244.0	734.0	51.1	0.66	0.711424	-3.35	-18.0	8.8
SH18004	-26.3733	32.62077	47	7.4	1160	723.6	67.2	16.5	126.1	6.7	165.6	44.0	297.5	48.7	0.19	0.712847	-4.36	-20.9	14.0
SH18005	-26.38359	32.63083	22	7.6	1005	678.2	41.1	18.7	129.2	5.5	129.6	38.0	316.0	48.1	0.19	0.712990	-3.95	-18.1	13.5
SH18006	-26.3808	32.63184	22	7.5	1096	734.2	53.3	21.6	124.7	5.7	128.9	44.0	356.0	48.7	0.22	0.712673	-3.81	-18.3	12.2
SH18007	-26.77963	32.82775	20	7.6	505	344.4	52.4	6.1	29.1	5.1	54.7	2.0	195.0	34.9	0.09	0.711327	-3.91	-17.7	13.6
SH18015	-26.50667	32.71009	14	7.2	2550	1451.2	98.6	52.1	308.9	10.0	427.6	428.0	125.7	33.0	1.04	0.709095	-3.84	-17.6	13.1
SH18016	-26.49804	32.71283	13	7.4	3010	1557.6	147.0	60.1	321.8	8.5	334.7	274.0	411.5	30.0	1.38	0.708962	-3.58	-17.5	11.1
SH18018	-26.22813	32.62112	39	7.7	1068	666.9	56.1	28.1	99.3	5.6	148.3	44.0	285.5	50.5	0.30	0.71130	-3.89	-19.4	11.7
SH18019	-26.22077	32.61886	41	7.9	831	537.1	35.9	19.3	83.6	7.0	91.4	32.0	268.0	45.1	0.19	0.71212	-3.69	-18.7	10.9
SH18021	-26.01537	32.52614	31	7.2	1116	611.7	24.7	15.6	148.1	6.2	197.2	47.0	173.0	52.9	0.14	0.71297	-3.55	-17.5	10.9
SH18022	-26.01951	32.5239	32	7.6	1720	962.4	53.0	26.5	215.2	5.8	307.4	109.0	245.5	46.9	0.26	0.71216	-3.61	-18.6	10.3

Sample ID	Latitude, S	Longitude, E	Elevation	pH	EC	TDS	Ca	Mg	Na	K	Cl	SO4	HCO3	SiO2	Sr	87/86Sr	δ18O	δ2H	d-excess
SH18023	-26.20181	32.61755	42	7.3	708	417.9	40.1	12.0	62.8	5.0	106.5	16.0	175.5	49.9	0.15	0.71303	-3.98	-18.7	13.1
SH18024	-26.19876	32.61234	41	7.0	312	179.0	8.6	4.4	33.3	3.2	52.5	18.0	59.0	24.6	0.04	-	-3.73	-18.4	11.5
SH18027	-26.22076	32.61891	41	7.7	811	541.1	32.9	18.7	83.7	7.8	93.6	32.0	272.5	43.3	0.19	0.71212	-3.66	-17.1	12.2
SH18029	-26.32442	32.56677	46	7.3	781	398.2	9.8	7.1	101.4	4.3	141.1	37.0	97.5	55.3	0.07	0.714098	-4.27	-20.5	13.7
SH18073	-25.72175	32.30906	77	6.9	677	513.0	45.6	29.5	57.9	0.9	59.7	12.0	307.5	20.4	0.35	0.710803	-0.38	-5.0	-1.9
SH18076	-25.69378	32.64908	30	6.3	272	159.8	25.5	1.3	22.9	2.9	53.6	4.0	49.5	12.0	0.06	0.716080	-0.76	-1.2	4.9
SH18077	-25.69442	32.65594	31	6.7	391	183.3	6.9	9.3	35.4	6.3	66.9	3.0	55.5	34.3	0.09	0.714172	-3.62	-17.1	11.9
SH18078	-25.68317	32.66511	30	5.6	387	190.2	1.0	2.1	61.8	8.2	93.6	14.0	9.5	33.7	0.02	0.714485	-2.98	-12.8	11.1
SH18079	-25.67322	32.65881	33	6.8	299	175.7	23.6	2.3	31.2	3.4	40.7	7.0	67.5	43.9	0.05	0.712757	-4.01	-19.6	12.5
SH18080	-25.66531	32.63169	51	7.1	369	245.9	37.4	3.5	27.8	5.7	64.1	7.0	100.5	33.7	0.05	0.717390	-4.23	-21.9	11.9
SH18081	-25.66356	32.62558	50	6.4	274	147.3	16.6	4.2	24.8	4.5	50.7	4.0	42.5	30.6	0.03	0.716160	-4.34	-22.0	12.7
SH18082	-25.65325	32.59703	55	7.4	334	219.0	21.2	4.2	45.1	3.3	49.2	9.0	87.0	37.3	0.07	0.715927	-4.22	-20.9	12.9
SH18086	-25.60964	32.67078	20	7.1	379	226.2	31.1	6.3	35.5	4.6	58.3	8.0	82.5	39.7	0.11	0.715441	-4.07	-20.6	12.0

3.1. Physiochemical Parameters

Groundwater samples in the study area have values of pH that range between 5.6 to 9.9 and values of EC that range between 119 to 12500 µS/cm. The average pH value is 7 (n= 71, σ = 0.6) and the average EC is 1379.8 µS/cm (σ=1849 µS/cm). EC and TDS measurements taken in the field correlate positively with an r^2 value of 0.82. Physiochemical parameters for each Zone are summarized in **Table 3-2**.

Zone C has the highest recorded pH value, 9.9 and has the highest average pH in the study area, 8.0. Zone D1 has the lowest recorded pH, 5.6 and Zone D2 has the lowest average pH in the study, 6.6.

Zone C, has the highest average EC, 3798 µS/cm (σ = 4627.5 µS/cm) and the highest recorded EC in the area is found in Zone D2, 12500 µS/cm. Zone A represents the lowest average EC in the study area, 321.6 µS/cm (σ= 147.9 µS/cm) and has the lowest recorded EC value in the study area, 119 µS/cm. Since large standard deviations are associated with the data median values for each parameter were assessed. Zone B2 had the highest EC median value of 1711.0 µS/cm, followed by Zone D2 which had a median value of 1619.0 µS/cm.

Table 3-2 Descriptive statistics of physiochemical parameters and major ions for each zone.

	pH	EC (uS/cm)	TDS (mg/L)	Ca^{2+} (mg/L)	Mg^{2+} (mg/L)	Na^{+} (mg/L)	K^{+} (mg/L)	Cl^{-} (mg/L)	SO_4^{2-} (mg/L)	HCO_3^{-} (mg/L)	SiO_2 (mg/L)
Zone A											
Min	6.5	189	80	1.4	1.9	20.1	1.7	28.8	2.0	22.5	19.2
Max	7.5	3200	1946	145.5	73.8	441.5	4.9	1017.1	17.0	254.5	75.1
Mean	7.0	890	527	35.7	18.0	117.2	2.9	216.9	6.4	129.8	48.3
Stdev	0.4	989	614	48.2	24.3	138.3	1.2	331.7	5.3	87.3	16.6
Median	6.9	510	272	16	7	59	2.5	79.2	4.5	105.0	46.6
Zone B1											
Min	6.4	465	290	13.1	9.6	46.1	1.4	81.0	2.0	102.5	28.2
Max	8.0	3680	2302	102.5	69.7	666.2	17.4	966.7	70.0	747.0	85.3
Mean	7.2	1548	957	46.6	31.1	216.3	4.3	273.2	20.4	365.2	63.3
Stdev	0.4	878	551	29.0	21.0	161.3	3.8	224.7	22.8	186.0	16.8
Median	7.2	1477	878.7	35.5	25.0	182.8	3.2	212.4	10.5	373.5	65.2
Zone B2											
Min	6.6	360	202	14.0	8.9	39.9	0.0	75.9	7.0	54.5	39.1
Max	7.7	1834	1088	90.0	54.2	255.9	7.1	469.7	25.0	534.0	85.3
Mean	7.0	1240	781	65.7	31.7	141.9	3.2	222.5	14.8	301.1	67.5
Stdev	0.4	709	381	32.6	20.0	83.2	3.2	162.2	9.3	198.7	21.5

Median	6.8	1711	1014	85.6	30.5	134.4	1.6	200.8	9.0	309.5	79.9
Zone C											
Min	7.2	381	246	12.8	9.4	39.2	0.2	31.7	5.0	138.0	42.7
Max	9.9	11760	7655	174.1	224.7	1839.0	6.7	2829.0	1516.0	1069.5	95.5
Mean	8.0	3798	2417	69.4	76.7	558.8	2.7	818.7	385.3	505.1	66.4
Stdev	1.3	5395	3530	74.2	100.4	862.6	3.0	1349.6	753.8	417.8	22.3
Median	7.5	1525	882.5	45.5	36.4	178.5	2.0	207	10.0	406.5	63.7
Zone D1											
Min	5.6	272	147	1.0	1.3	22.9	0.9	40.7	2.0	9.5	12.0
Max	7.9	4150	2533	147.0	80.9	604.2	10.0	750.1	428.0	734.0	55.3
Mean	7.2	1009	600	43.3	18.8	117.2	5.7	152.8	61.5	200.6	39.5
Stdev	0.5	966	560	34.4	20.1	132.7	2.2	161.7	104.9	162.0	11.1
Median	7.2	744.5	465.5	36.6	13.8	73.2	5.6	93.6	25	174.3	41.5
Zone D2											
Min	6.0	388	187	1.7	4.3	35.0	2.8	49.7	1.4	13.5	13.6
Max	7.5	12500	14904	438.7	530.7	4306.0	72.9	8206.2	1174.0	292.5	71.5
Mean	6.6	2423	2341	81.6	82.9	667.7	16.0	1216.6	215.7	132.4	33.8
Stdev	0.49	3155	4029	125.7	144.5	1224.8	20.4	2268.2	374.5	97.1	18.6
Median	6.6	1619	989.2	31.6	12.9	205.4	7.7	335.3	75.5	134.5	32.4

3.2. Major Ions

3.2.1. Charge Balance Error

A Charge Balance Error (CBE) was calculated for each sample using Na^+, K^+, Mg^{2+}, Ca^{2+}, Cl^-, HCO_3^- and SO_4^{2-}. The accuracy of the chemical analysis can be estimated from the CBE, whereby cations and anions are expressed in meq/L and their sum should be equal since water is electrically neutral (described in more detail in **Section 2.2.6**). Twenty-two percent of the sample has a CBE between 5-10%, these samples are included but interpreted with caution. Overall, sodium represents the most abundant cation in the study area, with an average of 229.5 mg/L (σ = 532.3 mg/L) followed by Ca^{2+} (46.5 mg/L, σ = 59.3 mg/L), Mg^{2+} (32.0 mg/L, σ = 63.9 mg/L) and K^+ (6.1 mg/L, σ = 9.0 mg/L). Chlorine represent the most abundant anion in the study area, with an average of 352.7 mg/L (σ = 967.3 mg/L), followed by HCO_3^- (230.2 mg/L, σ = 247.7 mg/L) and SO_4^{2-}. Descriptive statistics of the major cations and anions are presented in **Error! Reference source not found.**.

3.2.2. Water Type

3.2.2.1. Schoeller diagrams

Schoeller diagrams are used to show the relative concentrations of anions and cations (expressed in meq/L)

in groundwater samples. The diagrams can be used to demonstrate different hydrochemical water types and to identify ionically related waters. **Figure 3-1 A-F** displays the Schoeller diagrams for each zone. Most samples in Zone A and B1 display similar proportions of the relative anions and cations. In Zone B2, samples SH18068 and SH18058 show different proportions of $Na^+ + K^+$ and Mg^{2+}. Samples in Zone C display similar proportions of each ion but in different concentrations. Sample SH18033, however, has a higher proportion of SO_4^{2-}. In Zone D1, most of the samples have similar proportions of ions, but in varying concentrations. Sample SH18077 has a higher proportion of Mg^{2+}, SH18007, -73, - 79 and -82 has a higher proportion of HCO_3^- and samples SH003 and -29 have lower proportions of Ca^{2+}. In Zone D2, samples SH18002, -89, -10 have relatively higher proportions of SO_4^{2-}, samples SH013 and -08 have lower proportions of $HCO_3^-$and samples SH18089, -14 and -95 have lower proportions of Mg^{2+}.

Samples in Zone A have the lowest average Ca^{2+}, Mg^{2+} and Na^+ (35.7, 18.0 and 117.2 mg/L) concentrations and samples in Zone C have the lowest average K^+ concentration (2.7 mg/L) in the study. Zone D2, contains samples that have the highest average cation concentrations (Ca^{2+}= 81.6 mg/L, Mg^{2+} = 82.9 mg/L, Na^+ = 66.7 mg/L and K^+ = 16 mg/L), and highest average Cl^- concentration(1216.6 mg/L). Samples in Zone C have the highest average HCO_3^- (505.1 mg/L) and SO_4^{2-} (385.3 mg/L) concentration, whilst samples in Zone A have the lowest average SO_4^{2-} (6.4 mg/L) and HCO_3^- (129.8 mg/L) concentrations.

3.2.2.2. Piper Diagrams

Piper diagrams are a useful way of graphically representing the chemistry of water samples and distinguishing between different water types. Piper diagrams are trilinear representations of normalized anion and cation concentrations (meq/L), which can be subsequently divided into different fields representing different hydrochemical facies (**Error! Reference source not found.**). However, the limitation of Piper diagrams lies in the fact that it is a triangular diagram and samples that have very different concentration, but end-members in the same proportion can plot in the same place and be classified as the same water type.

Major anions and cations, expressed as meq/L, were plotted on a Piper diagram (**Figure 3-2**). Of the anions, 65% of the samples have Cl^- as the dominant anion followed by HCO_3^-> SO_4^{2-}, whilst the remaining samples are dominated by HCO_3^-> Cl^-> SO_4^{2-}. Of the cations, 48% of the samples have Na^+ >Mg^{2+}>Ca^{2+}>K^+ and 44% have Na^+>Ca^{2+}>Mg^{2+}>K^+. Two samples, SH18014 and -15 have Mg^{2+}>Ca^{2+}>Na^+>K^+, samples, SH18076, -80, 86, -07 in Zone D zone have Ca^{2+}>Na^+>Mg^{2+}>K^+.

In total, 63% of the samples plot within the Na-Cl water type and 30% plot within the Na-HCO_3 water type on the Piper Trilinear diagram. Both water types are present in each zone. Sample SH180 07, -76, -80, -86 (Zone D1) plot in the Ca-HCO_3 water type and sample SH18014 (Zone D2, near Bela-Vista) plots in the Mg-Na-Ca-Cl water type.

3.2.2.3. Chadha Plots

Chadha (1999) developed a diagram that defines the overall character of the water and gives insight into the various hydrochemical processes controlling the chemistry of the groundwater. The diagram is different with respect to Durov and Piper diagrams, in the sense that the two equilateral triangles are omitted, and the shape of the main study field is different. The diagram considers the difference between the alkaline earth (Ca^{2+} and Mg^{2+}) and alkalis (Na^{+} and K^{+}), and the difference between weak acidic anions (HCO_3^- and CO_3^{2-}) and strong acidic anions (Cl^- and SO_4^{2-}), expressed in milliequivalent percentages, and can be divided into four quadrants of different water types and mechanisms (**Figure 3-3**). The distribution of water types across the study are displayed in **Figure 3-4** – there are no obvious trends present across the study area in terms of changing water type.

Samples in Zone A plot in the lower left quadrant of the diagram, indicating Na-Cl water type and salinity as the major mechanisms controlling the composition of the water. In Zone B1, 38% of the samples plot in the Na-HCO_3 water type, indicating ion exchange as a major process controlling groundwater composition, and 43% fall within the Na-Cl water type. In Zone B2, samples are spread between the Ca-Mg-HCO_3 water type, indicating newly recharged waters, and Na-Cl waters. In Zone C, the samples plot between three quadrants, suggesting no dominant water type or mechanisms controlling groundwater chemistry. In Zone D1, most samples plot in the Na-Cl water type, followed by Ca-Mg-Cl water type (reverse ion exchange) and Na-HCO_3 water type (ion exchange). Lastly, in Zone D2, the major control of water chemistry is salinity, which is evident as the majority of samples plot in the Na-Cl water zone.

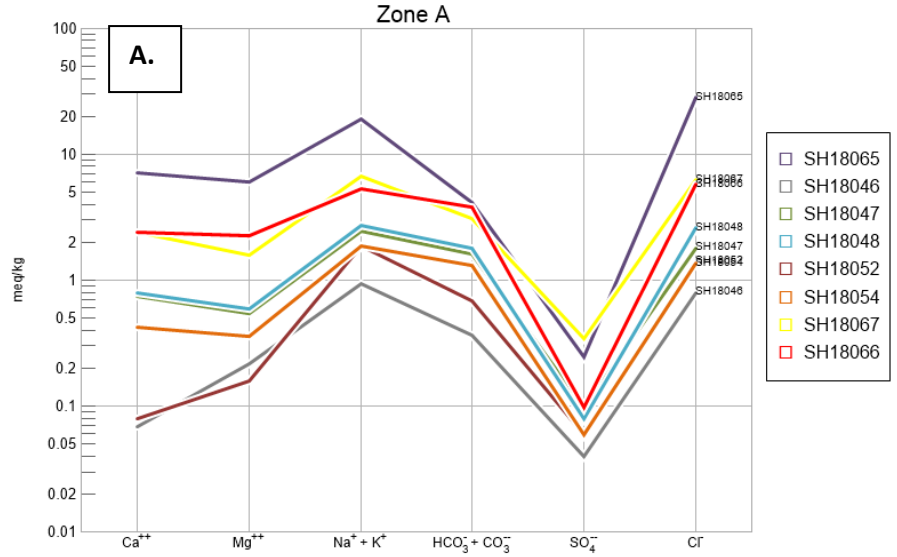
Zone A
A.
meq/kg
100
50
20
10
5
2
1
0.5
0.2
0.1
0.05
0.02
0.01
Ca++
Mg++
Na+ + K+
HCO3- + CO3--
SO4--
Cl-
SH18065
SH18048
SH18047
SH18046
SH18065
SH18046
SH18047
SH18048
SH18052
SH18054
SH18067
SH18066

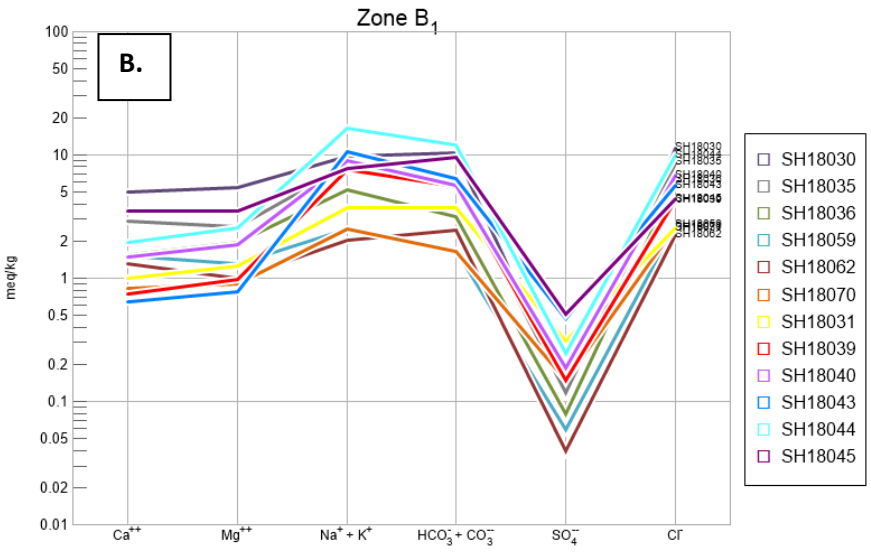
Zone B1
B.
meq/kg
100
50
20
10
5
2
1
0.5
0.2
0.1
0.05
0.02
0.01
Ca++
Mg++
Na+ + K+
HCO3- + CO3--
SO4--
Cl-
SH18030
SH18035
SH18036
SH18059
SH18062
SH18070
SH18031
SH18039
SH18040
SH18043
SH18044
SH18045

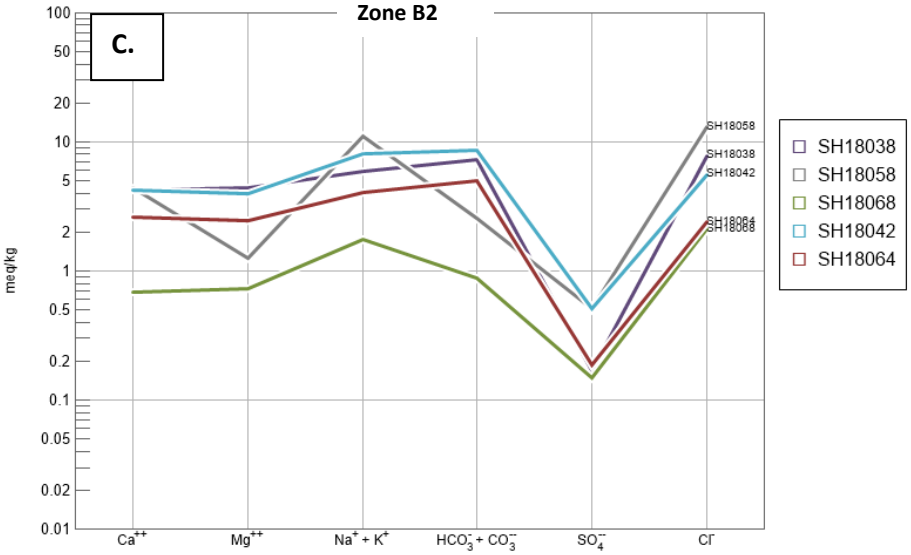
Zone B2
C.
meq/kg
100
50
20
10
5
2
1
0.5
0.2
0.1
0.05
0.02
0.01
Ca++
Mg++
Na+ + K+
HCO3- + CO3--
SO4--
Cl-
SH18058
SH18038
SH18042
SH18064
SH18068
SH18038
SH18058
SH18068
SH18042
SH18064

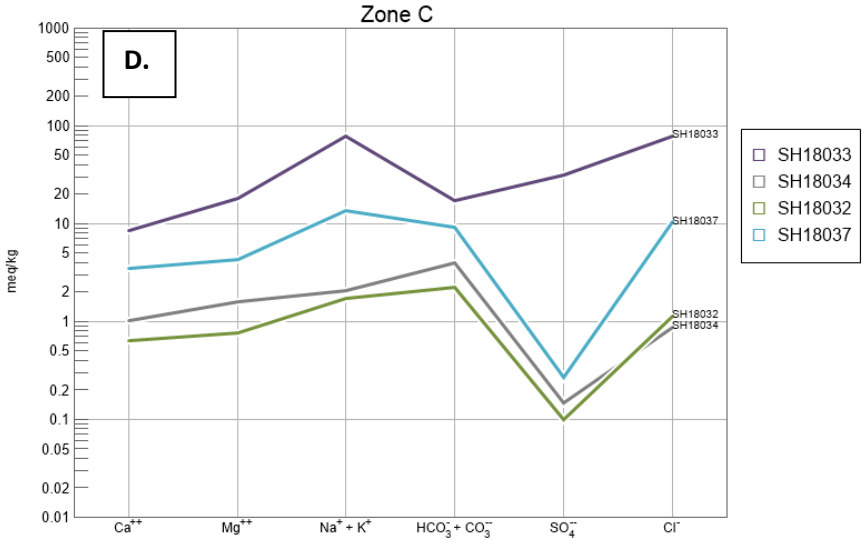
Zone C
D.
meq/kg
1000
500
200
100
50
20
10
5
2
1
0.5
0.2
0.1
0.05
0.02
0.01
Ca++
Mg++
Na+ + K+
HCO3- + CO3--
SO4--
Cl-
SH18033
SH18037
SH18032
SH18034
SH18033
SH18034
SH18032
SH18037

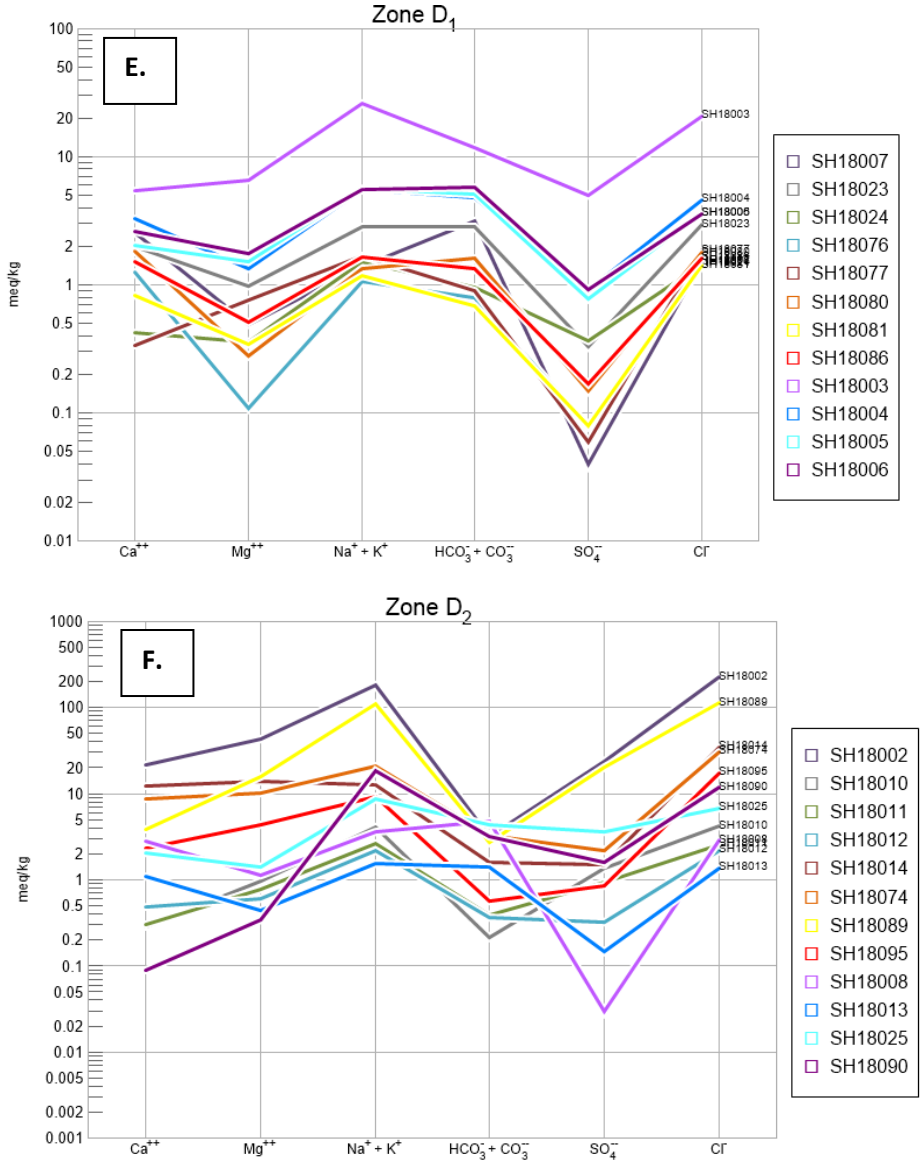

Figure 3-1 **Scholler Diagrams for each zone for major ions expressed in milliequivalents per litre to demonstrate different hydrochemical water types. A. Zone A, B. Zone B1. C. Zone B2. D. Zone C. E. Zone D1. F. Zone D2.**

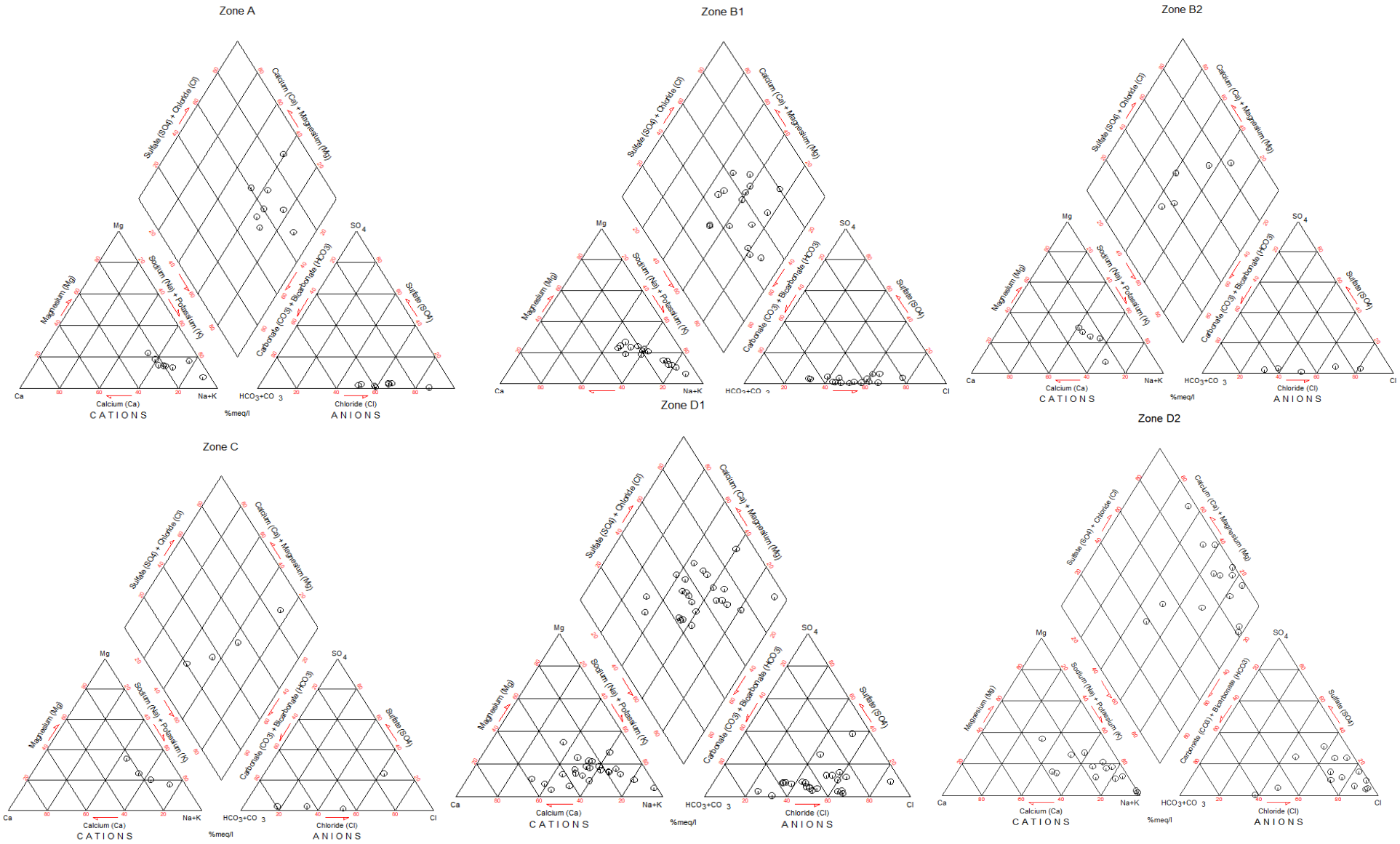

Figure 3-2 Piper diagrams for each Zone

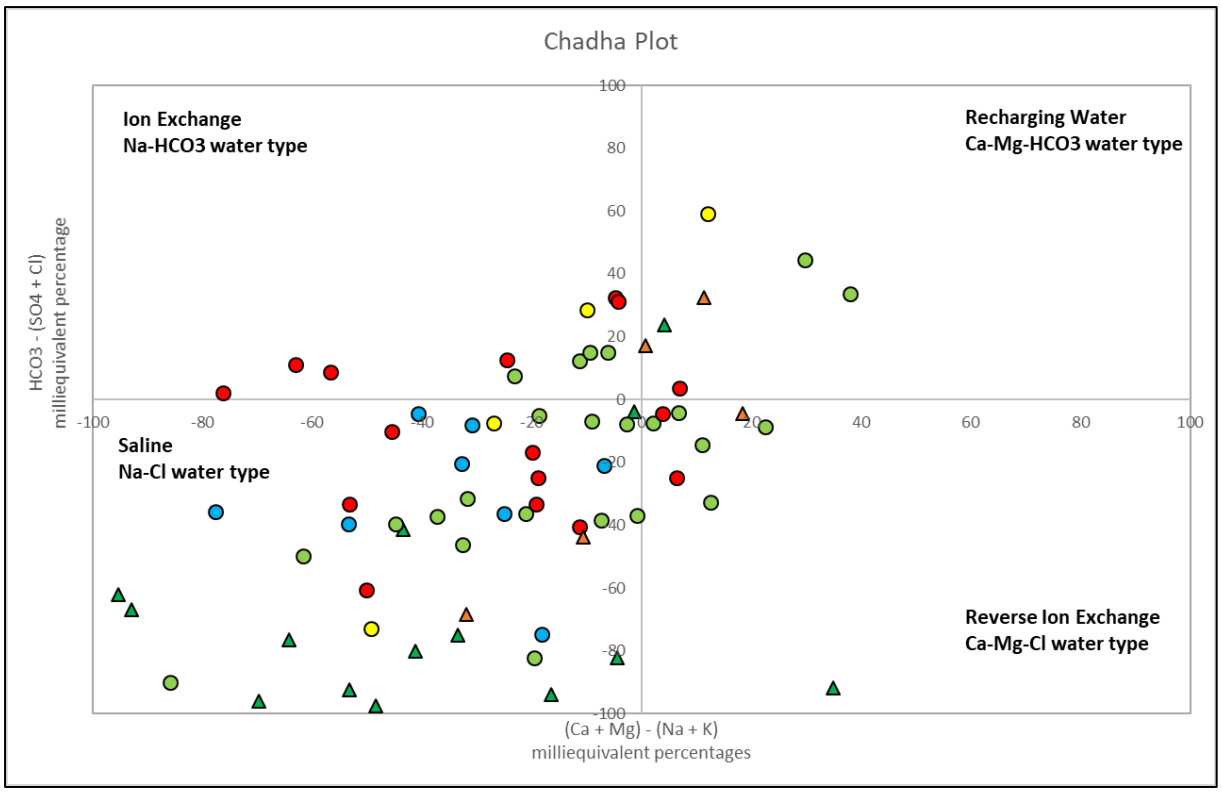
Chadha Plot
Ion Exchange
Na-HCO3 water type
Recharging Water
Ca-Mg-HCO3 water type
Saline
Na-Cl water type
Reverse Ion Exchange
Ca-Mg-Cl water type
HCO3 - (SO4 + Cl)
milliequivalent percentage
(Ca + Mg) - (Na + K)
milliequivalent percentages
100
80
60
40
20
0
-20
-40
-60
-80
-100
-100
-80
-60
-40
-20
0
20
40
60
80
100

Figure 3-3 **Chadha Plot diagram for geochemical classification of groundwater. Blue circles = Zone A, red circles = Zone B1, orange triangles = Zone B2, yellow circles = Zone C, green circles = Zone D1, green triangles= Zone D2.**

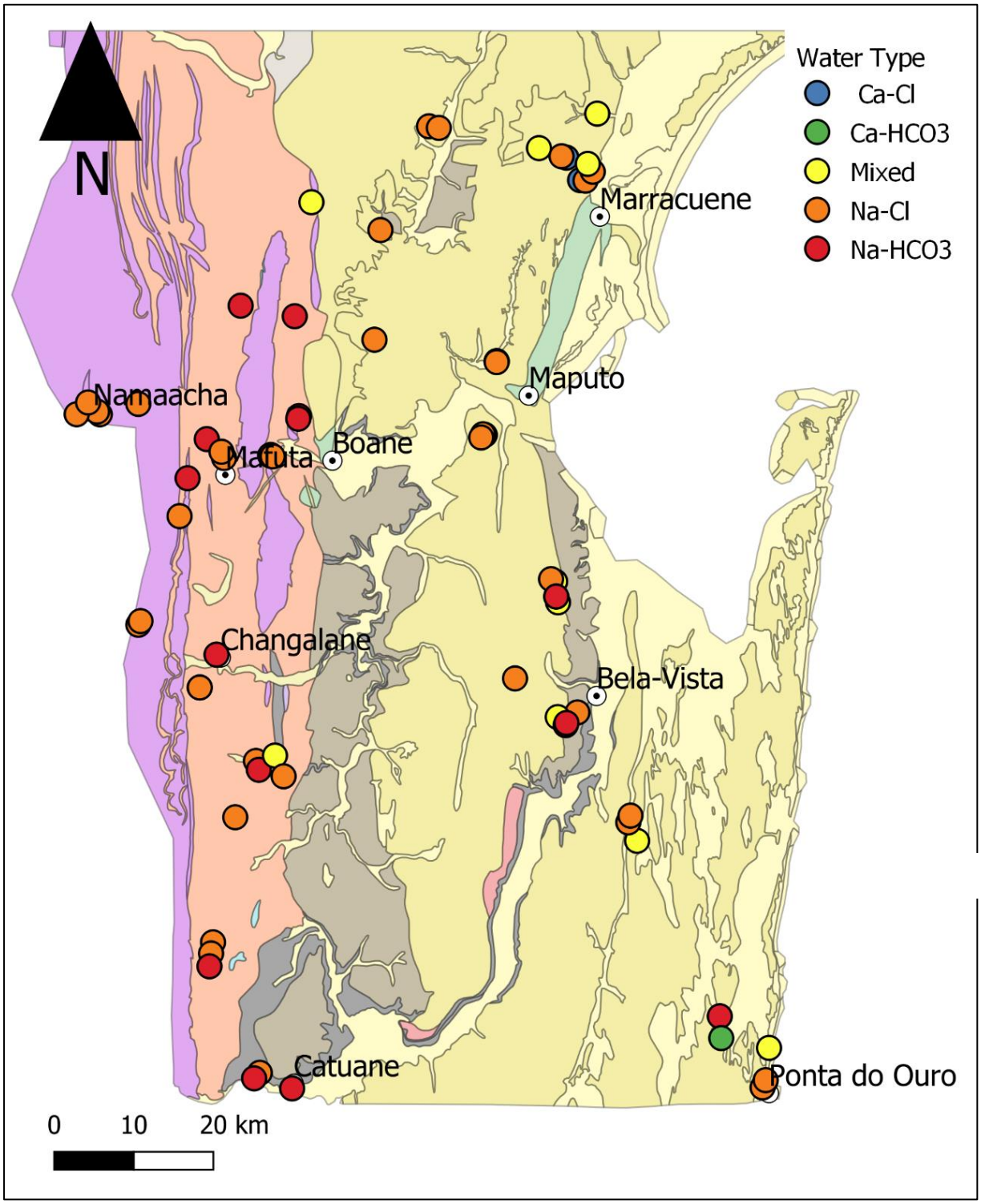

Figure 3-4 **Map displaying the distribution of water types across Southern Mozambique according to the Chadha plot.**

3.3. Isotopes $\delta^{18}O$, $\delta^{2}H$ and d-excess

Samples in the study have $\delta^{18}O$ values that range between —0.36‰ to —0.38‰, with an average value of —3.13 ‰. The average $\delta^{2}H$ isotopic composition is —15‰, ranging between —23‰ to 0‰. Samples in Zone D1 have the highest average $d^{2}H$ and $d^{18}O$ values, —17‰ and —3.56‰, and samples in Zone C have the lowest average $d^{2}H$ and $d^{18}O$ values, —9‰ and —2.30‰, respectively. The majority of samples plot between the LMWL and GMWL, a few exceptions, however, plot towards the composition of modern seawater (**Figure 3-5**). The average d-excess value in the study is 10.4‰, which plots close to the GMWL Samples in Zone B1 have the lowest average d-excess value, 7.80‰, whereas samples in Zone A have the highest average d-excess values, 11.91‰.

Samples in Zone A have $d^{18}O$ values that range between —3.86‰ to —3.10‰ and $d^{2}H$ values that ranges between —18‰ and —15‰. Samples plot away from the Pretoria MWL, intersecting the GMWL. D-excess values range between 9.79‰ to 13.6‰, with an average of 11.9‰. The $^{87}Sr/^{86}Sr$ ratio ranges between 0.70726 to 0.71636 and has an average of 0.70923.

The $d^{2}H$ and $d^{18}O$ values in Zone B1 ranges between —16‰ to 0‰ and —3.44‰ to —0.60‰ respectively. Samples plot along the Pretoria MWL and GMWL and intersect the composition of modern seawater. The average d-excess value is 7.80‰, ranging from 4.86‰ to 11.8‰. The $^{87}Sr/^{86}Sr$ ratio average is 0.70967 and ratios range between 0.70744 to 0.71102

Samples in Zone B2 have $d^{18}O$ values that range between —17.1‰ to —5.4‰ and a $\delta^{2}H$ composition that ranges between —4‰ to —2‰. Two samples, SH18063 and -58 plot on the GMWL, whilst the remaining samples plot away from the GMWL. The d-excess values range from 7.3‰ to 11.3‰, with an average of 8.8‰. The $^{87}Sr/^{86}Sr$ ratio ranges between 0.70676 to 0.71028 and the average ratio is 0.70872.

Samples in Zone C have $d^{2}H$ and $d^{18}O$ values that ranges between —14‰ to —5‰ and —2.65‰ to —1.91‰, respectively. The samples plot close to the GMWL. The average d-excess value is 9.7‰, ranging from 7.8‰ to 10.6‰. The $^{87}Sr/^{86}Sr$ ratio ranges between 0.70980 to 0.72208 and the average ratio is 0.71679.

Samples in Zone D1 have a $d^{18}O$ and $d^{2}H$ composition that ranges between —4.36‰ to —0.38‰ and —22‰ to —1‰, respectively. Most samples are clustered around the Pretoria MWL,

intersecting the GMWL. Samples SH18076 and SH18073 plot away from the GMWL, close to the composition of modern seawater. The d-excess values range between —1.92‰ to 13.99‰, with an average of 11.19‰. The average $^{87}Sr/^{86}Sr$ ratio is 0.71084, and ranges between 0.70648 to 0.71339.

In Zone D2, samples have d^2H values that ranges between —22‰ and —7‰ and a $d^{18}O$ composition that ranges between —4.28‰ and —2.03‰. Samples plot between the LMWL and GMWL. The average d-excess value is 11.72‰, ranging from 9.17‰ to 13.95‰. The average $^{87}Sr/^{86}Sr$ ratio is 0.71306, and ranges between 0.70896 to 0.71306.

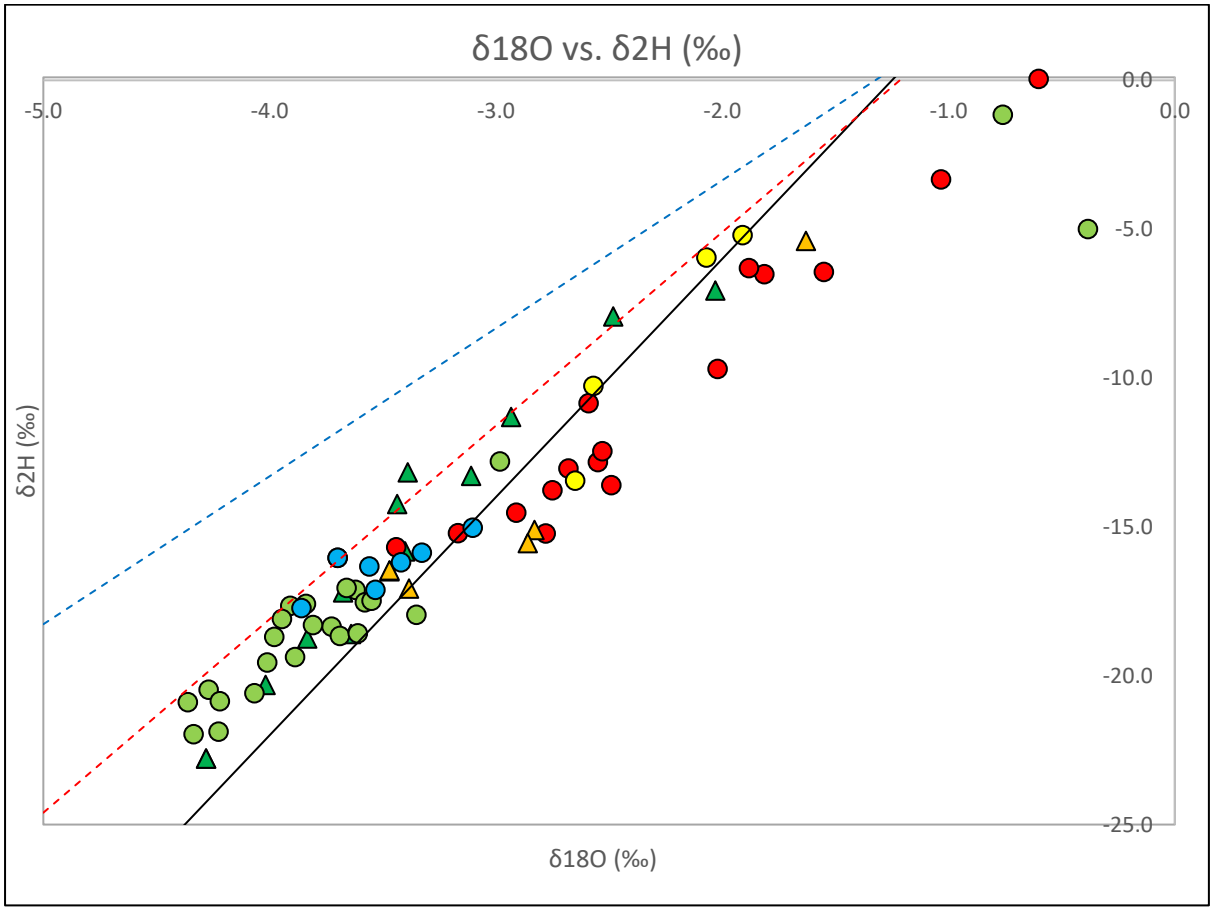

Figure 3-5 **Blue circles = Zone A, red circles = Zone B1, orange triangles = Zone B2, yellow circles = Zone C, green circles = Zone D1, green triangles = Zone D2. Solid black line = GMWL ($\delta^2H=8\delta^{18}O + 10$). Red dashed line = Pretoria LMWL ($\delta^2H=6.55\delta^{18}O + 7.9$). Blue dashed line = Durban LMWL ($\delta^2H=4.97\delta^{18}O + 6.58$)**

4. Discussion

This following section uses the physiochemical, hydrochemical and stable isotope compositions to characterize the water, delineate the source of dissolved salts and infer the recharge environment of groundwater in southern Mozambique. Piper diagrams and Chadha plots are used to characterize the different water facies in the study area and determine the major process controlling the hydrochemistry. A Gibbs diagram is used in conjunction with a simple silica-carbonate diagram to infer silicate/carbonate dissolution dominancy, which is further investigated using correlation plots of major ions. Standard $\delta^{2}H$ vs $\delta^{18}O$ diagrams are used to compare the data obtained in this thesis with the Local Meteoric Water Lines and isotopes of precipitation from Pretoria and Durban (GNIP; Ndlovu, 2019) to determine the source of water and infer the hydrological processes prior to infiltration.

4.1. Origin of variation in Groundwater Chemical Composition

Major ion evolution can be described by the Chebotarev sequence (1955) in which groundwater tends to evolve towards the composition of seawater. This is accompanied by changes in dominant anion species (**Figure 4-1**). The progressive evolution of anions is dependent on two variables – mineral solubility and mineral availability (Freeze and Cherry, 1979).

Water chemistry is influenced by a number of factors, but they can be narrowed down into a few 'mechanisms', as described by Gibbs (1970). Although the Gibbs diagram was first developed for river systems, it is widely used in hydrogeological studies to infer the major mechanisms controlling the water chemistry. Gibbs (1970) suggested that there are three main mechanisms that control the chemistry of surface and groundwaters – the first being atmospheric precipitation, whereby the chemistry of the water is primarily influenced by the chemistry of rainwater, which is essentially diluted sea-water. This would be typical in the vadose zone after a rainfall event. The second mechanism describes weathering processes as the major influence of water chemistry and is termed 'the rock-dominance zone' and the third mechanism is 'evaporation-fractional crystallization', whereby the concentration of TDS increases as a result of evaporation and the precipitation of certain ionic species is controlled by the loss of solids from solution (Eby, 2004).

The mechanisms controlling groundwater chemistry can be inferred from a Gibbs diagram (Gibbs, 1970), by plotting TDS (mg/L) vs. $Na^{+}/(Na^{+} + Ca^{2+})$ mg/L. Samples that plot in the rock- dominance zone indicate the dissolution of silicate bearing minerals (Skeiky and Narany *et al.*, 2014), whereas samples that plot in the evaporation/crystallization zone indicate the dissolution of carbonate minerals and silicate

minerals. Samples that plot in the evaporation/crystallization, more to the right hand side indicate silicate weathering, whereby sodium starts to dominate again due to mixing with seawater, or extreme evapoconcentration, which would result in the precipitation of carbonate minerals. Shifts in concentration of elements results in a shift in the equilibrium which will result in the precipitation or dissolution of minerals. However, in many groundwater investigations around the world, it has been noted that shallow (upper zone) groundwater samples are lower in dissolved solids, whereas samples in deeper (lower zone) parts of the same system have higher amounts of dissolved solids (Freeze and Cherry, 1970). According to the Chebotarev (1955) sequence, samples in the 'upper zone' are characterized by HCO_3^- as the dominant anion, and a low TDS as a result of active flushing, whereas samples in the 'lower zone' are characterized by high TDS content and high Cl^- content.

Hounslow (1995) used a simple bicarbonate-silica ratio to distinguish between carbonate and silicate weathering. Typically, carbonates dissolve without releasing silica, whereas silicates may dissolve releasing significant amounts of silica. An HCO_3^-/SiO_2 ratio of less than five indicates silicate dissolution and a value greater than 10 is indicative of carbonate weathering – between five and 10 is taken to be ambiguous. It should be noted, however, that a high ratio is not always necessarily indicative of the dissolution of either component if neither component is present in high concentrations. It is imperative to assess this ratio in combination with the TDS values of each sample. Rock dominance weathering yields TDS values between 50 -1000 mg/L (Gibbs Diagram). Overall, 60% of the samples reveal a ratio of less than five, eight percent are above 10 and the remaining samples are ambiguous, indicating silicate weathering as the dominant process in the study area.

In Zones B2, and C the majority of samples plot within the rock dominance zone on the Gibbs diagram (**Figure 4-2**). Most samples in Zone D1 and D2 plot in the evaporation/ crystallization zone. Samples that are in equilibrium or oversaturated with respect to calcite and dolomite (SI>1) have HCO_3^-/SiO_2 ratios greater than 10, indicating carbonate dissolution. Most samples in Zone A, B1 and D1 are undersaturated with respect to calcite and dolomite (SI<0.1), have HCO_3^-/SiO_2 ratios less than 5, and plot within the rock weathering zone of the Gibbs diagram. These samples also have higher than average Cl^- values (12.39 mg/L), indicating longer residence times. In order to confirm if these waters have longer residence times however, radiogenic dating would need to take place on the groundwater samples.

Figure 4-3 presents the relationship between $Ca^{2+} + Mg^{2+}$ (meq/L) vs $HCO_3^- + SO_4^{2-}$ (meq/L) for groundwater within the study area. Previous studies have shown that samples that plot above the 1:1 line are indicative of carbonate weathering whereas samples that plot below the 1:1 line can be explained by silicate weathering (Datta *et al*., 1996; Rajmohan and Elango, 2004). From Figure 4.6, 25% of the samples plot around the 1:1 line, indicating that it is not clear whether carbonate or silicate mineral weathering is the dominant process. The conclusion is that it is inconclusive and that either one of the two processes

occur, or both. Around 56% of the samples are indicative of silicate weathering and the remaining samples suggest carbonate weathering. This is in good accordance with the HCO_3^-/SiO_2 ratios mentioned above. A study by McLean and Jankowsi (2000) suggested that samples that plot below the 1:1 line are indicative of ion exchange, in which case HCO_3^- and SO_4^{2-} are enriched with respect to Ca^{2+} and Mg^{2+}.

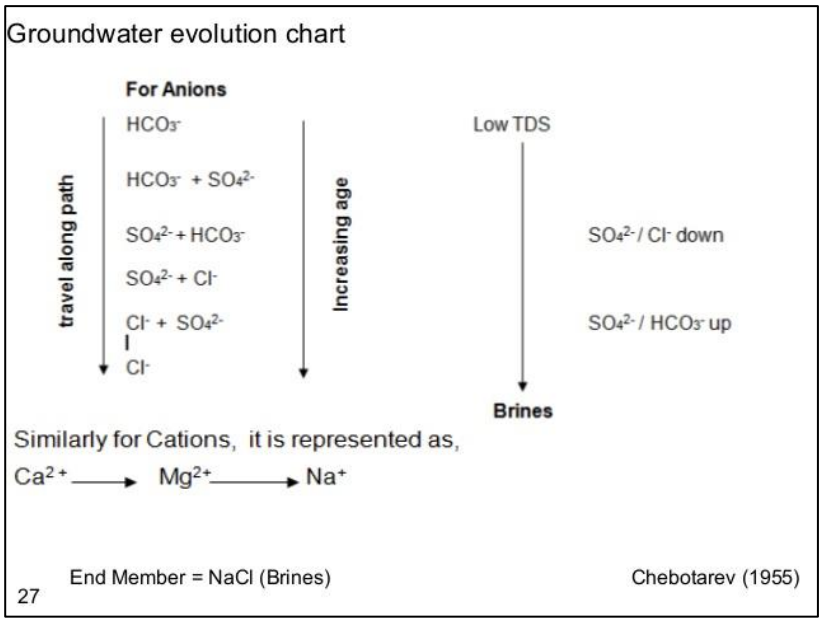

Figure 4-1 **Chebotarev sequence depicting the evolution of major anion and cation species as groundwater moves through an aquifer. Generally, the longer the groundwater remains in contact with the aquifer matrix, the greater the amount of material it will take into solution.**

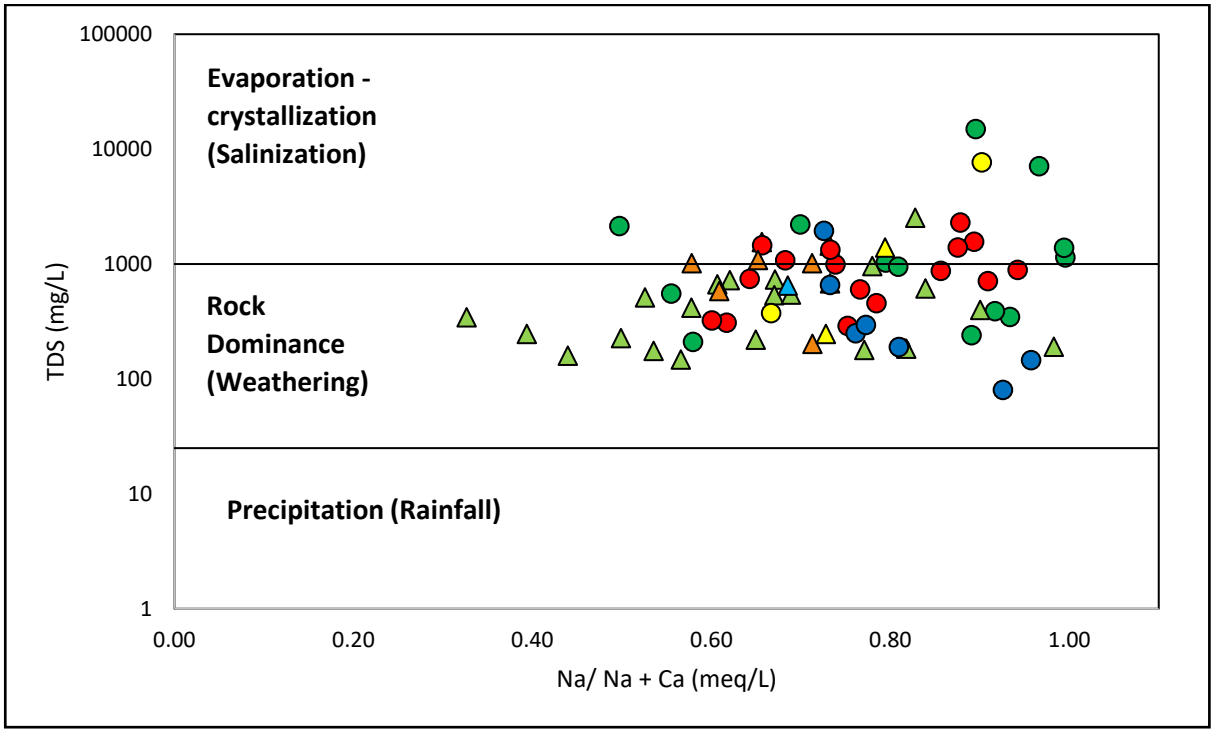

Figure 4-2 **Gibbs diagram, plotting TDS (mg/L) as a function of the ratio of $Na^+/(Na^+ + Ca^{2+})$ (meq/L). Blue circles = Zone A, red circles = Zone B1, orange triangles = Zone B2, yellow circles = Zone C, green circles = Zone D1, green triangles = Zone D2**

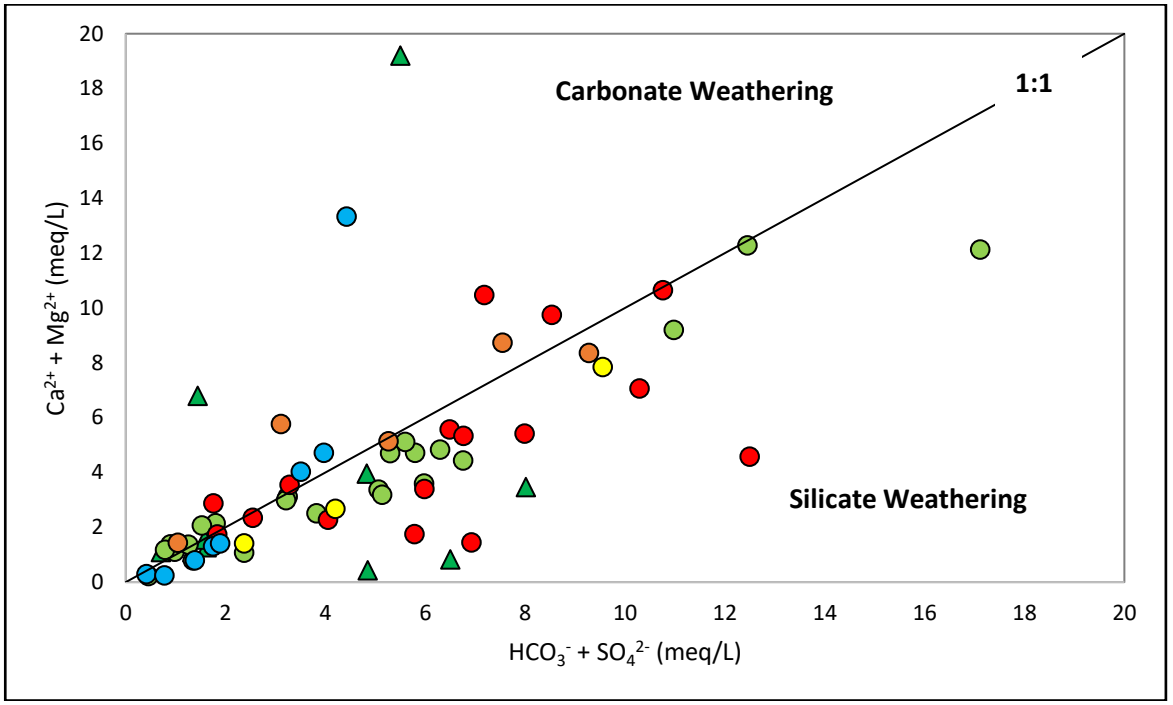

Figure 4-3 **$Ca^{2+} + Mg^{2+}$ (meq/L) vs $HCO_3^- + SO_4^{2-}$ – delineating weathering type. Blue circles = Zone A, red circles = Zone B1, orange triangles = Zone B2, yellow circles = Zone C, green circles = Zone D1, green triangles = Zone D2**

4.1.1. Saturation Indices

A statistical summary of the saturation indices is presented in **Table 4-1**. All samples are undersaturated with respect to halite and gypsum, suggesting that these minerals are not present in high enough concentrations in the aquifer matrix to make an influence on the chemistry of the water. The conditions are thermodynamically favor for their dissolution. Samples in Zone A are undersaturated with respect to calcite and dolomite. In Zone B and C, the majority of samples (67% and 75%) are saturated or in equilibrium with respect to calcite, driving them to precipitate out of solution. In Zone D, 66% of the samples are undersaturated with respect to calcite and dolomite.

Table 4-1 **Statistical summary of calculated Saturation Indices of calcite, dolomite, gypsum, and halite.**

	Calcite	Dolomite	Gypsum	Halite		Calcite	Dolomite	Gypsum	Halite
Zone A					**Zone C**				
Min	-2.96	-5.53	-4.71	-7.76	Min	-0.82	-1.37	-3.49	-7.38
Max	-0.08	-0.09	-2.52	-4.99	Max	2.45	5.54	-0.91	-4.02
Mean	-1.24	-2.34	-3.52	-6.65	Mean	0.56	1.52	-2.58	-6.08
Stdev	1.05	1.91	0.81	0.87	Stdev	1.38	2.91	1.16	1.61
Zone B1					**Zone D1**				

Min	-1.72	-3.28	-3.62	-6.98	Min	-4.68	-8.63	-4.11	-7.45
Max	0.56	1.27	-1.93	-4.84	Max	0.65	1.28	-1.10	-5.00
Mean	-0.14	-0.08	-2.87	-6.04	Mean	-0.57	-1.15	-2.60	-6.65
Stdev	0.63	1.30	0.52	0.60	Stdev	1.21	2.37	0.78	0.69
Zone B2					**Zone D2**				
Min	-1.66	-3.19	-3.29	-7.06	Min	-3.35	-6.03	-3.54	-7.30
Max	0.90	1.96	-2.22	-5.52	Max	0.24	0.96	-0.70	-3.23
Mean	-0.29	-0.53	-2.68	-6.26	Mean	-1.52	-2.64	-2.39	-5.68
Stdev	0.97	2.00	0.43	0.61	Stdev	1.30	2.46	0.87	1.20

4.1.2. Dissolution and Weathering Processes

Chlorides are amongst the most conservative constituents of groundwater and can be regarded as chemically inert (Porowski, 2017). Sources of chlorine are limited in the geological environment and are usually associated with diagenetic rock water interactions, dilution and water evaporation (Carpenter, 1978; Hem, 1989; Hounslow, 1995; Appelo and Postma, 1996; Porowski, 2017). Primary sources of chloride are rock salt deposits and seawater. As a result, older waters usually have higher concentrations of Cl^- than younger waters (Freeze and Cherry, 1970). In addition to this, Cl^- is readily transported through the soil, whereas Na^+ may be removed by cation exchange, this may result in Cl^- enrichment in shallow aquifers that have a low TDS content (Chenini *et al*., 2010).

4.1.2.1. Sodium and Chloride

The correlation between Na^+ and Cl^- is strong in the sample set (r^2=0.878 to r^2=0.999), suggesting a common source. Halite is formed as a result of subaerial evaporation of rainwater on the ground and the dissolution of halite is represented by a Na^+/Cl^- (meq/L) ratio of 1. **Figure 4-4 A** presents the relationship between Na^+ vs Cl^- (meq/L)- sixty-two percent of the samples plot above the line of halite dissolution, suggesting an enrichment of Na^+ over Cl^-. All samples in Zone C and most samples in Zone A, B1, and D2 have a Na/Cl ratio greater than 1, whilst around half the samples in zones, D2 and B2 have a Na^+/Cl^- (meq/L) ratio less than 1. This is further supported by halite being undersaturated in the system. Samples that have a Na^+/Cl^- molar ratio greater than one indicates ions are likely to be derived from silicate weathering, ion exchange processes or anthropogenic sources, whilst samples that have a ratio less than one, suggest reverse ion exchange processes or seawater intrusion.

Weathering of high-temperature alumino-silicates, such as albite, can releases cations and silica whilst forming an array of more stable clay minerals such as kaolinite. Zone A is situated within rhyolites, where the rock matrix is composed of quartz, alkali-feldspars, and biotite - Na^+ enrichment may be due to the dissolution of albite (R1). The $SiO_2/(Na^+{+}K^+)$-Cl^- ($mmol/dm^3$) ratio for most of the samples is between 1 and 2, confirming albite weathering as the dominant process in Zone A.

$$2NaAlSi_3O_{8\ albite} + 9H_2O + 2H^+ \rightarrow 2Na^+ + Al_2SiO_5(OH)_{4\ Kaolinite} + 4H_4SiO_4^o \text{ .....(R1)}$$

Other sources of Na^+ and Cl^- include seawater/brine water and atmospheric deposition. According to Duce and Hoffman (1976), between 30 to 75% of particulates in the atmosphere come from sea aerosol and around 10% of the salts are deposited on land. Seawater has a Na^+/Cl^- (meq/L) ratio of 0.86 +/- 0.05. and this value remains constant during subaerial evaporation until halite starts to precipitate (Carpenter, 1978). Half the samples in Zone B2 and D2 and a third of the samples in Zone D1 have a Na^+/Cl^- ratio within the range of what is typical for halite and ocean water. Due to the lack of petrographic evidence of halite in the rock matrix, sodium-chloride mineralization, in this case, could be a result of varying degrees of subaerial evaporation of rainwater during rainfall and infiltration or reverse ion-exchange (Porowski, 2017).

4.1.2.2. Calcium and Magnesium

Calcium and magnesium are present in groundwater in varying concentrations in this study, and sources are numerous. The solubility of magnesium and calcium are governed on carbonate/bicarbonate equilibrium and thus pH and temperature. **Figure 4-4 B**, **C** and **D** indicate the dissolution of calcite (R2), dolomite (R3) and gypsum (R4). Samples that plot above the 1:1 lines of dissolution indicate alternative sources of either/or both calcium and magnesium, either from silicate weathering or reverse ion exchange processes. Samples that plot below the 1:1 lines of dissolution indicate precipitation either calcite, gypsum or dolomite, or they represent young waters. The HCO_3^-/SiO_2 ratio for four samples in Zone D, one sample in Zone B1 and one sample in Zone C are greater than 10, indicating carbonate weathering. Calcite is the main component in many marine sedimentary rocks and can be found associated with hydrothermal veins and in pockets of basalts and other rocks. The correlation between Ca^{2+} and HCO_3^- is moderate in zones A, B1&2 and D1 (r^2=0.29 to 0.71), weak in Zone D2 (r^2=0.062) and strong in Zone C (r^2=0.99), suggesting variable sources of both constituents. The Ca^{2+}/HCO_3^- (meq/L) ratio for 36% of the samples in Zone D is greater than one, indicating alternative sources of Ca^{2+} other than calcite whilst most samples in all other zones plot below the 1:1 line of calcite dissolution indicating an additional source of HCO_3 from either silicate weathering of dolomite, or from young waters recharging into the system. Since dolomite is undersaturated in Zone D, the conditions are thermodynamically favored for the dissolution of dolomite.

$$CaCO_{3\ calcite} + CO_2 + H_2O \leftrightarrow Ca^{2+} + 2HCO_3^- \text{.....(R2)}$$

$$2H^+ + CaMg(CO_3)_{2dolomite} \leftrightarrow Ca^{2+} + Mg^{2+} + 2HCO_3^- \text{.....(R3)}$$

$$CaSO_4.2H_2O_{gypsum} \rightarrow Ca^{2+} + SO_4^{2-} + 2H_2O \text{.....(R4)}$$

In Zone D, 37% of the samples have a Ca^{2+}/HCO_3^- greater than 1. Most of these samples have a Ca^{2+}/SO_4^{2-} and $(Ca^{2+} + Mg^{2+})/HCO_3^-$ (meq/L) ratio also greater than 1 and an HCO_3^-/SiO_2 ratio less than 5, confirming the silicate weathering dominance. Sample SH058 and -65 in Zone B2 and A, respectively also confirm silicate weathering dominance. Samples, SH18016, SH79 (Zone D) and -59 (Zone B1) plot on the line of calcite dissolution, however, only sample SH18016 has an HCO_3/SiO_2 ratio greater than 10, the other two samples have ratios less than 5.

In 28% of the samples in Zone D the Ca^{2+}/SO_4^{2-} ratio is less than one, indicating ion exchange processes or precipitation of another Ca-bearing mineral. Of these samples, SH18025, -90, -91 and -29 in Zone D have Ca^{2+}/HCO_3^- and $(Mg^{2+} + Ca^{2+})/HCO_3^-$ ratios less than one. Only sample SH18025 suggests gypsum dissolution accompanied by dolomite and calcite precipitation (gypsum SI <-0.1 and calcite and dolomite SI >0.1). The remaining samples suggest silicate weathering or ion exchange. Samples SH1802 and -03 (Zone D) plot on the line of gypsum dissolution and carbonate weathering is confirmed by the HCO_3^-/SiO_2 ratio being greater than 10. Ca^{2+} and SO_4^{2-} correlate moderately (r^2=0.2 to 0.6) indicating variable sources of either component. In Zone C, however, the correlation is strong (r^2=0.89) indicating a common source.

Dolomite dissolution is represented by $(Ca^{2+} + Mg^{2+})/HCO_3^-$, **Figure 4-4 D** indicates that several samples plot along the dolomite dissolution line. Around 20% of the samples in Zone D and B plot along the 1:1 line of dolomite dissolution. These samples have an HCO_3^-/SiO_2 ratio either between 5-10 or greater than 10. Mg^{2+} and Ca^{2+} correlate strongly (r^2= 0.77 to r^2=0.99) suggesting a common source. For samples that have an HCO_3^-/SiO_2 ratio greater than 10, an $Mg^{2+}/(Mg^{2+} Ca^{2+})$ a value >0.5 would indicate dolomite dissolution. Sample SH18003, -29 (Zone D1), -44 (Zone B1) and -07 (Zone C1) indicate dolomite dissolution. For most samples that have an HCO_3^-/SiO_2 value between 5-10, indicating either silicate or carbonate weathering, the $Mg^{2+}/(Mg^{2+} + Ca^{2+})$ ratio is also >0.5, suggesting either ferromagnesian mineral weathering or dolomite dissolution. To delineate the source of Mg^{2+} in this case in non-mafic and ultramafic rocks, samples that have a $SiO_2/(Na^+ + K^+) - Cl^-$ value >2 would indicate ferromagnesian mineral weathering, possibly by biotite dissolution (R5). Samples SH18011, -29, -18, -78 (Zone D), -57 (Zone B), -46, -48, -67 (Zone A) all suggest ferromagnesian weathering as the main source of Mg^{2+}.

$$KMg_3(AlSi_3O_{10})(OH)_{2\ biotite} + 7H^+ + ½\ H_2O \rightarrow K^+ + 3Mg^{2+} + 2H_4SiO_4^o + ½\ Al_2Si_2O_5(OH)_{4\ kaolinite} \ldots\ldots \text{(R5)}$$

Additional sources of Ca^{2+} include the dissolution of tremolite, actinolite and most importantly anorthite. Anorthite dissociates in water, liberating Ca^{2+} ions and forming kaolinite. (R6). Anorthite is a component of basalt and aeolian derived sediments and its dissolution could explain the presence of Ca^{2+} in

Zone B, C and D. However, anorthite is not a mineral usually associated with rhyolite, and that would explain the lower concentration of Ca^{2+} (average concentration of 1.78 meq/L) in Zone A.

$$CaAl_2Si_2O_{8\ anotrthite} + H_2O + 2H^+ \rightarrow Ca^{2+} + Al_2Si_2O_5(OH)_{4\ kaolinte} \text{.....(R6)}$$

In mafic and ultramafic rocks, $Mg^{2+}>Ca^{2+}$ and low TDS can be expected. Samples in Zone B, plot within basalts, whereby the rock matrix is composed of olivine (R7), clinopyroxene (R8) and plagioclase. The Mg^{2+}/Ca^{2+} ratio for all samples, except for three, is greater than 1, confirming ferromagnesian weathering as a source of Mg^{2+}.

$$(Mg/Fe)_2SiO_{4\ olivine} + 4H^+ \rightarrow 2Mg^{2+}/Fe^{2+} + 2H_4SiO_4^o \text{.....(R7)}$$

$$Ca(Mg,Fe)Si_2O_{6\ pyroxene} + 4H^+ + 2H_2O \rightarrow Ca^{2+} + Mg^{2+}/Fe^{2+} + 2H_4SiO_4^o \text{.....(R8)}$$

4.1.2.3. Bicarbonate

Bicarbonate is primarily derived from carbon dioxide, either from precipitation or soil/organic matter in the unsaturated zone. The unsaturated zone represents an open system, whereby soil CO_2 and organics replenish the acidity consumed by mineral dissolution. The production of organic acids drives mineral weathering to consume the acid portion (H^+), leaving HCO_3^- in solution. This subsequently also increases the dissolved inorganic carbon (DIC) and pH of the groundwater (R9). As water moves into the saturated zone, the amount of CO_2 is limited to the amount gained through recharge. As water moves through the aquifer, more reactions will lower the H_2CO_3 content and increase the HCO_3^- and CO_3 content.

In locations where calcite is present (Zone B, C, D), dissociation liberates CO_3^{2-}, which is converted to HCO_3^- in the presence of H^+ (R10). This in effect, causes more H_2CO_3 to dissociate and more CO_2 to diffuse into solution. However, because CO_2 is limited in these cases as all samples are taken in the saturated zone, the rate of carbonate dissolution is limited to the amount of CO_2 available and therefore the amount of carbonic acid. In locations where silicates weathering is dominant (Zone A, B, and D), CO_2 charge waters liberate hydrogen ions and HCO_3^-. Hydrogen ions react with silicates to liberate cations and form stable clays and silicic acid (R 9 and 10).

$$CO_2 + H_2O \leftrightarrow H_2CO_3$$

$$H_2CO_3 \leftrightarrow H^+ + HCO_3^-$$

$$HCO_3^- \leftrightarrow H^+ + CO_3^{2-} \text{.....(R9)}$$

$$CaCO_3 \leftrightarrow Ca^{2+} + CO_3^{2-}$$

$$H_2CO_3 + CaCO_3 \rightarrow Ca^{2+} + 2HCO_3^{-} \text{.....(R10)}$$

4.1.2.4. Sulphate

Sulfate is either derived from the dissolution of gypsum, pyrite, arsenopyrite, seawater or deposition from the atmosphere. The saturation index for gypsum and anhydrite is below -0.1 for all samples and Ca^{2+} and SO_4^{2-} correlate weakly (r^2 = 0.375), suggesting different sources of Ca^{2+} and SO_4^{2-}. Low sulfate concentrations could be attributed to sulfate reduction by bacterial reactions in a reduced environment (i.e. in the saturated zone).

4.1.2.5. Potassium

Potassium is ubiquitous in the environment and is most commonly associated with feldspars and micas. Both these mineral groups are present in the geology associated with each Zone And their respective dissociation could explain the presence of K^+ in the groundwater.

$$2KalSi_3O_{8\ orthoclase} + 9H_2O + 2H^+ \rightarrow 2K^+ + Al_2Si_2O_5(OH)_4 + 4H_4SiO_4^o \text{.....(R11)}$$

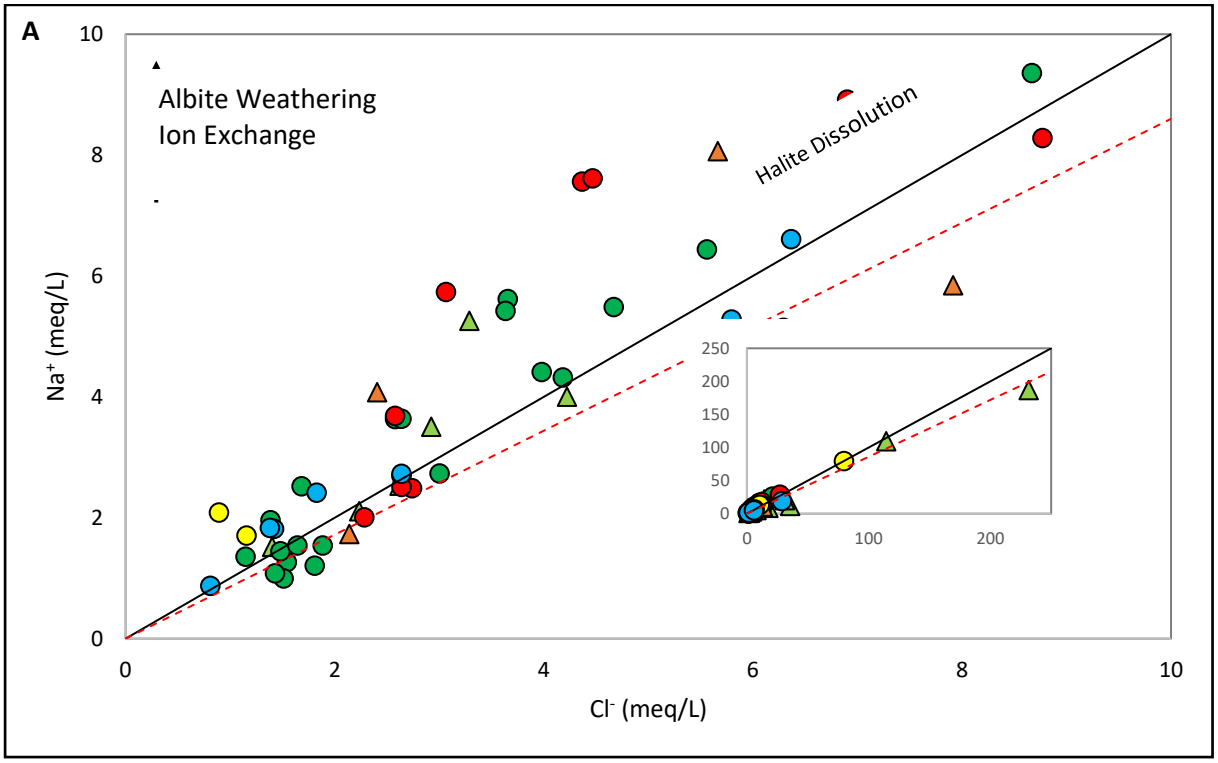

Solid black line = halite dissolution. Red dashed line = composition of seawater. Blue circles = Zone A, red circles = Zone B1, orange triangles = Zone B2, yellow circles = Zone C, green circles = Zone D1, green

triangles = Zone D2

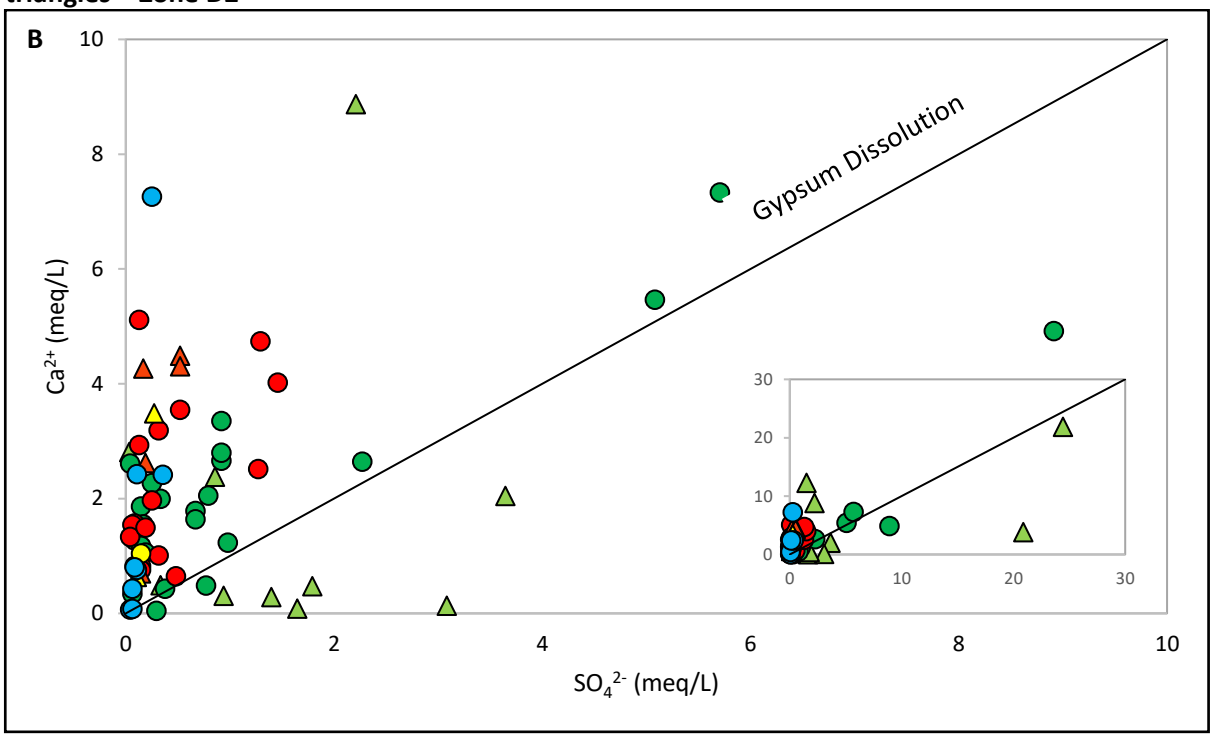

Black sloid line = gypsum dissolution line. Blue circles = Zone A, red circles = Zone B1, orange triangles = Zone B2, yellow circles = Zone C, green circles = Zone D1, green triangles = Zone D2

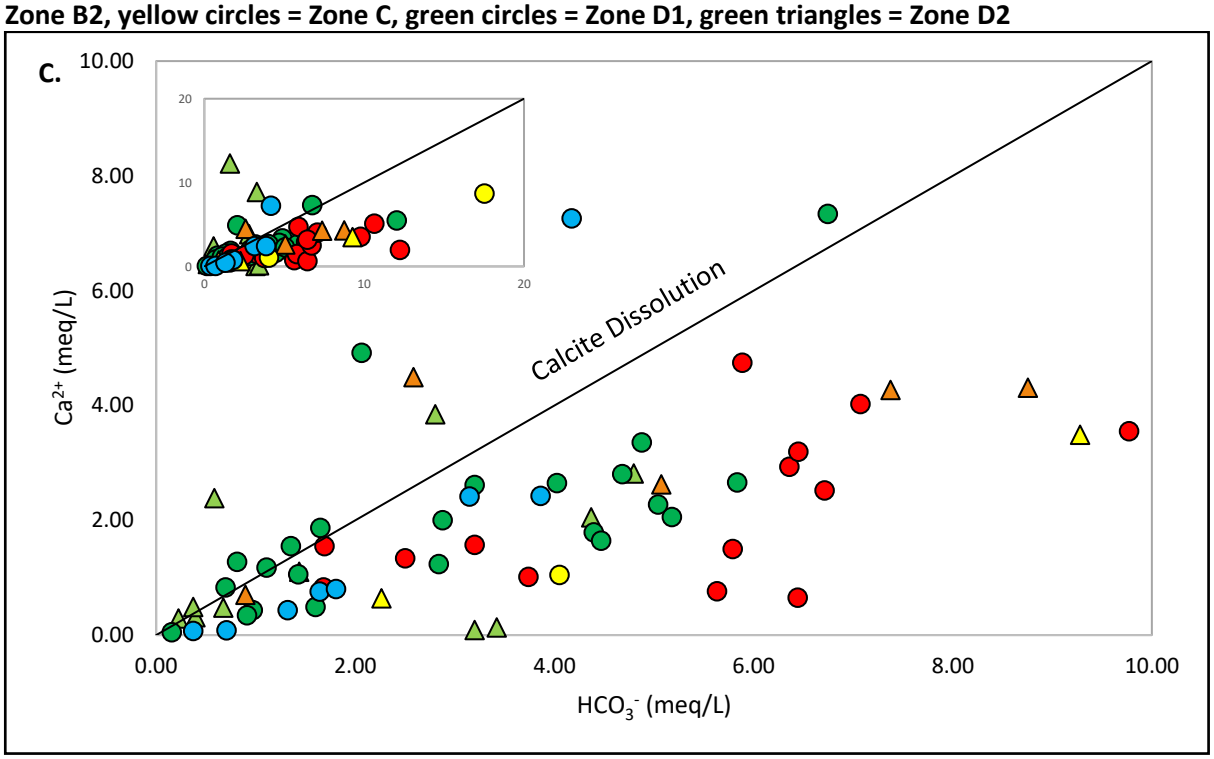

Black sloid line = calcite dissolution line. Blue circles = Zone A, red circles = Zone B1, orange triangles = Zone B2, yellow circles = Zone C, green circles = Zone D1, green triangles = Zone D2

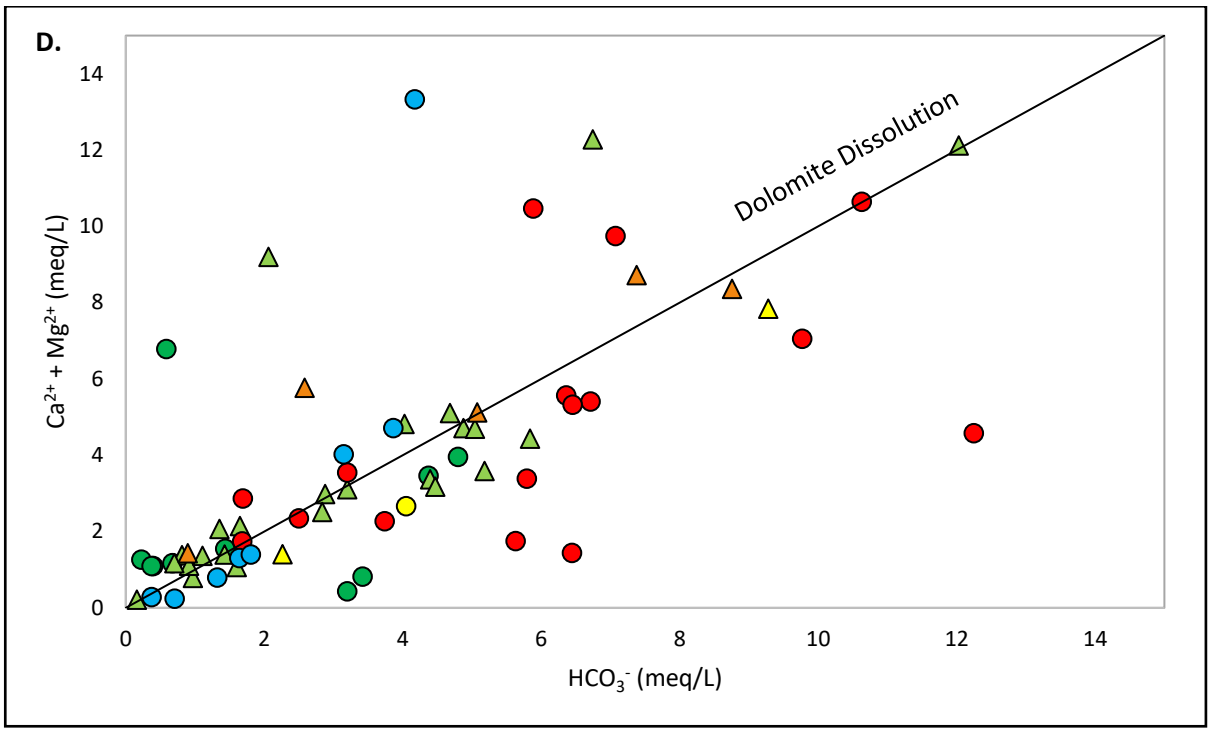

Figure 4-4 **A. Na^+ vs Cl^- (meq/L) plot B. Ca^{2+} vs SO_4^{2-} (meq/L) plot C. Ca^{2+} vs HCO_3^- (meq/L) plot D. $Ca^{2+} + Mg^{2+}$ vs HCO_3^- (meq/L). Blue circles = Zone A, red circles = Zone B1, orange triangles = Zone B2, yellow circles = Zone C, green circles = Zone D1, green triangles = Zone D2**

4.1.3. Ion Exchange Processes

Ions in solution tend to be attracted onto solid surfaces due to the electrical charge. The tendency for absorption amongst major cations is as follows- $Ca^{2+}>Mg^{2+}>K^+>Na^+$, whereby sodium ions are less likely to be absorbed onto surfaces than calcium ions.

The $SiO_2/(Na^+ + K^+)$-Cl^- ratio is commonly used to identify the sources of silica and non-halite sodium. The index reflects the hydrolysis of alkali feldspars or the ion exchange between clay minerals and water (Hem, 1989; Houslow, 1995). An excess of silica over sodium is indicative of the weathering of granites or basalts. Values that are between 1 and 2 indicate the hydrolysis of albite as the major source of Na^+ ions in solution and values between 1 and 0 suggest that cation exchange as a probable source of excess Na^+. Around 42% of the samples (all samples in Zone B2, around half the samples in Zone B1, C and D1 and a third of the samples in Zone D2) have a $SiO_2/(Na^+ + K^+)$- Cl^- ratio between 1 and 2, and a Na/Cl ratio greater than 1, suggesting ion exchange as source of excess Na^+. Around 7% of the samples (in Zone A, C, and D1) have a value between 1 and 2, and a Na^+/Cl^- ratio greater than 1, indicating albite weathering as a source of Na^+.

Figure 4-4 A and **B** shows that most samples plot away from the 1:1 line of halite and calcite

dissolution. This would suggest that other hydrogeochemical processes are affecting the chemical composition of the water. Samples that plot above the halite dissolution line and below the calcite dissolution line indicate enrichment of Na^+ over Ca^{2+} as a result of cation exchange (R11), whereby Ca^{2+} cations are preferentially adsorbed onto the surfaces of clays, and Na^+ is released in the water. In the case where samples plot below the line of halite dissolution and above the line of calcite dissolution, an enrichment of Ca^{2+} over Na^+ indicates reverse cation exchange (R12) (Apello and Postma, 1995). In zones B, C and D1, most of the samples display enrichment of Na^+ over Ca^{2+}, indicating cation exchange and the $SiO_2/(Na^+ + K^+)$- Cl^- values are below 1, confirming this. In Zone D2 however, 50% of the samples indicate revers cation exchange.

$$Ca^{2+} + 2Na\text{-}Clay \rightarrow Ca\text{-}Clay + 2Na^+ \text{ .....(R11)}$$

$$2Na^+ + Ca\text{-}Clay \rightarrow Ca^{2+} + 2Na\text{-}Clay \text{ .....(R12)}$$

4.2. Stable Isotopes

The O- and H-isotope composition of water can be used to trace different sources of water and, in addition to this, they can provide insight into different processes in the hydrological cycle. In most cases, the isotopic composition of groundwater represents the weighted average isotopic composition of precipitation that fell in the local recharge areas (Sharp, 2005). The following section will explore the seasonal and geographic variations of $\delta^{18}O$ and $\delta^{2}H$ composition.

4.2.1. Local meteoric water line (LMWL)

During the 1960s, the International Atomic Energy Agency (IAEA) established a worldwide isotope monitoring network, known as the Global Network for Isotopes in Precipitation (GNIP) (IAEA, 2006a; IAEA, 2006b). Stable isotopes of precipitation can be used to derive the LMWL per specific geographic area. However so, there is no established monitoring network in southern Mozambique, so LMWL derived from monitoring station in Pretoria, and established by Abiye *et al.,* (2011) will be used in this study, as well as the Durban LMWL that was calculated using stream and groundwater samples from a paper written by Ndlovu et al, (2019) . Pretoria and Durban are used as a reference for this study due to similar climatic and similar latitude/longitude (see **Figure 4-7**). It must be noted however that Durban is at lower altitudes, and Pretoria is at a different longitude and altitude than the study area.

Rainfall collection has been ongoing in Pretoria, South Africa since 1958 and $\delta^{2}H$ and $\delta^{18}O$ samples were collected intermittently between April 1961 to December 2001. The Durban LMWL is $\delta^{2}H = 4.97\delta^{18}O + 6.58$,

and was calculated using the RMA method using 32 borehole samples collected around the Durban Metropolitan area in a study conducted by Ndlovu *et al.*, (2019). The Pretoria LMWL is $\delta=6.55\delta^{18}O + 7.9$. Figure 4.8 illustrates $\delta^{18}O$ versus $\delta^{2}H$, with three Meteoric Water Lines (MWL) – Durban, Pretoria and the GMWL. Overall, the groundwater samples plot along a line of regression $\delta^{2}H=5.5\delta^{18}O + 2.39$, which slightly deviates away from the Pretoria LMWL and the Durban LMWL. The slope of the line of the groundwater samples is similar to the slope of the Durban LMWL. Samples that were collected in the first sampling round, in March 2018, plot on the line $\delta^{2}H=5.5\delta^{18}O + 2.82$ and samples that were collected plot on the line $\delta^{2}H=5.5\delta^{18}O + 2.14$. The small difference in the line of regression for the two sampling rounds indicates that either there is only a small difference in the isotope composition of precipitation between the two seasons and/or that recharge is relatively slow and seasonal difference is not picked up.

As mentioned previously in **Section 1.2.5,** Dansgaard (1964) proposed the concept of deuterium excess to quantify the deviation of the LMWL from the GMWL. This can be used to trace the source of water vapor and to identify secondary processes that influence the atmospheric vapor content (Bodag, et al 2016, Chen et al., 2010). D-excess can vary considerably with geographic position and it is influenced by several parameters, such as temperature differences, aridity, rate of evapotranspiration, and sources of air masses. However so, the major driver is related to changes in relative humidity rather than changes in temperature in areas where evaporation takes place (Dansgaard, 1964). Hoefs (1997) noted the relationship between relative humidity and isotopic composition of precipitation, known as the 'dilution effect' – high relative humidity makes isotopic exchange reactions faster. A small d-excess value indicates a high relative humidity and little evaporation of water on the surface, whereas a large d-excess value indicates low relative humidity and high evaporation.

In order to understand the evaporation effect on the physicochemical characteristics of the groundwater samples, $\delta\ ^{18}O$ vs Cl^- concentration (mg/L) (**Figure 4-5 A**) and d-excess vs Cl^-(meq/L) (**Figure 4-6 B**) plots have been used to assess the possibility of evaporation. **Figure 4-6 A** presents the relationship between chloride concertation as a function of $\delta^{18}O$. A slight increase in $\delta^{18}O$, coupled with an increase in Cl^- (mg/L) indicates that evaporation may be a possible source of salinity in Zone A (r^2=0.62). Zones B1, D1 and D2, the evaporation effect is strong, indicated by the samples 'veering' off the LMWLs. Isotopic enrichment is coupled with a moderate increase in chloride, indicating a strong evaporation effect.

If the cause of high salinity is evaporation, then d-excess should decrease with an increasing Cl^- concentration. From **Figure 4-6 B**, it is evident that evaporation is a minor cause of salinity in Zone A (r^2=0.59) and to a lesser extent in Zone B1 and D1. However, in Zones C, B2 and D2, d-excess values are inconsistent with increasing Cl^- values, suggesting that evaporation is not a major process influencing the

salinity of the groundwater.

By examining the d-excess values, the δ^2H, $\delta^{18}O$ values, and the evaporation effect it is probable to say that the deviation of the line of regression of samples in the study area from the GMWL, Durban LMWL and the Pretoria LMWL is not a result of evaporation but is rather a reflection of the LMWL of the study area. This, however, would need to be confirmed by collecting isotope rainfall samples from the study area.

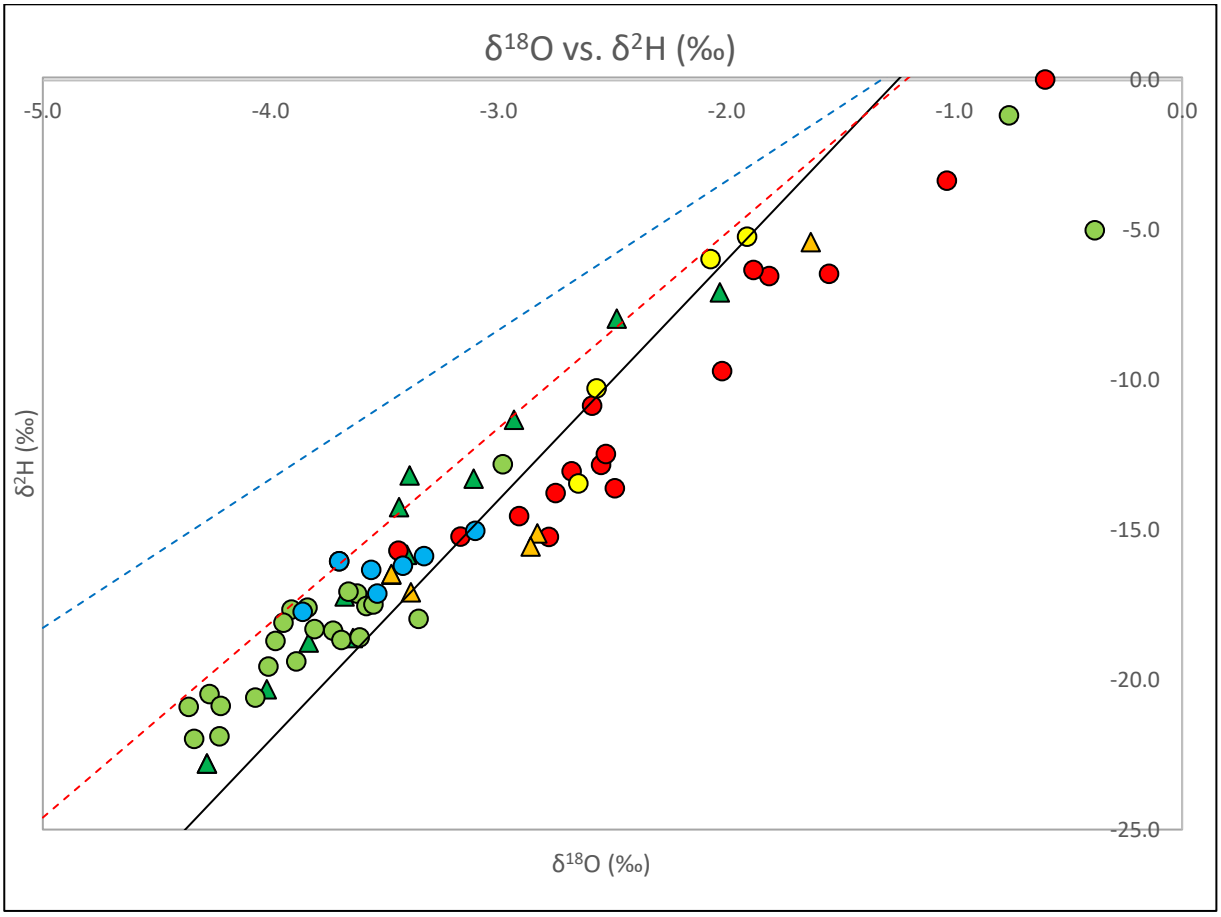

Figure 4-5 Blue circles = Zone A, red circles = Zone B1, orange triangles = Zone B2, yellow circles = Zone C, green circles = Zone D1, green triangles = Zone D2. Blue dashed line = Central Mozambique LMWL ($\delta^2H=8.7\delta^{18}O + 15.5$). Solid black line = GMWL ($\delta^2H=8\delta^{18}O + 10$). Red dashed line = Pretoria LMWL ($\delta^2H=6.55\delta^{18}O + 7.9$). Blue dashed line = Durban ($\delta^2H=4.97\delta^{18}O + 6.58$)

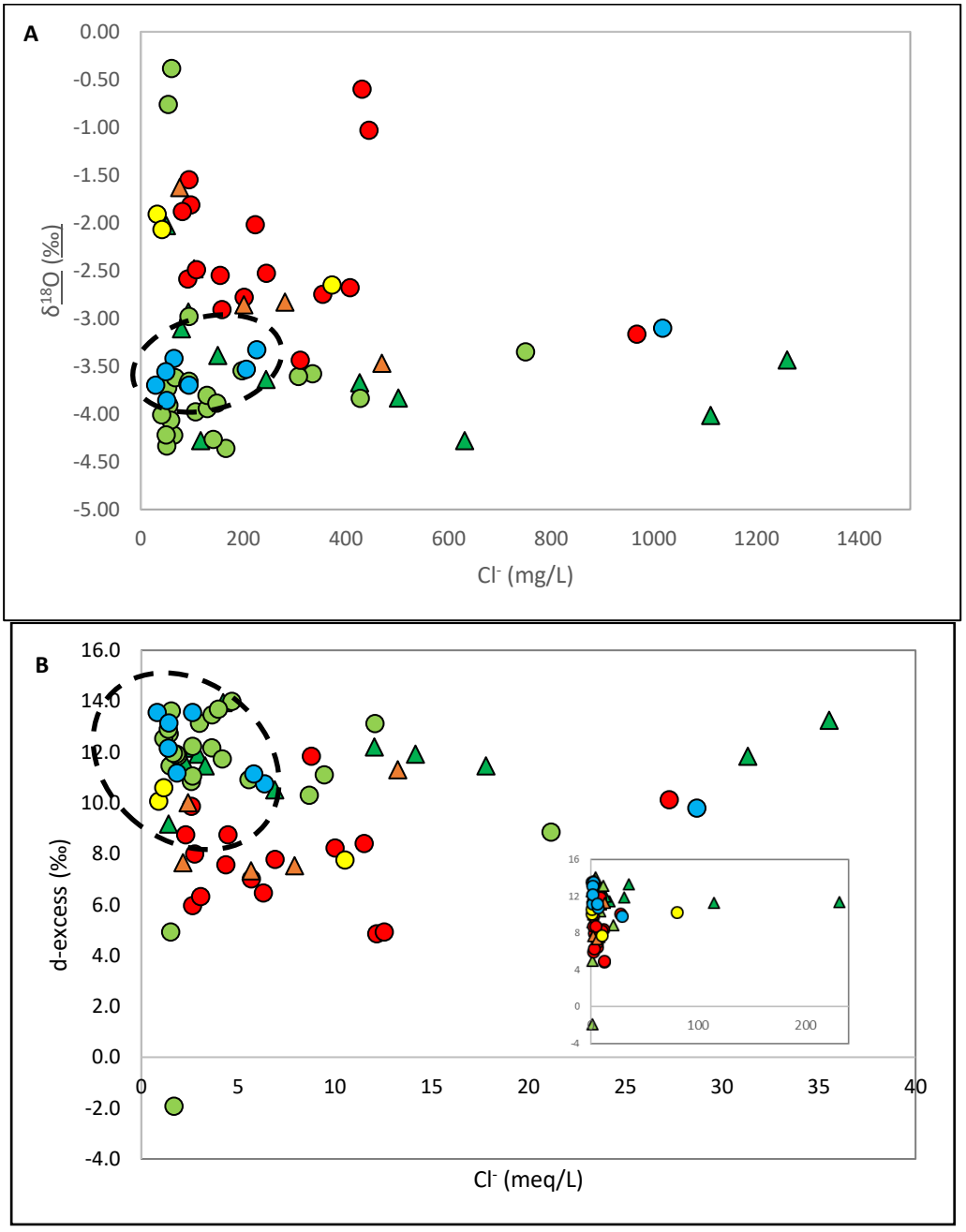

Figure 4-6 A. Cl (mg/L) vs $\delta^{18}O$ (‰) B. Cl^- (meq/L) vs d-excess (‰) Blue circles = Zone A, red circles = Zone B1, orange triangles = Zone B2, yellow circles = Zone C, green circles = Zone D1, green triangles = Zone D2

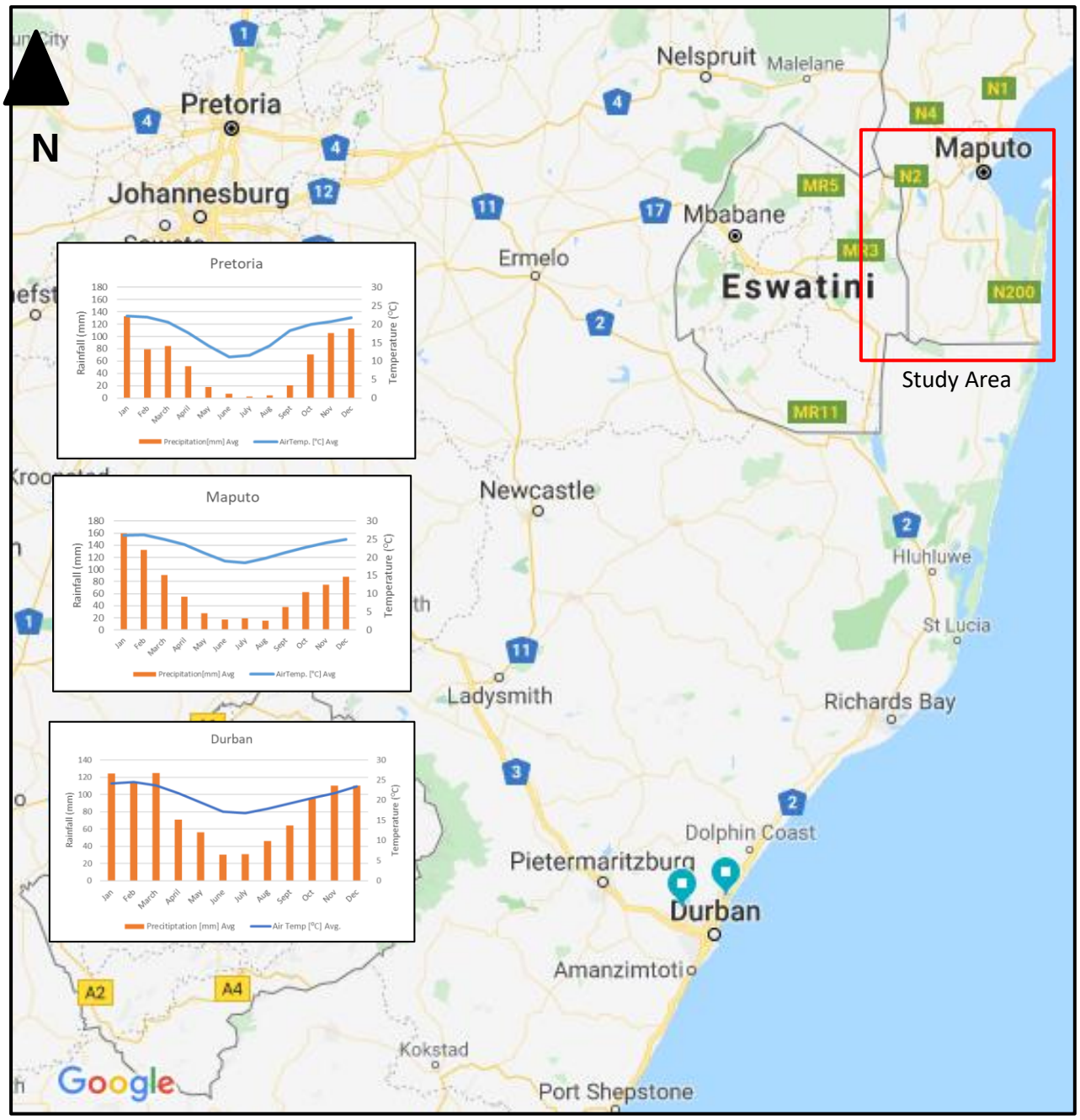

Figure 4-7 **Map of the study area and corresponding Local Meteoric Water Lines used in this study. Average rainfall and temperature data for Pretoria, Durban and Maputo displayed to demonstrate similar climatic regimes.**

4.2.2. Seasonal Variations

In southern Mozambique, March is the warmer, more humid and wetter season than September. The average d-excess value in March is slightly higher (d-excess = 10.9 ‰) than in September (d-excess = 9.6 ‰). This suggests that isotopes of precipitation are more affected by secondary evaporation processes in March than in September. However, the difference is small and is within the error margin of the wavelength-scanned cavity ring-down spectrometer and therefore the difference can be negligible. **Table**

4-2 compares seasonal variations between each zone. The average d-excess values and $\delta^{18}O$ for each zone is higher in March than in September, apart from Zone B2 and D2. Zone B2 and D2 represent boreholes with a depth greater than 40m, and it is, therefore, possible that seasonal variations are not reflected as prominently due to longer recharge rates.

Figure 4-8 depicts GNIP average isotope rainfall data collected from Pretoria. Average values for March and September are circled in black, whilst groundwater samples (from the study) that were collected in March 2018 are presented as green circles and samples collected in September 2018 are presented as red squares. Table 4.3 lists the average $\delta^{18}O$ and $\delta^{2}H$ for rainfall collected from the GNIP station in Pretoria – in general, March has higher $\delta^{2}H$ and $\delta^{18}O$ values than September. It is apparent that groundwater samples collected in March 2018 are clustered in the lower left side of the graph (with a higher $\delta^{18}O$ and $\delta^{2}H$ values), plotting close to the average rainfall isotope signature for March. Groundwater samples collected in September 2018 are more spread-out across the graph, with some samples plotting close to the rainfall data collected in September. In addition to this, similarities in the isotopic composition between the GNIP data and the groundwater samples indicate that groundwater recharge is primarily due to precipitation recharge with minimal evaporation effect.

Table 4-2 Statistical summary of $\delta^{18}O$, $\delta^{2}H$ and d-excess (‰) for March and September in each zone.

		$\delta^{18}O$ (‰)	$\delta^{2}H$ (‰)	d-excess (‰)	$\delta^{18}O$ (‰)	$\delta^{2}H$ (‰)	d-excess (‰)
		March			September		
Zone A	Mean	-3.65	-17	12.7	-3.32	-16	10.6
	Stdev	0.17	1	1.04	0.22	1	0.69
Zone B1	Mean	-2.67	-13	8.39	-1.79	-7	7.0
	Stdev	0.38	2	1.61	0.86	5	2.01
Zone B2	Mean	-2.85	-15	7.43	-2.83	-13	9.7
	Stdev	0.02	0	0.14	1.04	7	1.85
Zone C	Mean	-2.30	-9	9.68	-	-	-
	Stdev	0.37	3.86	1.30	-	-	-
Zone D1	Mean	-3.81	-18	12.0	-3.18	-16	9.8
	Stdev	0.27	1.09	1.48	1.54	8	5.02
Zone D2	Mean	-3.05	-1.23	11.7	-3.93	20	11.7
	Stdev	0.55	3.85	1.49	0.33	3	0.35

Table 4-3 Monthly GNIP data from Pretoria

Month (GNIP PRETORIA)	$\delta^{18}O$[‰] Avg	$\delta^{2}H$[‰] Avg	d-excess[‰] Avg
January	-3.88 ± 2.53	-18.7 ± 13.8	11.9 ± 8.8
February	-3.21 ± 2.43	-15.2 ± 17.6	9.6 ± 9.1
March	-4.00 ± 3.35	-21.6 ± 23.3	11.9 ± 8.5
April	-3.03 ± 2.45	-12.7 ± 19.7	12.8 ± 7.2

May	-2.47 ± 1.68	-8.7 ± 10.6	10.9 ± 9.3
June	-1.35 ± 1.90	-0.3 ± 10.5	12.6 ± 8.3
July	-0.49 ± 1.74	10.4 ± 14.1	9.0 ± 5.9
August	0.44 ± 1.79	12.0 ± 16.9	7.3 ± 7.1
September	-1.52 ± 2.02	2.3 ± 14.1	11.0 ± 6.9
October	-2.16 ± 1.41	-0.7 ± 10.3	15.5 ± 5.5
November	-2.26 ± 1.79	-9.2 ± 11.6	11.0 ± 8.2
December	-3.70 ± 2.77	-16.7 ± 16.2	13.8 ± 5.8

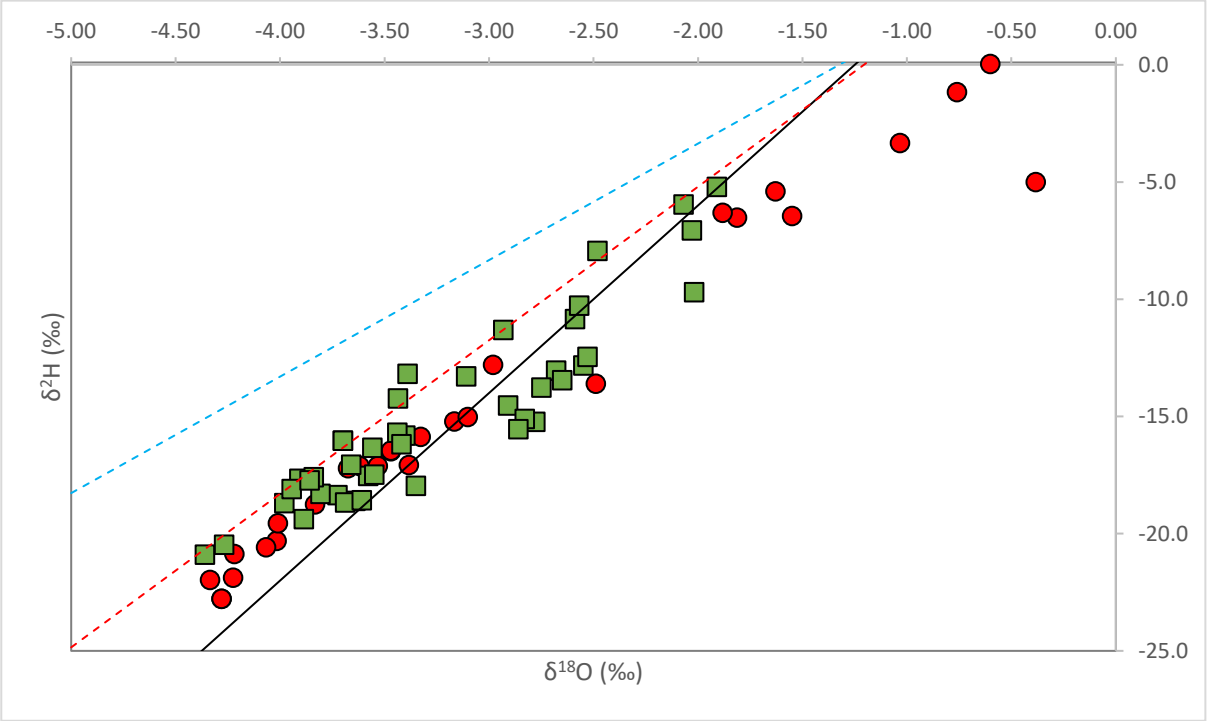

Figure 4-8 **$\delta^{18}O$ vs. $\delta^{2}H$ plot for groundwater samples from the study and rainfall samples from Pretoria. Red Circles = samples taken in September, Green Squares = samples taken in March, Solid black line = GMWL. Red dashed line = Pretoria LMW. Blue dashed line = Durban LMWL.**

4.2.3. Geographic Variations

As an air mass moves farther from its source and over continents, the $\delta^{2}H$ and $\delta^{18}O$ of precipitation increases as it undergoes more cycles of precipitation (Dansgaard,1960). **Figure 4-9** gives a map of the study area and the distribution of $\delta^{18}O$ values and **Figure 4-10 A** depicts the relationship between distance from coast and $\delta^{18}O$. No obvious correlation is present - zones B2 and D2 have a low negative correlation (r^2= 0.46 and r^2=0.48). Zone B2 has higher $\delta^{2}H$ and $\delta^{18}O$ values with increasing distance from the coast, whereas Zone D2 shows lighter $\delta^{18}O$ values with increasing distance from the coast. Zones A, B1, C, and D1 have low correlation coefficients, ranging between r^2= 0.05 to r^2=0.12.

Dansgaard (1964) noted that the $\delta^{2}H$ and $\delta^{18}O$ values increase with increasing latitude and altitude. **Figure 4-10 B** depicts the relationship between $\delta^{18}O$ and latitude (decimal degrees). Overall, from south to

north, no obvious trend is present. All zones have low to negligible correlations (r^2=0.05 to r^2 = 0.77), suggesting no relationship between latitude and $\delta^{18}O$.

There is a relationship between elevation and temperature. Lower temperatures associated with higher elevations lead to lower δ^2H and $\delta^{18}O$ values. **Figure 4-10 C** shows the relationship between $\delta^{18}O$ and elevation (m). In Zone A, samples are taken between 100 to 600 meters and around the same latitude – the higher the elevation, the more enriched in heavier isotopes. The remaining samples have negligible correlations, showing no relationship between altitude and $\delta^{18}O$.

As previously stated, stable isotopes can provide insight into the recharge environment of groundwater. **Figure 4-9** depicts the distribution of $\delta^{18}O$ samples across the study area. Contrasting $\delta^{18}O$ values of proximal samples suggest different recharge environment at the time of infiltration.

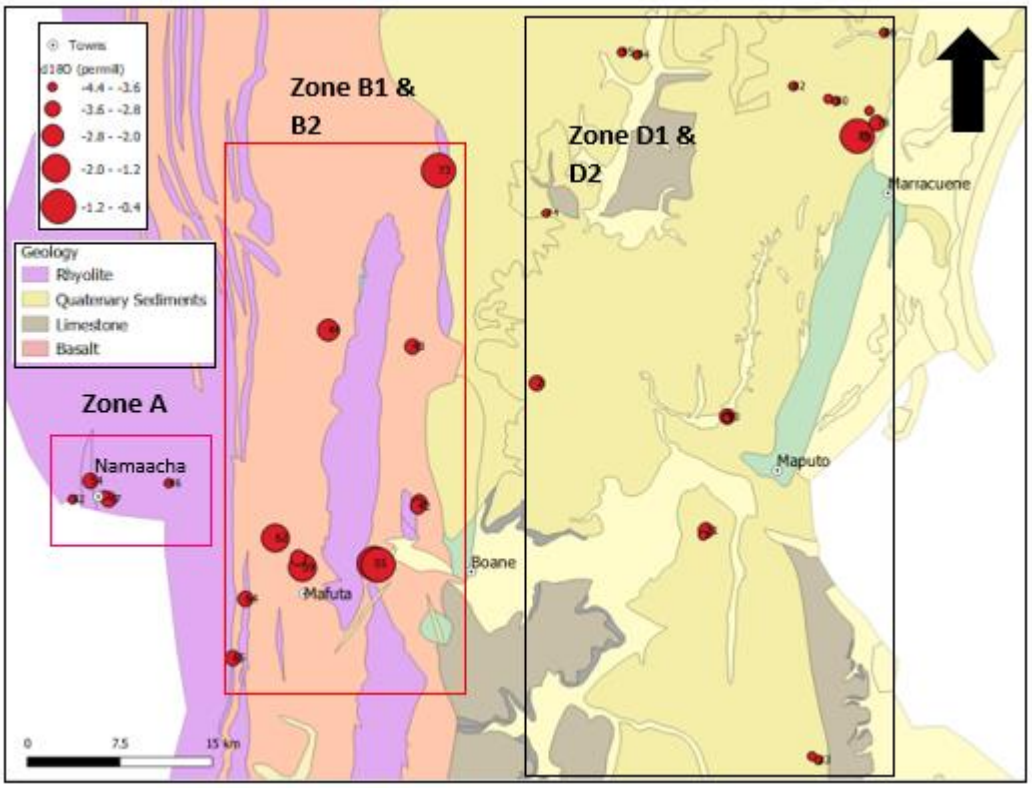

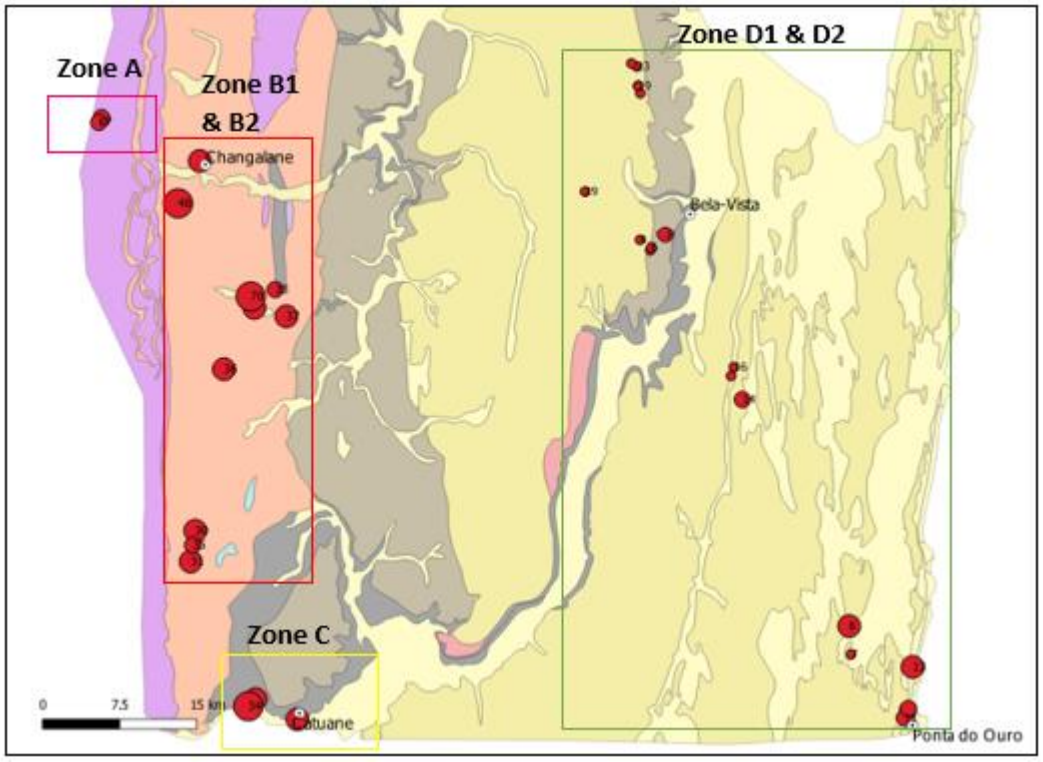

Figure 4-9 **A and B. Map of study area displaying the distribution of δ ^{18}O (‰) in the study area. Areas highlighted in pink squares plot within Rhyolites (Zone A). Red squares are samples that plot in Basalts (Zone B1 and B2). Yellow squares are samples that plot in Limestone (Zone C). Green squares are samples that plot in Quaternary sediments (Zone D1 and D2). Similar size circles suggest similar recharge conditions of the proximal sample.**

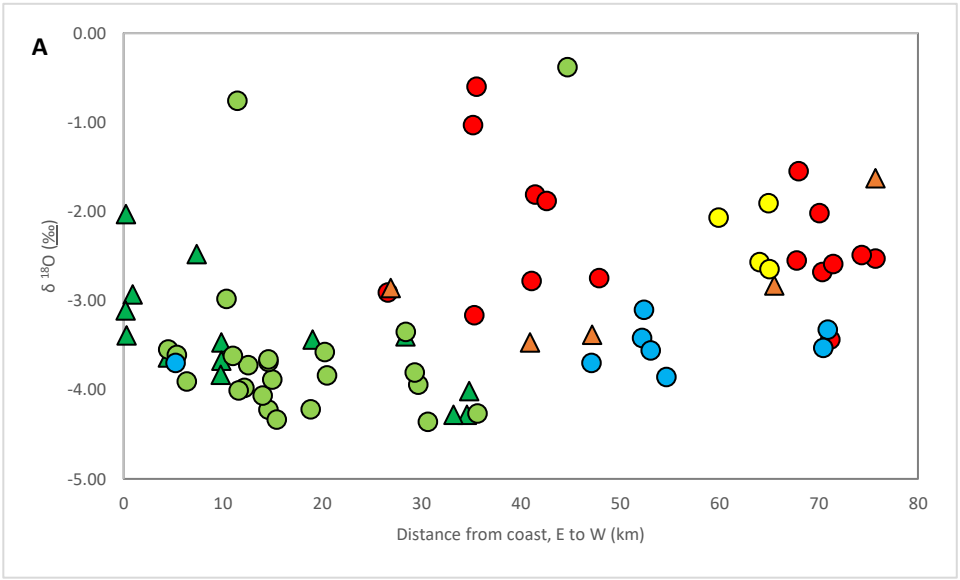

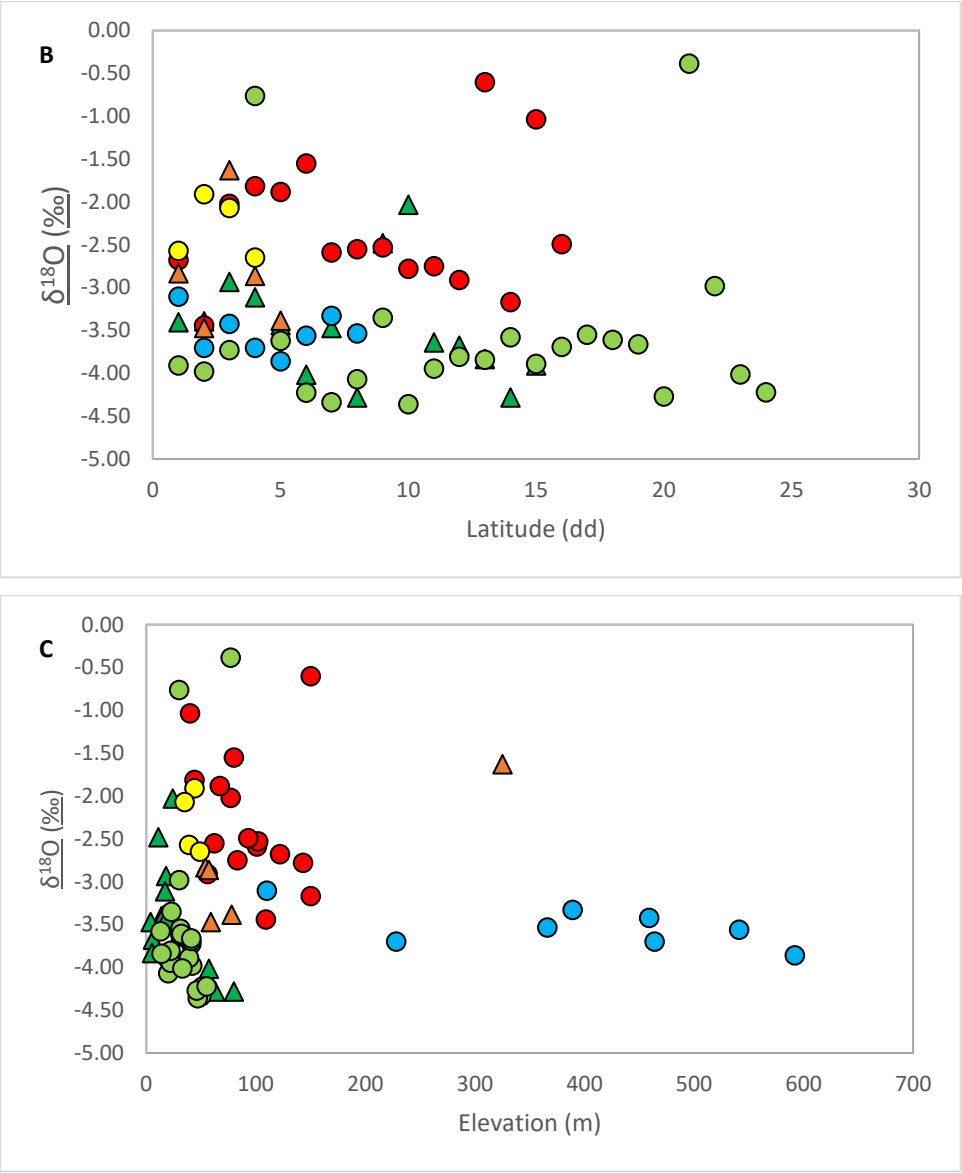

Figure 4-10 **A. δ ^{18}O (‰) vs Distance from the coast (km), measured from east to west, representing the continental effect. B. Elevation (m) vs. δ ^{18}O (‰), representing the altitude effect. C. Latitude (decimal degrees) vs δ ^{18}O (‰). Blue circles = Zone A, red circles = Zone B1, orange triangles = Zone B2, yellow circles = Zone C, green circles = Zone D1, green triangles = Zone D2**

4.3. Radiogenic Isotopes

Strontium isotope (^{87}Sr/^{86}Sr) ratios are widely used in hydrological studies for delineating different sources of water bodies – whether it be waters form different rock-water interactions, connate seawater in alluvial deposits, seawater intrusion, pollution plumes, or freshwater that infiltrates into the groundwater. This is because ^{87}Sr/^{86}Sr ratios vary widely in nature, due to the radioactive decay of rubidium (^{87}Rb) to strontium (^{87}Sr), and therefore different sources of water will yield different ^{87}Sr/^{86}Sr ratios. In addition to this, different mixing processes can be delineated, by constraining the relationship between the Sr concentration ratios and the Sr isotopic composition (Négrel, 1999; Hogan et al., 2000; Négrel, 2004).

According to Faure (1886), Sr derived from marine sediments and seawater should have a low $^{87}Sr/^{86}Sr$ ratio and a high Sr^{2+} concentrations, whilst Sr derived from the dissolution of Rb-rich minerals, such as micas and K-feldspars will have a higher ratio and a lower concentration. In addition to this, the $^{87}Sr/^{86}Sr$ ratio in continental rocks, such as granites and rhyolites will have a higher ratio than oceanic rocks, such as basalts.

Zones A, C, D1 and D2 all have very strong positive r^2 values for Sr^{2+} and Ca^{2+}, and Sr^{2+} and Cl^- (**Figure 4-11 A** and **B**). This might reflect an Sr^{2+} input, attributed to either, silicate weathering, mineral reaction in the unsaturated zone and/or dissolution of carbonate (Monjerezi et al., 2011). For Zones B1 and B2, low correlations reflect dissimilar sources of these components.

Strontium isotope values from different lithologies may impart distinctive isotopic ratios to the groundwater. Various petrography studies conducted across the region have measured the isotope ratios for the Mbuluzi Rhyolites and the Movene Basalts. As expected, The Movene Rhyolites have a higher isotope ratio, 0.71424 than the Movene Basalts, 0.70517. In addition to this, modern seawater has an $^{87}Sr/^{86}Sr$ ratio of 0.70920, whilst cretaceous seawater has an $^{87}Sr/^{86}Sr$ ratio of 0.70750.

The large spread of $^{87}Sr/^{86}Sr$ ratios in each zone cannot be attributed to the host lithology per zone (**Figure 4-12**). This indicates that mixing of different waters occurs in each zone. For example, in Zone A, where Mbuluzi Rhyolites are dominant, all samples except for one have relatively low $^{87}Sr/^{86}Sr$ ratios approximately 0.708, and plot below the $^{87}Sr/^{86}Sr$ ratio of the Movene Rhyolites (0.71424). The low concentration of Sr^{2+} and relatively low $^{87}Sr/^{86}Sr$ ratio suggests mixing of waters has occurred in this area. In contrats, samples in zones B1 and B2, where basalts are the dominant geology, the $^{87}Sr/^{86}Sr$ ratios plot around the value of modern seawater, 0.70920, whereas the Movene Basalts have a low $^{87}Sr/^{86}Sr$ ratio, of 0.70517. The higher $^{87}Sr/^{86}Sr$ ratio in these zones indicate mixing of waters with a higher $^{87}Sr/^{86}Sr$ ratio.

A few samples in Zone D1, D2, and B1 plot along the line of modern seawater. Samples that are derived from marine sediments should have low $^{87}Sr/^{86}Sr$ ratios, but high Sr^{2+} concentrations. The low concentrations of Sr in both D1 and D2, could be attributed to cation exchange with Ca^{2+}, due to the similar size, and therefore modern seawater influence could be possible. However, for Zone B1, the distance from the coast makes it unlikely that modern seawater influenced the $^{87}Sr/^{86}Sr$ ratio. This ratio is more likely a result of mixing of waters from different aquifers.

In many groundwater studies, a binary mixing relationship is calculated between two end members using the strontium isotope ratio and strontium concentration. End members would include distinct isotope

signature from dominant lithology of the aquifer, fresh-water samples from the rivers or precipitation and seawater. However, in this study, no end members are identified, and therefore the binary mixing relationship is not calculated. For future studies, precipitation samples, river samples, and seawater samples could be collected to assess the mixing relationships.

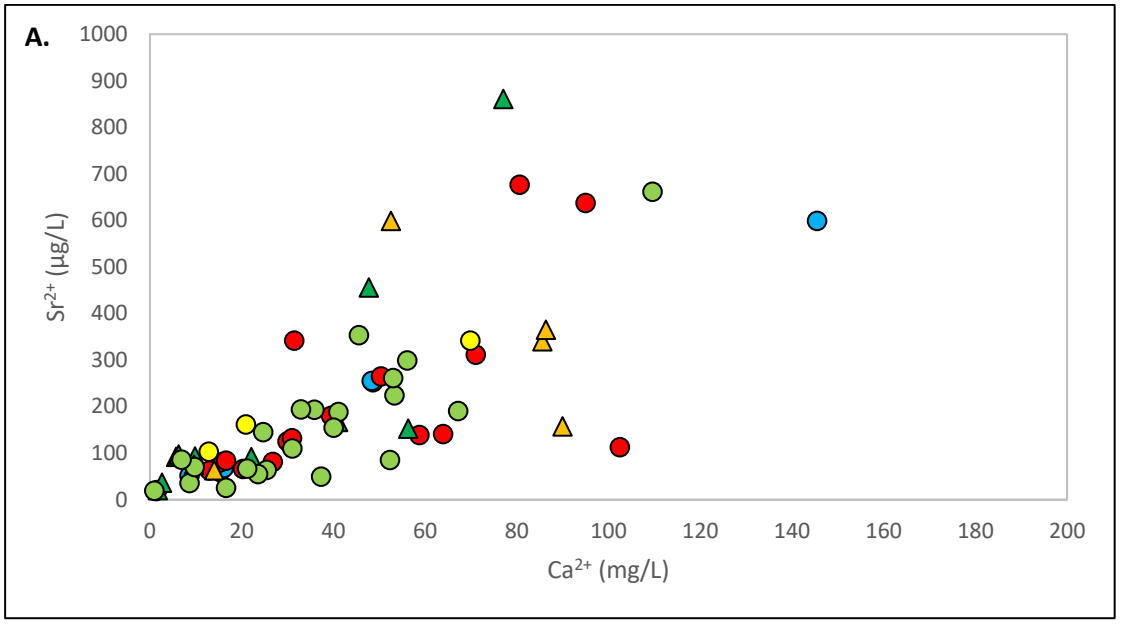

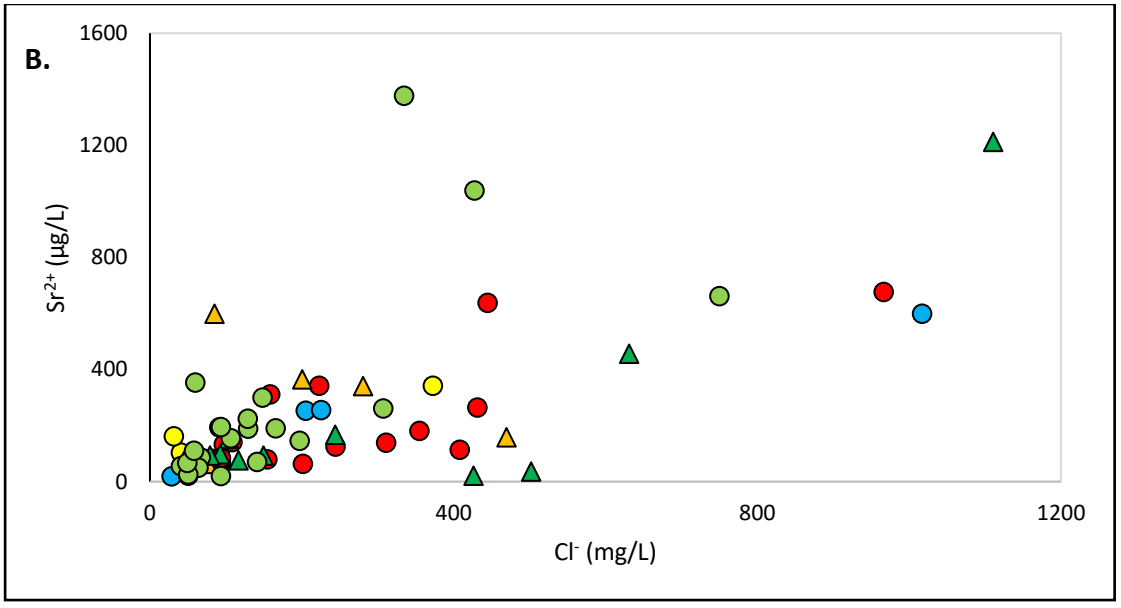

Figure 4-11 ***A. Ca (mg/L) vs. Sr (mg/L) and B. Cl (mg/L) vs Sr (mg/L). Blue circles = Zone A, red circles = Zone B1, orange triangles = Zone B2, yellow circles = Zone C, green circles = Zone D1, green triangles = Zone D2***

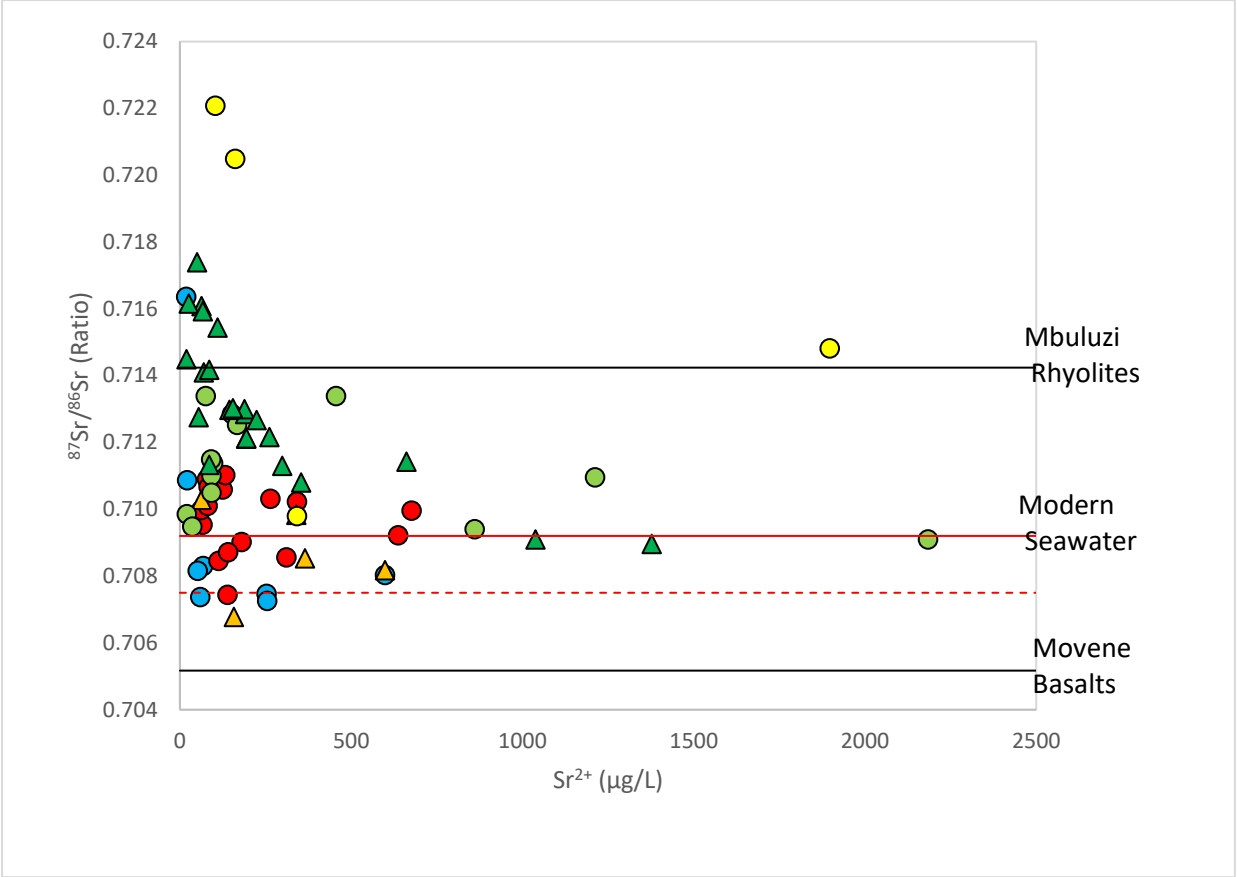

Figure 4-12 ***$^{87}Sr/^{86}Sr$ vs. Sr^{2+} (µg/L). Blue circles = Zone A, red circles = Zone B1, orange triangles = Zone B2, yellow circles = Zone C, green circles = Zone D1, green triangles = Zone D2***

4.4. Water Quality

Water quality is a term used to describe the chemical, physical and biological characteristics of water with respect to its suitability for the intended use (DWAF, 2011). It is therefore important to have a complete understanding of the controls governing water quality before its supply for domestic, agricultural or industrial usage (Kumar et al., 2014). In order to establish the potability of water in the study, parameters such as pH, EC, and major anion and cation concentrations are reviewed and compared to guidelines set by the World Health Organization (WHO) and the Department of Water Affairs of South Africa (DWAF, 2008) (**Table 4-5**).

Water can be categorized as 'freshwater', 'brackish', 'saline' and 'brine' based on EC values, see **Table 4-4** (Freeze and Cherry, 1970). In Zone A, D1 and D2 samples located close to the towns Maputo, Ponta do Ouro, Marracuene, and Namaacha have average EC values between 150 to 1500 µS/cm, classifying the groundwater as 'brackish'. In zones, C, B1, B2 and a few select samples in Zone D1 and D2

(around the greater Maputo and Bela-vista) EC values are between 1500 to 15000 µS/cm and are classified as 'saline'. From Figure 4.16 the majority of samples fall within the 'brackish' category.

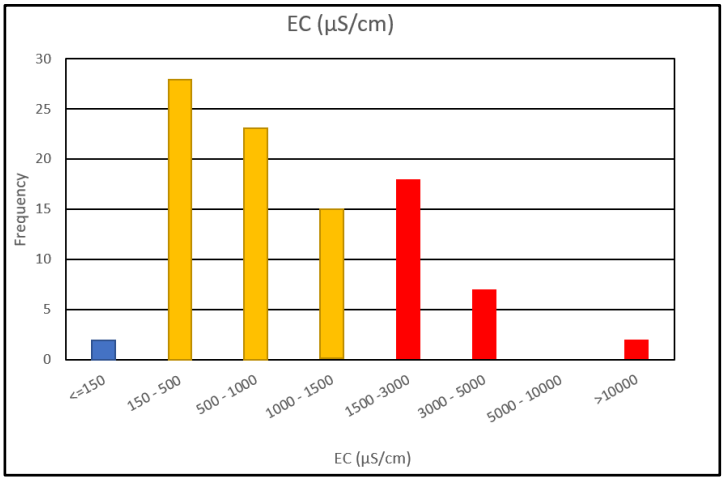

Figure 4-13. ***Histogram depicting the spread EC data in the study according to the classification of Freeze and Cherry (1970). Blue bars indicate samples categorized as 'Fresh', yellow bars indicate 'Brackish', red bars indicate 'Saline' waters.***

Table 4-4 **Classification of salinity, expressed in EC (µS/cm) according to Freeze and Cherry, 1970**

EC Range (µS/cm)	Class
<150	Freshwater
151 – 1500	Brackish water
1501 – 15000	Saline
>15001	Brine

According to the WHO guidelines, pH has no known impact on water consumers and therefore there are no health-based guidelines. However, lower pH values in waters tend to make them more corrosive (WHO,2011). For groundwater systems, the natural range in pH is usually between 6 to 8.5. The average pH of samples in Zone A, B2 and D2 ranges between 6.2 to 7, indicating a neutral to slightly acidic nature. Samples in Zone B1, C and D2 range between 7.2 to 8, indicating a slightly basic nature. Table 4.5 summarizes the health effects and recommended drinking guidelines for different elements.

Sulfate is soluble in water and is ubiquitous in groundwater and the concentrations can vary depending on the natural and/or anthropogenic sources (Minnesota Pollution Control Agency, 1999). The primary sources of sulfate in groundwater include atmospheric deposition, sulfide mineral oxidation and sulfate mineral dissolution (Krouse and Mayer, 1999). The combustion of fossil fuels releases sulfur in the atmosphere, where is it oxidized to sulfate and deposited through dry deposition or with precipitation. Sulfate occurs naturally in many minerals such as gypsum ($CaSO_4.2H_2O$), which is commonly associated with

sedimentary deposits, limestones, dolostone, sandstone, and hydrothermal veins.

Sulfate does not have a health-based guideline, but a value of 500mg/L would cause effects on the taste of the groundwater. The average SO_4^{2-} content in all zones is below the 500 mg/L recommended value, ranging between 2.8 to 259 mg/L. Sample SH18002 and SH18089 in Zone D2 have SO_4^{2-} values of 1174 mg/L and 1003 mg/L.

Chloride inputs to groundwater can arise from several anthropogenic and natural sources, including sewage effluent discharges, inorganic fertilizers, various industrial processes, and seawater intrusion. Although there are no health-based guidelines, a value of 250 mg/L is recommended by the WHO (2011). Values above this may be above the corrosion threshold and may also alter the taste of the water. Zone A, B2, and D1 have average Cl^- values below the recommended value and Zone B1, C and D1 have Cl values above the 250 mg/L threshold.

Sodium is prevalent in groundwater as most rocks and soils contain sodium compounds, which are readily dissolvable. The most notable sources of sodium in groundwater include erosion from salt deposits and sodium bearing minerals, saltwater intrusion in coastal areas, naturally occurring brackish water and anthropogenic sources such as sewage effluent, irrigation leaching, and infiltration of leachate from landfills and/or industrial sites. (Water Stewardship Information Series, 2007). There is no health-based guideline set for sodium; however, a value above 200 mg/L would affect the taste of water and its use for agricultural purposes. Zones A, B2, and D1 have average Na^+ values below the 200 mg/L threshold, whilst the remaining zones have average Na values above the recommended value.

Magnesium is a common constituent of groundwater and sources include mineral dissolution, naturally occurring brine water and seawater. Common minerals of Mg^{2+} include magnesium carbonates, commonly found in limestones and dolostones, and various magnesium silicates (DWAF,2011). The solubility of magnesium is governed by pH, whereby the solubility of magnesium hydroxide decreases with an increasing pH. Magnesium, together with calcium is responsible for the hardness of water which may cause scaling problems. Scaling issues can occur with a Mg^{2+} content between 30 to 50 mg/L. Health-based effects include diarrhea can occur with a magnesium content above 70 mg/L. Although the WHO does not give a guideline, a target range of 0-30 mg/L is ideal (DWAF, 1996). Zones A, B1, B2 and D1 have average Mg^{2+} values below 30 mg/L, whereas the zones C and D2 have values above the ideal Mg^{2+} content.

Calcium inputs to groundwater commonly occur via mineral dissolution. Many rocks and minerals are composed of Ca^{2+} including; limestone, marble, calcium carbonates, bicarbonate, phosphates and

sulfates. The solubility of calcium in groundwater is influenced by pH and temperature, especially for carbonate/bicarbonate reactions. Together with Mg^{2+}, Ca^{2+} is responsible for the harness in water. No health-based guidelines are set by the WHO. A Ca^{2+}content between 0 to 32 mg/L is recommended as a target range before scaling issues are induced. All zones have an average Ca^{2+} concentration greater than the recommended value.

Potassium is commonly present in groundwater as many K^+ compounds are highly soluble. Common minerals that contain K^+ include feldspars and micas. In addition to this, K^+ is a component of fertilizer and urine and may occur as runoff or sewage. In water, K^+ is always associated with anions – Cl^- most commonly, but it can also occur with SO_4^{2-} , HCO_3^- , or NO_3^-. Health-based effects of excessive potassium may induce kidney-related diseases due to electrolyte imbalances. The DWAF recommends a K^+ range between 0 to 50 mg/L. All zones have an average of less than 50 mg/L. Samples SH18002 and SH18089 in Zone D2 have elevated K^+ concentrations, of 50.6 and 72.9 mg/L respectively.

With regard to water quality, samples around the towns of Maputo, Ponta do Ouro and Marracuene (in Zone D1), Namaacha (Zone A) all have average cation and anion concentrations below the recommended guideline set by WHO and DWAF (except for Ca^{2+}). These zones represent the best water quality in the whole study. Samples were taken near the towns of Boane, Bela-Vista, greater Maputo (Zone D1 and D2), Catuane (Zone C), Changalane, Brewery and Mafuta (Zone B1 and B2) on the other hand, have anion and cation concentrations above the recommended guidelines.

Table 4-5 **A list of selected chemical constituents; their natural concentrations observed in seawater and freshwater; their DWA guideline value; their associated environmental and health issues; and the exceedances observed in this study.**

		Cl^-	SO_4^{2-}	Na^+	Mg^{2+}	Ca^{2+}	K^+
Occurrence (mg/L)	**Freshwater**	-	0 - 100	-	4 - 10	15	2 - 5
	Seawater	19,800	900	11,000	1,300	400	400
Sources	**Natural**	Salt-water, dissolution of Cl bearing minerals	Dissolution of minerals - gypsum	Salt deposits, seawater intrusion, minerals, brines	Magnesium carbonates and silicates	Calcium carbonate, phosphate, sulphate	Minerals – feldspars and micas
	Anthropogenic	Irrigation return flows, sewage effluent, industrial waste	Acid mine drainage, industrial waste, fossil fuel burning	Industrial waste, run-off from irrigation	-	-	Fertilizer, urine
Issues		Salty taste, corrosion effects	Salty and bitter taste, increase erosion rate of metals	Salty taste	Scaling and taste	Scaling	Bitter taste
Health-issues with elevated concentrations		Electrolyte imbalance	Diarrhoea	Electrolyte imbalance	Diarrhoea		Electrolyte disturbances, vomiting
Recommended concentration (mg/L)		0 – 200	0 - 500	0 – 200	0 – 30	0 – 32	0 – 50
Zones less than recommended amount		Maputo, Ponta do Ouro, Marracuene (Zone D1 and D2) Namaacha (Zone A), One World University (Zone B1 and B2)	Zone A, B1, B2,	Maputo, Ponta do Ouro, Namaacha, Marracuene, One World University	Maputo, Ponta do Ouro, Namaacha, Marracuene, One World University	Maputo, Ponta do Ouro, Namaacha, Marracuene, Brewery	All
Zones greater than		Boane, Bela-Vista,	-	Boane, Bela-	Boane, Bela-Vista,	Maptuo,	-

recommended concentration (mg/L)	Catuane, Changalane, Brewery, Mafuta		Vista, Catuane, Changalane, Brewery, Mafuta	Catuane, Changalane, Brewery, Mafuta	Boane, Bela-Vista, Catuane, Changalane, Mafuta,	

5. Conclusions and Recommendations

The aim of this study was to characterize the isotopic and hydrochemical composition of groundwater in the study area. The chemical composition, various ion ratio and saturation indices were used to gain better insight into the factors that control the overall chemical character of the groundwater. Isotopes were used to delineate external processes (i.e. evaporation processes) prior to infiltration and infer the source of groundwater.

Samples were divided into different zones based on the dominant geology in which the borehole is sited, and furthermore, the depth of the borehole. Samples in Zone A situated in the rhyolites that form a part of the Lebombo monocline in the far west of the study. All boreholes are community hand pumps and are less than 40m in depth. Zone B plotted within the basalts that are present in the center of the study area. This zone was divided into boreholes that are less than 40m depth, Zone B1 and boreholes that are greater than 40m depth, Zone B2. Zone C represents boreholes that are situated within limestones in the southern part of the study area. Lastly, Zone D represents boreholes that plot within the Quaternary sediments on the eastern side of the study area. Borehole less than 40m depth is in Zone D1 and boreholes greater than 40m depth is in Zone D2.

Overall, the dominant anions and cations are as follows; $Cl^{-}>HCO_3^{-}>SO_4^{2-}$ and $Na^{+}>Ca^{2+}=Mg^{2+}>K^{+}$. According to the Piper diagram, 68% of the samples fall within the Na-Cl water type and 30% plot within the Na-HCO_3 water type. A Chadha plot was used in conjunction with the Piper diagrams to verify the major water types and dominant mechanisms controlling the water chemistry. Across the study area, there are no obvious trends relating to the water type. In Zone A and D2, water chemistry is controlled by salinity and the water type is of Na-Cl character. In zone, B1 salinity and ion exchange processes control the chemistry of the water and samples are of Na-CL and Na-HCO_3 type. In Zone B2 however, waters are represented by recharge waters and salinity as the mechanisms controlling the chemistry. Samples are Ca-Mg-HCO_3 and Na-Cl dominant. In Zone C and D1 there is no obvious mechanism that controls the chemistry and there is no dominant water type in these zones.

Gibbs diagrams, HCO_3^{-}/SiO_2 and $Ca^{2+} + Mg^{2+} / HCO_3^{-} + SO_4$ ratios reveal rock-water interactions and silicate weathering are dominant processes that control the hydrochemical character of the water for 60% of the boreholes. Whereas 30% of the boreholes are controlled by evaporation/crystallization and carbonate and silicate dissolution. Most samples in Zone B2, C and D2 plot within the evaporation/crystallization zone of the Gibbs diagram. These samples are oversaturated with respect to

calcite and dolomite according to the SI values - confirming carbonate dissolution. In Zones A, B1 and D1, samples plot within the rock-dominance zones. Additionally, samples are undersaturated with respect to calcite and dolomite, confirming silicate mineral dissolution. The saturation indices reveal that all samples are undersaturated with respect to gypsum and halite, suggesting that these minerals are not present in high enough concentrations to contribute to the overall chemical character of the water.

The sources of major anions and cations can be inferred by looking at various ratios and their degree of correlation. In this study, Na^+ and Cl^- correlate strongly, suggesting a common source. Sixty-two percent of the samples have a Na^+/Cl^- ratio greater than one, indicating enrichment of Na^+ over Cl^-. This is indicative of silicate weathering. The remaining samples, in Zone B2, B1 have a ratio of less than 1, suggesting reverse ion exchange, halite dissolution or seawater intrusion. However, the SI values indicate that halite is not present in high enough concentrations to contribute to the Na and Cl^- content in the groundwater. Sea-water intrusion is unlikely since samples do not plot within the δ^2H and $\delta^{18}O$ of seawater. In addition to this, samples that are enriched with respect to Cl^- over Na^+, have a Ca-Cl water type, suggesting reverse ion exchange as a dominant process. In Zone A, the $SiO_2/(Na^+ + K^+) – Cl^-$ ratio is greater than 1 indicating albite weathering as a source of Na^+ in this zone.

Sources of Ca^{2+} and Mg^{2+} include carbonate minerals such as calcite and dolomite, as well as ferromagnesian silicates, such as biotite. In Zone B, the $SiO_2 /(Na^+ + Ca^{2+}) – Cl^-$ is greater than two, suggesting the dissolution of ferromagnesian minerals such as biotite as a source of Ca^{2+} or Mg^{2+}. In Zone C, the Ca^{2+}/HCO_3^- and $(Ca^{2+} + Mg^{2+})/HCO_3^-$ ratios plot around the 1:1 line and SI values that samples are oversaturated with respect to calcite and dolomite. The sources of Ca^{2+} and Mg^{2+} in Zone D are variable, suggesting either silicate weathering or carbonate mineral dissolution.

Sources of HCO_3^- include dissolved CO_2 from rainfall, the decay of organic matter in the vadose zone or dissolution of calcite/dolomite all of which liberate HCO_3^- into the groundwater. In Zones, C and D, calcite and dolomite dissolution is a major contributor to HCO_3^- in the groundwater. In addition to this, SO_4^{2-} is not present in high concentrations in the groundwater throughout the study area. The SI values indicate that gypsum is undersaturated in all samples of groundwater. Low SO_4^{2-} concentrations are indicative of a reducing environment, in which sulfate reduction occurs, liberating sulfur from the sulfate molecule.

Although no rainfall samples were collected for this study, several meteoric water lines have been used as a proxy for a local meteoric water line. Overall, samples were found to best match the LMWL of Durban and Pretoria. Low d-excess values, that are less than 10 suggest that little evaporation took place prior to groundwater infiltration. Furthermore, isotopic effects, such as seasonal variations, latitude,

elevation, and distance from coast appeared to not be such a major factor affecting the isotopic composition.

Strontium isotopes, and elemental strontium concentrations indicate that groundwater mixing likely occurred in each zone. No end-members could be identified however, so mixing relationships were not defined. The relationship between Cl^- vs Sr^{2+} and Ca^{2+} vs Sr^{2+} suggested that silicate weathering and carbonate weathering were the dominant processes controlling salinity in groundwater in Zones A,C, D1 and D2.

Several limitations are evident in the study. First, three different methods were used at two different labs to measure concentrations of the different anion species, whereas all cations were measured at the same lab using the same technique and machine - bicarbonate anions were measured using the Metrohm 905 Titrano Autotritrator at the Department of Soil Science at Stellenbosch University, whereas the chloride anions were measured using 0.02N Silver Nitrate titration using the Metrohm 904 Titrando at Bemlabs in Somerset West. In addition to this, Sulphate concentrations were analyzed using the ICP-OES Agilent 700 ICP series at Bemlabs. Furthermore, cations were measured at the Center of Analytical Facilities at Stellenbosch University using the Agilent 7700 ICP-OES machine. For future studies, to decrease the error margin on the analysis, it is recommended that the same technique at the same lab is used to measure the concentrations of the major ions.

In addition to this, the sampling locations between the two different sampling trips were different and as a result, the seasonal difference between major ions and isotopes could not be inferred in this study. In order to be able to observe seasonal and spatial differences, the same borehole should be sampled in different seasons.

Lastly, in order to better understand the origin of groundwater, stable isotope $\delta^{18}O$ and $\delta^{2}H$ of precipitation around the study area should be collected for 10 years in order to infer the LMWL of southern Mozambique. This will aid in better characterizing the source of the groundwater in the study area.

6. References

Afonso, R.S., Araujo, J.R., Ferro, B.P., Rebolo, J.F., Oberholzer, W., &Perlico, L.C., 1969. *Carta geologica de rigiao de Tambara-Doa*, Sheet Sul-E36, (Sheet 1936), Servico Geologico e Minas, Lourenco Marques.

Afonso, R.S., Marques. J.M. and Ferrara, M., 1998. *A evolucao geologica de Mocambique: Uma sintese*, Lisboa.

Appello, C. A. J., & Postma, D., 1996. *Geochemistry, Groundwater and Pollution*, Second Edition. A.A. Balkema Publishers, Amsterdam, 536 pp.

Beuster, J., Clarke, F.A., 2008. *Basin Characteristics, Land Use and Water Resources Infrastructure*.
Campbell, I.H., Griffiths, R.W., 1990. *Implications of mantle plume structure for the evolution of flood basalts*

Carpenter, A.B., 1978. *Origin and Chemical evolution of brines in sedimentary basin*. Oklahoma Geological Survey Circular, 79, 60-76

Carta Hidrológica Executada pela direcção nacional de águas com apoio da UNICEF, de Acordo com a igneda interenacional para cartas hidrogeológicas da UNESCO,1992

Castelino, J.A., Reichert, C., Klingelhoefer, F., Aslanian, D., 2015. *Mesozoic and Early Cenozoic sediment influx and morphology of the Mozambique Basin*, Marine and Petroleum Geology 66,pp. 890-905

Chadha, D.K., 1999. *A proposed new diagram for geochemical classification of natural waters and interpretation of chemical data*, Hydrogeology Journal, Volume 7, issue 5, pp. 431-439

Chairuca, L., Naafs, A., van Haren, I., Upton, K., Ó Dochartaigh, B.É. and Bellwood-Howard, I. 2018. *Africa Groundwater Atlas: Hydrogeology of Mozambique*, British Geological Survey, Accessed [April 2018]. http://earthwise.bgs.ac.uk/index.php/Hydrogeology_of_Mozambique

Chebotaev, I. I., 1955. *Metamorphism of natural waters in the crust of weathering – 1*, Geochimica et Cosmochimica Acta, Volume 8, Issue 1-2, pp. 22-32

Chebotaev, I. I., 1955. *Metamorphism of natural waters in the crust of weathering* – 2, Geochimica et Cosmochimica Acta, Volume 8, Issue 3, pp. 137-170

Chenini, I., Mammou, A. B., May, M. E., 2010. *Groundwater Recharge Zone Mapping Using GIS-Based Mutli-criteria Analysis: A case study in central Tunisia*, Water Resource Management, Volume 24, Issue 5, pp. 921-939

Clarke, I. D., Fritz, P., 1997. Environmental Isotopes in hydrology. 1 ed. New York: Lewis Publishers
Cleverly, R.W., Bristrow, J.W., 1979. *Revised volcanic stratigraphy of the Lebombo Monocline*, Transactions of the Geological Society of South Africa 82,2, pp. 227-230

Coplen T., 1993. *Normalization of oxygen and hydrogen isotope data*, Chemical Geology (isotope Geoscience), Volume 72, pp. 293-297

Coster, P.W., Lawrence, R., Fortes, G., 1989. *Mozambique: a new framework for hydrocarbon Exploration*, Journal of Petroleum Geology 12, pp. 205-230

Cox, K.G., 1970. *Tectonics and volcanism of the karoo period and their bearing on the postulated*

fragmentation of Gondwanaland, Jounral of African Magmatism, pp. 211-235

Cox, K.G., 1972. *The Karoo volcanic cycle*, Journal of the Geological Society of London 128, pp. 311-336

Cox, K.G., 1972. *Flood basalts, subduction, and the break-up of Gondwanaland*. Nature 274, pp. 47-49

Cox, K.G., Bistrow, J.W., 1984. *The Sabie River Basalt Formation of the Lebombo Monocline and south-east Zimbabwe*, In: Erkland, A.J., (ed.), Petrogenesis of the volcanic rocks of the Karoo Province, Geological Society of South Africa, Special Publication 13, pp. 125-147

Cox, K.G., 1992. *Karoo igneous activity, and the early stages of the break-up of Gondwanaland*. Special Publication of the Geological Society of London 68, pp. 137-148

Craig, H., 1961. *Isotopic Variations in Meteoric Water*. Volume 133, pp. 1702-1703.

Dansgaard, W., 1960. *Stable Isotopes in precipitation*. Tellus, pp. 336-368

Dansgaard, W., 1964. *Stable Isotopes in Precipitation*. Tellus 16, pp. 436-468

Darracott, B.W., Kleywegt, R.J., 1974. *The structure of the southern portion of the Lebombo volcanic belt deduced from gravity data*. Transactions of the Geological Survey of South Africa, 77 (Part 3), 301-308
Datta, P.S., Tyagi, S.K., 1996. *Major Ion Chemistry of Groundwater in Delhi Area: Chemical Weathering Processes and Groundwater Flow Regime*. Journal Geological Society of India. Volume 47, Feb, 1996, pp. 179-188

Department of Water Affairs., 2011. *Water Quality Guidelines*.

DNA., 1989. *Review of the Water Resources of Maputo Province*. World Bank Study. Arnhem, Euroconsult. Maputo. DNA

Duce, R.A., Hoffman, E.J., 1976. *Chemical fractional at the air/sea interface*. Ann. Rev. Earth Planet. Sci.4, pp. 187-228

Eales, H.V., Marsh, J.S., Cox, K.G., 1984. *The Karoo igneous province: and introduction*. In Erkland, A.J., (ed.) Petrogenesis of the volcanic rocks of the Karoo Province, Geological Society of South Africa, Special Publication 13, pp. 1-26

Eby, G.N., 2004. *Principals of Environmental Geochemistry*. Brooks/Cole, Belmont, USA.

Faure G. Principles of Isotope Geology, 2nd ed.; John Wiley & Sons: 1986; p 539.

Flores, G., 1961. *Outline of the geology of Mozambique*. Rel. ined., Mozambique Gulf Oil Co., Serv. Geol. Minas, Lourenco Marques.

Flores, G., 1970. *Suggested origin of the Mozambique Channel*. Transactions of the Geological Society of South Africa Part 1(1), pp. 1-16

Flores, G., 1973. *The Cretaceous and Tertiary sedimentary basins of Mozambique and Zululand*. In: Sedimentary Basins of the African Coasts, Symposium, Part 2, South and East Coast. Association of African Geological Surveys, Paris, pp. 81-111

Freeze, R. A., Cherry, J.A. 1979. *Groundwater*. Prentice-Hall, Eaglewood Cliffs.

Gallagher, K., Hawkesworth, C.J., 1992. *Dehydration melting and the generation of continental flood basalts*. Nature 358, pp. 57-59

Gat, J. R., 1996. *Oxygen and Hydrogen Isotopes in the Hydrologic Cycle*. Earth Planet Science, Volume 24, pp. 225-262

Gibbs, R. J., 1970. *Mechanisms Controlling World Water Chemistry*. Science. New Series, 170, pp. 1088-1090

Gwavava, O., Swain, C.J. Podmore, F., Fairhead, J.D., 1992. *Evidence of crustal thinning beneath the Limpopo Belt and the Lebombo Monocline of Southern Africa based on regional gravity studies and implications for the reconstruction of Gondwana*. Tectonophysics 212, pp. 1-20

Hem, J, D., 1989. *Study and Interpretation of the Chemical Characteristics of Natural Water*. Water Supply Paper 2254. Department of the Interior U.S. Geological Survey, Alexandria, pp. 118, 190, 194.

Hoefs, J., 1997. *Stable Isotope Geochemistry*. Springer, Cham.

Hogan, J.F., Blum, J.D., 2003. *Tracing hydrologic flow paths in a small forested watershed using variations in 87Sr/86Sr, [Ca]/[Sr], [Ba]/[Sr] and delta d18O*. Water Resour. Res. 39, 1282–1293.

Hounslow, A., 1995. *Water Quality Data: Analysis and Interpretation*. Lewis Publishers, Boca Raton, pp. 67, 77-85, 90, 99-100, 102-103, 105-106, 112-115

IAEA, 2007. *Atlas of Isotope Hydrology – Africa*. International Atomic Energy Agency, Vienna.

IAEA/WMO. 2006a. *Global Network of Isotopes in Precipitation*.

IAEA/WMO. 2006b. *Isotope Hydrology Information System*.

Johnson, M.R., Anhaeusser, C.R., Thomas, R.J., 2006. *The Geology of South Africa*, 1st Edition, Council for Geosciences/Geological Society of South Africa, Johannesburg.

Jourdan, F., Feraud, G., Bertrand, H., Watkeys, M.K., 2007a. *From flood basalts to the inception of oceanization: example from the $^{40}Ar/^{39}Ar$ high-resolution picture of the Karoo large igneous province*. Geochemistry Geophysics Geosystems 8, Q02002. Doi:10.1029/2006GC00139

Manninen, T., Eerola, T., Mäkitie, H., Vuori, S., Luttinen, A., Sénvano, A., Manhiça, V., 2008. *The Karoo volcanic rocks and their related intrusions in southern Mozambique*. Geological Survey of Finland, Special Paper 48, pp. 211-250

Mashaba, V., Altermann, W., 2015. *Calculation of water saturation in low resistivity gas reservoirs and pay-zones of the Cretaceous Grudja Formation, onshore Mozambique basin*. Marine and Petroleum Geology 67, pp. 249-261

Mclean, W., Jankowski, N., 2000. *Groundwater Quality and sustainability in an alluvial aquifer, Australia*, Groundwater: Past achievements and future challenges, Cape Town, November 2000

Matthews, A., Lawrence, S.R., Mamad, A.V., Fortes, G., 2001. *Mozambique basin may have a bright future under new geological interpretations*. Oil Gas Journal 2,pp. 70-76

Melluso, L., Cucciniello, C., Petrone, C.M., Lustrino, M., Vincenzo, M., Tiepolo, M., Vasconcelos, L., 2008. *Petrology of Karoo volcanic rocks in the southern Lebombo Monocline Mozambique*. Journal of African Earth

Sciences 52, pp. 139-151

Miller, J.A., Harris, C., 2007. *Petrogenesis of the Swaziland and Northern Natal rhyolites of the Lebombo rift margin, South East Africa*. Journal of Petrology 48, pp. 185-218

Minnesota Pollution Control Agency 1999, *Sulfate in Minnesota's Ground Water*. <https://www.pca.state.mn.us/sites/default/files/sulfate7.pdf>

Monjerezi, M., Vogt, R., Aagaard, P., Gebru, A., Saka, J. 2011. *Using 87Sr/86Sr, $\delta^{18}O$ and $\delta^{2}H$ isotopes along with major chemical composition to assess groundwater salinization in lower Shire valley, Malawi.* Applied Geochem. 26, 2201-2214

Narany, T. S., Ramli, M. F., Aris, A. Z., Sulaiman W. N. A., Juahir, H., Fakharia, K., 2014. *Identification of the Hydrogeochemical Processes in Groundwater Using Classic Integrated Geochemical Methods and Geostatistical Technique in Amol-Babol Plain, Iran*. Hindawi, Volume 2014.

Ndlovu, M.S., Demile, M., Butler, M., 2019. *Hydrogeological setting and hydrochemical characteristics of the Durban metropolitan district, eastern South Africa*. Geological Society of South Africa.

Négrel, P., 1999. *Geochemical study of a granitic area— the Margeride Mountains, France: chemical element behavior and 87Sr/86Sr constraints*. Aquatic Geochemistry 5 (2), 125–165.

Négrel, P., Petelet-Giraud, E., Widory, D., 2004. *Strontium isotope geochemistry of alluvial groundwater: a tracer for groundwater resources characterisation*. Hydrology and Earth System Sciences 8 (5), 959–972.

Piteau and Assoicates., 1992. *Groundwater Resources Swaziland. Report prepared for the Swaziland Department of Geological Surveys and Mines and the Canadian International Development Agency*.
Porowski, A., 2017. *Hydrogeological settings and origin of groundwater composition in the southern part of the Gorce Mts, Kowaniec Maly catchment*. Annales Societatis Geologorum Poloniae.

Rajmohan, N., Elango, L., 2004. *Identification and evolution of hydrogeochemical processes in the groundwater environment in an area of the Palar and Cheyyar River Basins, Southern India. Environmental Geology, Volume 46, pp. 47-61*

Rapela, C.W., Pankhurst, R.J., 1992. *The granites of northern Patagonia and the Gastre Fault System in relation to the break-up Gondwana*. Geological Society of London, Special Publication 68, pp. 209-220
Said, A., Moder, C., Clark, S., Ghordal, B., 2015. *Cretaceous-Cenozoic sedimentary budgets of the Southern Mozambique Basin: Implications for uplift history of the South African Plateau*. Journal of African Earth Sciences, 109, pp. 1-10

Salman, G., Abdula, I., 1995. *Development of the Mozambique and Ruvuma sedimentary basins, offshore Mozambique.* Sedimentary Geology 96, pp. 4-41

Sharp, Z., 2005. *Principals of Stable Isotope Geochemistry*, Volume 2, pp. 3-1 – 3-24

Soares, A. F., Silva, G.H., 1970. *Contribuicao para o estudo da Geologia do Maputo. Estratigrafia e paleontologica de Madubula e suas relacoes com areas visinhas*. Rev. Cienc. Geol. Univ., Lorenco Marques.

Storey, B.C., Alabaster, T., Pankhurst, R.J., 1992. *Magmatism and the causes of continental break-up.* Geological Society of London, Special Publication 68, pp. 404

Vaz, A., van der Zaag, P., 2001. *Sharing the Incomati Waters; Cooperation and Cometition in the Balance.* UNSECO-Green Cross.

White, R.S., Mckenzie, D., 1995. *Mantel plumes and flood basalts*. Journal of Geophysics Research 100 17543-17585Water Stewardship Information Series, 2007. *Sodium in Groundwater* >https://www.rdn.bc.ca/cms/wpattachments/wpID2284atID3807.pdf<
World Bank. 2007. *Mozambique Country Water Resources Assistance Strategy: Making Water Work for Sustainable Growth and Poverty Reduction*. AFTWR, Africa Region, August 2007.

World Health Organization, 2011. *Guidelines for Drinking Water-Quality*. Volume 4 >https://apps.who.int/iris/bitstream/handle/10665/44584/9789241548151_eng.pdf;jsessionid=600BFB814747BDA3D652CAF40916635D?sequence=1<

WorldWeatherOnline.com. 2018. *Maputo City Monthly Climate Averages, 2018*. [online] Available at <https://www.worldweatheronline.com/maputu-city-weather-averages/maputo/mz.aspx>

WorldWeatherOnline.com. 2018. *Namaacha Monthly Climate Averages, 2018*. [online] Available at <https://www.worldweatheronline.com/namaacha-weather-averages/maputo/mz.aspx>